INSTITUTE OF GRADUATE STUDIES

DEPARTMENT OF MEDICAL MICROBIOLOGY AND CLINICAL MICROBIOLOGY

ASSESSMENT OF DEEP LEARNING MODELS FOR CUTANEOUS LEISHMANIA PARASITE DIAGNOSIS USING MICROSCOPIC IMAGES

Ph.D. THESIS

ALI MANSOUR ABDELMULA

Nicosia

June - 2025

NEAR EAST UNIVERSITY

INSTITUTE OF GRADUATE STUDIES

DEPARTMENT OF MEDICAL MICROBIOLOGY AND CLINICAL MICROBIOLOGY

ASSESSMENT OF DEEP LEARNING MODELS FOR CUTANEOUS LEISHMANIA PARASITE DIAGNOSIS USING MICROSCOPIC IMAGES

Ph.D. THESIS

ALI MANSOUR ABDELMULA

Supervisor

Prof. Dr. Hüseyin Kaya Süer

Co-Advisor

Assist. Prof. Dr. Omid MIRZAEI

Nicosia

June - 2025

Approval

We certify that we have read the thesis submitted by **ALI MANSOUR ABDELMULA** titled "**Assessment of Deep Learning Models for Cutaneous Leishmania Parasite Diagnosis Using Microscopic Images**" and that in our combined opinion it is fully adequate, in scope and in quality, as a thesis for the degree of doctoral of Medicin.

Examining Committee:	**Signature**
Head of the Committee:	
PROF. DR. Emrah Ruh	.....
Committee Member:	
Assoc. Prof. Dr. Hakan Evren	.....
Prof. Dr. Meryem Güvenir	.....
Assoc. Prof. Dr. Ayşe Arikan Sarioğlu	.....
Prof. Dr. Hüseyin Kaya Süer	.....

Approved by the Head of the Department 04./06./2025

Prof. Dr. Emrah Ruh .....

Approved by Head of the Institute of Graduate Studies:

.../.../2025

Prof. Dr. Kemal Hüsnü Can Başer .....

Declaration

I hereby declare that all information, documents, analyses, and results presented in this thesis have been collected and reported in accordance with the ethical guidelines established by the Ethical Committee at Emhammed Almgarif Health Center, Al-Murqub district, which approved the research (Reference No: EMHC. REF. 22.08.1063, dated 5 August 2022), and the ethical standards of the Institute of Graduate Studies, Near East University. I further affirm that all sources of information and data not original to this study have been properly cited and referenced in full compliance with academic integrity and ethical research conduct.

Ali Mansour Abdelmula

23/05/2025

Acknowledgments

This dissertation would not have been possible without the support and contributions of many individuals to whom I am deeply grateful.

First, I would like to express my sincere appreciation to the faculty and staff of the Near East University Graduate School for their continued support and dedication to my academic journey. I am especially thankful to my Primary Investigator, Prof. Dr. Kaya Süer, for his invaluable wisdom, guidance, encouragement, and unwavering support throughout the course of this project, as well as to the entire staff of the Near East Hospital Laboratory for their assistance and collaboration.

I would also like to extend my gratitude to the esteemed members of my PhD dissertation committee. Assist. Prof. Dr. Omid Mirzaei provided vital guidance and reassurance in my research on the *Assessment of Deep Learning Models for Cutaneous Leishmania Parasite Diagnosis Using Microscopic Images*. His support in the areas of statistical modeling and machine learning has been particularly instrumental. I am equally thankful to Assist. Prof. Dr. Emrah Güler for his important contributions and support in advancing my work on cutaneous leishmaniasis diagnosis.

My heartfelt thanks also go to Prof. Dr. Emrah Ruh, Head of the Department of Medical Microbiology and Clinical Microbiology, for his leadership and support, as well as to all the instructors in our department at Near East University who have guided me throughout my academic journey. As well as, I am deeply grateful to Prof. Dr. Nedim Çakır, whose expertise and mentorship helped me find a strong sense of community and direction in this field. His experience and support have played a meaningful role in the completion of this work.

Above all, I am profoundly grateful to my family for their unwavering love and support throughout my journey in this program. My parents and my wife have stood by me unconditionally, through every moment and challenge, and I am deeply thankful for their presence in my life. I love them dearly. I also extend my heartfelt appreciation to my brothers, sisters, uncles, aunts, cousins, and grandparents, whose constant encouragement has been a source of strength. Their support has truly been a blessing.

Dedication

I dedicate this thesis to my parents and wife, who taught me the value of hard work and education. Your unwavering support made this journey possible.

Özet

Kutanöz leishmaniasis (KL), ciltte çoğunlukla ülseratif yapıda lezyonların oluşmasıyla karakterize edilen yaygın bir paraziter hastalıktır ve genellikle vücudun açık bölgelerinde görülür. Her ne kadar esasen tropikal bölgelerde endemik olsa da, son yıllarda bu ihmal edilen tropikal hastalığın (İTH) Kuzey Afrika'nın özellikle Libya kıyılarında görülme sıklığında dikkat çekici bir artış yaşanmıştır. Bu artışın sebeplerinden biri, 2011'deki çatışmalar ve sonrasında yaşanan siyasi istikrarsızlık dönemlerinde sağlık altyapısındaki gerileme ve hükümetin kayıtsızlığı olabilir. Bu çalışma, enfeksiyonun farklı evrelerinde Leishmania amastigotlarının tespitine yönelik alternatif tanı yöntemlerini evrişimli sinir ağları (CNN'ler) kullanarak değerlendirmeyi amaçlamaktadır. Ayrıca, beş farklı önceden eğitilmiş derin öğrenme modelinin sınıflandırma görevlerindeki etkinliği karşılaştırmalı olarak analiz edilmiştir. Araştırma, kutanöz leishmaniasis ile enfekte bireylerden elde edilen ultra ince cilt yayma görüntülerinden oluşan bir veri kümesi kullanarak çeşitli sınıflandırma modellerini değerlendirmeye odaklanmıştır. EfficientNetB0, DenseNet201, ResNet101, MobileNetV2 ve Xception olmak üzere çeşitli önceden eğitilmiş derin öğrenme modelleri, kutanöz leishmaniasis tanısı için uygulanmıştır. Modellerin farklı veri alt kategorilerindeki performanslarının güvenilirliğini ve sağlamlığını doğrulamak amacıyla beş katlı çapraz doğrulama stratejisi kullanılmıştır. Farklı modellerin kapsamlı değerlendirme ve karşılaştırılması sonucunda, yaklaşık %99,15 doğruluk oranına ulaşan DenseNet-201 en yüksek başarıyı göstermiştir. Bunu yaklaşık %99,07 doğrulukla EfficientNet-B0 modeli takip etmiştir. Her iki model de diğerlerine kıyasla olağanüstü sınıflandırma performansı sergilemiştir.

Xception ve MobileNet-V2 orta düzeyde sonuçlar elde ederken, ResNet-101 yaklaşık %98,52 ile en düşük doğruluğu göstermiştir. Model performanslarını değerlendirmek için kullanılan bir diğer ölçüt ise F1 skoru olmuştur. Test edilen mimariler arasında, yaklaşık %99,1 F1 skoru ile en yüksek performansı DenseNet-201 göstermiştir. Bunu yine yaklaşık %99,1 ile EfficientNet-B0 takip etmiştir. MobileNet-V2 yaklaşık %98,7 ile biraz daha düşük performans göstermiş, onu yaklaşık %98,5 ile ResNet-101 izlemiştir. Buna karşın, Xception modeli yaklaşık %98,3 ile değerlendirilen modeller arasında en düşük performansı sergilemiştir. Ayrıca, Grad-CAM yöntemiyle oluşturulan ısı haritası, modelin pozitif bir sonuç tahmin ederken odaklandığı bölgeleri vurgulayarak pozitif tanıya katkı sağlayan kilit özellikleri ortaya koymuştur. Ek olarak, tüm modeller pozitif ve negatif vakaları ayırt etmede güçlü bir performans göstermiştir; bu durum, modellerin AUC değerleri ile de desteklenmiştir.

Anahtar Kelimeler: kutanöz leishmaniasis; amastigot evresi; CNN'ler; derin öğrenme.

Abstract

Cutaneous leishmaniasis (CL) is a prevalent parasitic disease characterized by the development of skin lesions, predominantly ulcerative in nature, on exposed areas of the body. Although it is primarily endemic to tropical regions, recent years have witnessed a notable increase in the incidence of this neglected tropical disease (NTD) along the northern coast of Africa, particularly in Libya. The decline in healthcare infrastructure and the government's apathy during the 2011 conflict and the ensuing periods of instability in politics may be partially responsible for this increase. The present study aimed to evaluate alternative diagnostic methodologies for the detection of Leishmania amastigotes at various stages of infection through the application of convolutional neural networks (CNNs). Furthermore, conduct a comparative analysis of the effectiveness of these five pre-trained deep learning models for classification tasks. The research also focused on evaluating various classification models using a dataset of ultra-thin skin smear images from individuals infected with cutaneous leishmaniasis. Several pre-trained deep learning models, EfficientNetB0, DenseNet201, ResNet101, MobileNetV2, and Xception are applied to the task of diagnosing cutaneous leishmaniasis. To confirm the reliability and strength of the model performances across different subcategories of the dataset, a five-fold cross-validation strategy is employed. Following a thorough analysis and comparison of the various models, DenseNet-201 developed as the highest performer, achieving an accuracy of approximately 99.15%. It was closely followed by EfficientNet-B0, which accomplished an accuracy of around 99.07%. Both models demonstrated exceptional classification performance compared to the others. Xception and MobileNet-V2 carried moderate results, while ResNet-101 showed the lowest accuracy at

approximately 98.52%. The other evaluation metric used to quantity performance of the model was the F1 score. Among the tested architectures, DenseNet-201 appeared as the maximum performer, achieving the highest F1 score of nearly 99.1%, indicating higher effectiveness. Close behind was EfficientNet-B0, which also achieved roughly 99.1%. MobileNet-V2 demonstrated slightly lower performance with about 98.7%, followed by ResNet-101 at approximately 98.5%. In contrast, the Xception model recorded the lowest performance among the evaluated models with around 98.3%. Moreover, Grad-CAM generated a heatmap that highlights the regions the model focused on when predicting a positive outcome, revealing key features that contributed to the positive diagnosis. Additionally, all models demonstrated strong performance in differentiating between positive and negative cases, as indicated by their respective AUC values.

Keywords: cutaneous leishmaniasis; amastigotes stage; CNNs; deep learning

Table Of Contents

Chapter III

Chapter IV

List of Figures

List of Tables

List of Abbreviation

CL:	Cutaneous Leishmaniasis
VL:	Visceral Leishmaniasis
MCL:	Mucocutaneous Leishmaniasis
DCL:	Diffuse Cutaneous Leishmaniasis
ACL:	Atypical Cutaneous Leishmaniasis
OWCL:	Old World Cutaneous Leishmaniasis
ZCL:	Zoonotic Cutaneous leishmaniasis
DNA:	Deoxynucleic Acid
M-CSF:	Macrophage Colony-Stimulating Factor
HIV:	Human Immunodeficiency Virus
TNF-α:	Tumor Necrosis Factor-Alfa
ELISA:	Enzyme-Linked Immunosorbent Assay
MALDI-TOF:	Matrix-Assisted Laser Desorption Ionization Time-of-Flight
PCR:	Polymerase Chine Reaction
PCR-RFLP:	"Polymerase Chain Reaction-Restriction Fragment Length Polymorphism"
PCR-HRM:	"Polymerase Chine Reaction-High Resolution Melting"
IIF:	Indirect Immunofluorescence Test
IFAT:	Immunofluorescence Antibody Test
DAT:	Direct Antiglobulin Test
rk39- ICT:	rK39 rapid immunochromatographic test (ICT)
MLEE:	Multilocus Enzyme Electrophoresis
MSLT:	Multiple Sleep Latency Test
LAMP:	Loop-mediated isothermal amplification
AI:	Artificial Intelligence

ANN:	Artificial Neural Networks
SML:	Supervised Machine Learning
CNN:	Convolution Neural Network
PPV:	Positive Predictive Value
NPV:	Negative Predictive Value
AUC:	Area Under Curve
ROC:	Receiver Operating Characteristic
Grad-CAM:	Gradient-Weighted Class Activation Mapping
MCC:	Matthew's Correlation Coefficient
SOTA:	Transferring State-of-the-Art
CT:	Computed Tomography
MRI:	Magnetic Resonance Imaging
ReLU:	Rectified Linear Unit
LRN:	Local Response Normalization
PCA:	Principal Component Analysis
SVM:	Support Vector Machines
KNN:	K-Nearest Neighbors
RF:	Random Forest
CDC:	"Centers for Disease Control and Prevention"
FDA:	"Food And Drug Administration"
BCE:	Before Common Era
WHO:	World Health Organization
NCBI:	the National Center for Biotechnology Information

Chapter I

1 Introduction

1.1 Background

The genus Leishmania contains obligatory intracellular digenetic parasites called leishmaniases, which cause serious zoonotic and anthroponotic illnesses that are major public health concerns worldwide(Al Jawaldeh, Osman, Tawfik, & Organization, 2014). Excluding Oceania, every continent is affected by this neglected tropical disease, which impacts nearly a hundred countries across Asia, Latin America, southern Europe, and northeastern Africa(Alvar et al., 2012). The most common form, cutaneous leishmaniasis (CL), is a neglected tropical and subtropical skin condition of significant public health concern. It is characterized by skin lesions that may lead to blistering, permanent scarring, disfigurement, and social stigma(Gabriel et al., 2019; Hay & Asiedu, 2018). The disease is transmitted through the bites of infected sand flies *Phlebotomus* species in the Old World and *Lutzomyia* species in the New World—which carry the parasites responsible for causing either cutaneous or visceral forms of leishmaniasis in humans and other vertebrates(Roque & Jansen, 2014).

The World Health Organization (WHO) reports that there are more than 20 different species of Leishmania in the world. The Leishmania species *L. tropica, L. major,* and *L. aethiopica*, which are exclusively found in the Old World, as well as *L. mexicana, L. amazonensis, L. venezuelensis, L. braziliensis, L. shawi, L. guyanensis, L. panamensis,* and *L. peruviana*, which are only found in the New World, all cause CL in humans (Espinosa, Serrano, Camargo, Teixeira, & Shaw, 2018; Roque & Jansen, 2014). Leishmaniasis is categorized into three types: cutaneous, mucocutaneous, and visceral leishmaniasis based on the causal agent and

clinical presentation. The local ulcer or nodules is the most typical clinical manifestation of CL.

The disease currently affects 12 to 15 million individuals, and 350 million people worldwide are at risk of contracting it. An estimated 70,000 people are killed and 1.5 to 2 million new cases are reported each year.(Markell, John, & Krotoski, 1999) (Torres-Guerrero, Quintanilla-Cedillo, Ruiz-Esmenjaud, & Arenas, 2017). An estimated 2.4 million "disability-adjusted life years (DALYs)" are lost due to leishmaniasis, 1.0 to 1.5 million new cases of CL occur year, and a sizable population is at risk in endemic places, according to a World Health Organisation report(Gabriel et al., 2019; Volpedo et al., 2021).

The course of CL and its clinical consequences are significantly influenced by the immune system's response to the parasite that causes it(Hawash, Ismail, Abdel-Wahab, & Khalifa, 2018). An important cytokine implicated in inducing apoptosis is interferon gamma. Nitric oxide, a powerful mediator involved in killing Leishmania both intracellularly and extracellularly, is produced by activated macrophages(Kak, Raza, & Tiwari, 2018). M1 macrophages exhibit increased nitric oxide levels and nitric oxide synthase expression, which prevents parasite development. Disease development is linked to Th2 cells' production of IL-4, IL-13, IL-10, TGF-, and macrophage colony-stimulating factor (M-CSF), which raises arginase 1 activity and polyamine synthesis and promotes parasite proliferation(Aoki et al., 2019; N. Wang, Liang, & Zen, 2014).

The disease presents a wide array of clinical symptoms, making it challenging to accurately diagnose both recent and past infections and to identify the specific etiological agent. For example, cutaneous leishmaniasis lesions can vary greatly in size, appearance, duration, and

tendency for spontaneous healing(Romero, de Farias Guerra, Paes, & Macêdo, 2001). The leishmanial parasite is commonly detected in skin smears or biopsy samples through direct microscopy, a method that often lacks sufficient sensitivity and specificity(Juliana Quero Reimão, Coser, Lee, & Coelho, 2020). Identifying the causative agent and accurately determining the species responsible for the disease's clinical manifestations remain significant challenges with current laboratory diagnostic techniques. Light microscope examination of skin smears or histopathological subsections, in vitro culture, antigen identification assays, and molecular diagnostics based on DNA detection and amplification are examples of common diagnostic techniques(Aronson et al., 2016).

Leishmaniasis is typically diagnosed using parasitological techniques that rely on seeing Leishmania amastigote formations in clinical specimens(Srivastava, Dayama, Mehrotra, & Sundar, 2011). When evaluating stained lesion samples (obtained by excision, punch biopsy, scrape, smear, or imprinting) for cutaneous leishmaniasis (CL), light microscopy shows a sensitivity of 50–70% for identifying Leishmania species from Africa, Asia, and Europe. However, for Leishmania species that are found in the Americas, its sensitivity decreases to 15–30%(Carmen Maria Sandoval Pacheco et al., 2018). A portion of the biopsied tissue can be utilized for implantation in a growth media as an alternative to enhancing sensitivity by direct inspection, albeit this is rarely done in ordinary clinical practice. For the molecular approaches of confirming Leishmania illness and species confirmation, isolation followed by in vitro cultivation is helpful(Juliana Quero Reimão et al., 2020).

In particular for CL-causing species that may be caused by many parasite species, PCR-based assays are strongly advised for species typing. For instance, at least seven genera have been linked to CL in Brazil. The benefits of employing PCR-based techniques are generally its applicability, safety, and dependability in a representative laboratory(Thakur, Joshi, & Kaur, 2020).

An other technique for identifying single-celled organisms, including both prokaryotes and eukaryotes, is matrix-assisted laser desorption ionisation time-of-flight (MALDI-TOF) mass spectrometry(Seng et al., 2010; Van Veen, Claas, & Kuijper, 2010). This strategy was then enhanced by creating a standard mass-spectral library for Leishmania identity containing 33 species of 10 structures, which was subsequently examined with a panel of 268 separate samples from various origins (Lachaud et al., 2017).

CL skin lesions frequently heal on their own, but occasionally they need to be treated. In many regions of the world, pentavalent antimonial medicines continue to be the mainstay of care(Copeland & Aronson, 2015). According to the accepted practices, doctors treat CL by applying liquid nitrogen during cryotherapy or by locally injecting sodium stibogluconate. Over the past 20 years, intra-lesional has been used as the first-line treatment for CL. According to estimates, 10 IL-SSG injections administered once a week are often necessary for healing(Silva et al., 2021; Siriwardana, Deepachandi, Gunasekara, Warnasooriya, & Karunaweera, 2019). In many countries around the world, SSG is the basis of leishmaniasis management(Cordeiro, de Andrade Júnior, & de Oliveira, 2019).

Artificial intelligence (AI) principles have enormous potential for a wide range of applications, including risk modeling and classification,

self-detection, diagnostics, including the classification of small molecules into illness subgroups, and the prediction of treatment response and prognosis. AI is increasingly being used in medical and biological research as well as therapeutic treatment(Ong et al., 2023; Rajkomar, Dean, & Kohane, 2019). Several preclinical and clinical studies on healthcare have been conducted recently using supervised machine learning (SML) and various AI technologies. In terms of e-health care, particularly the accurate identification and classification of diseases, SML has changed almost every industry internationally. For many aspects of healthcare, multiple university and industry labs are creating AI technologies(A. Kumar, Gadag, & Nayak, 2020). There are numerous applications based on medical imaging investigations, including the identification and diagnosis of squamous cell carcinoma(Cao, Song, & Zhao, 2019), lung diseases(Gunjan, Singh, Shaik, & Roy, 2022). Medical image analysis has recently benefited greatly from deep learning applications(Niu, Gu, Zhao, & Lu, 2021).

Convolutional neural networks (CNN) have produced exceptional classification and segmentation results for images. Clinical prediction frameworks have been developed and significant linkages explained thanks to the application of data analysis, machine learning, and deep learning algorithms in modern healthcare(Mabrouk, Diaz Redondo, Dahou, Abd Elaziz, & Kayed, 2022; Öztürk, 2022). CNN is a deep training algorithm that primarily focuses on object and image classification algorithms(Uppamma & Bhattacharya, 2023). The first layer of a convolutional neural network is composed of the convolutional layer and the pooling layer together, while the final layer is the fully connected layer(Vaz & Balaji, 2021). The density between these layers can be scaled up to capture more fine detail, but doing so will require more computer

power depending on the complexity of the images(Guo, Li, Sun, Li, & Wang, 2022; Li, Liu, & Chan, 2014). The foundational component of CNN is where the majority of computations take place. After the first conversion layer, there could be a second conversion layer. During the convolution process, a kernel or filter within this particular layer shifts throughout the image's receptive fields to assess whether a characteristic is present(Gu et al., 2018; Salehi et al., 2023). The input parameter count is decreased by the pooling layer, but some data are also lost as a result. Positively, this layer streamlines operations and increases the CNN's effectiveness(Modarres, Astorga, Droguett, & Meruane, 2018). Complete connection refers to the connection of all inputs or nodes from one layer to each activated unit or cluster from the following layer(Melville, Alguri, Deemer, & Harley, 2018).

1.2 **Aim of study**

The aim of this study is to evaluate alternative diagnostic methods for detecting cutaneous leishmaniasis parasites by utilizing a convolutional neural network (CNN) model. This approach seeks to address the limitations of traditional diagnostic techniques, which are often slow, costly, and disposed to inaccuracy due to variations in species and sizes. The study aims to improve detection efficiency, accuracy, and treatment orientation in complex scenarios where expert knowledge is required.

- One of the key achievements of this study was the implementation of pre-trained models (MobileNet-v2, ResNet101, EfficientNet-B0, DenseNet201, and Xception) for classifying microscopic images as either positive or negative.

- The performance of these models evaluated using various metrics such as accuracy, sensitivity, specificity, precision, F1-Score, Cohen's kappa, Area Under the Curve (AUC), Matthew's Correlation Coefficient (MCC), Receiver Operating Characteristic (ROC) curve, and Negative Predictive Value.
- The main objective of this investigation was to assess and compare the effectiveness of these five different pre-trained deep learning models in the context of classification tasks.

1.3 **Significant of study**

Despite the recent advances in diagnostic tools, diagnosing leishmaniases still imposes substantial challenges in the remote areas of endemic countries around the globe. Moreover, due to its complex transmission cycle, involving the various biological entities, identifying the responsible Leishmania species is crucial in disease control and interventions(Chambers, 2011). Early and accurate detection as well as improving patients' outcomes also provides imperative data for eco-epidemiological studies to monitor and assess the outbreak and evaluate current control measures that are in place in endemic regions(Vink et al., 2018). A diagnosis of leishmaniases is often made by evaluating the clinical manifestations of the disease in the patient(Ahyun Hong, Zampieri, Shaw, Floeter-Winter, & Laranjeira-Silva, 2020). The creation and application of artificial intelligence techniques in pathology services has significantly increased over the last ten years. It is expected that this trend would continue, possibly revolutionising the field soon. A paradigm change has occurred with the combination of AI and computational pathology technologies, which has improved the flexibility and efficiency of pathology services to meet the needs of precision medicine.

Nevertheless, despite AI models' encouraging performance, their transfer from research to actual clinical practice has been slow. The gap between discrete scientific endeavours and real-world therapeutic application is still wide and frequently disregarded.(Rakha et al., 2021). Therefore, the primary motivation of this work is to support pathologists in making microscopic analysis more efficient, reproducible, and accurate through automated evaluation procedures.

1.4 Barriers to Research Advancement

Several interdisciplinary articles were created throughout this initiative and independently verified by a peer-review procedure. The goal of these projects is the same: to improve the health of people and animals by integrating cutting-edge research into clinical practice to enable faster and more accurate diagnosis. The code and, where possible, the data-associated with each publication have been made publicly available in order to encourage repeatability and real-world application.

1.5 Limitation of study

The requirement for big datasets in deep learning, especially ones that include a broad range of cases, including different demographics, illness stages, hardware configurations, and imaging techniques, is one of the primary issues covered in this dissertation. It is much more challenging to obtain such data in medical imaging than in domains such as computer vision and optical photography. Consequently, one of the main obstacles to using deep learning for medical picture reconstruction is the scarcity of training data. The problem of incomplete and inadequate data in this setting is the main topic of this research.

Chapter II

2 Literature Review

2.1 Introduction

Leishmaniasis is a vector-borne disease caused by flagellated protozoa belonging to the genus Leishmani s prevalent in tropical and subtropical regions and occurs in 98 countries worldwide (Alvar et al., 2012). Leishmaniasis is a disease caused by protozoan parasites of the genus Leishmania, typically transmitted through the bite of infected sandflies. Archaeologically, it has been predominant in tropical and subtropical regions across Europe, Africa, Asia, and the Americas. In humans, Leishmania parasites duplicate within host cells and generally manifest as either visceral or cutaneous forms of the disease(Maxfield & Crane, 2024). Leishmaniasis has incredible historical significance, with documented disease thousands of years before Common Era (BCE) (C. M. Sandoval Pacheco et al., 2018). An analysis of ancient Egyptian and Christian Nubian mummies dating from 3500 to 2800 BCE exposed successful amplification of *Leishmania donovani* DNA. The disease is believed to have been announced into Egypt during the Middle Kingdom period, a time noticeable by increased occupation and military activity with Nubia (modern-day Sudan). Notably, DNA evidence of leishmaniasis is absent in earlier samples, supporting the idea of a later introduction. Additionally, some sources suggest that Sudan may have been the original of visceral leishmaniasis (VL)(Zink et al., 2006). Additionally, The Ebers Papyrus, a medical manuscript dating back to 1500 BC, described a skin condition believed to be cutaneous leishmaniasis, then referred to as the "Nile Pimple." Reflecting the ancient understanding of disease, an early form of vaccination was practiced in the Middle East and Central Asia.

This complicated collecting exudate from active lesions and inoculating it into the bottoms of children in an attempt to boost immunity(Akhoundi et al., 2017).

2.2 Leishmaniases Epidemiology

2.2.1 Definition

Leishmaniasis is a disease produced by protozoan parasites of the genus Leishmania, most commonly conducted through the bite of infected sandflies. Historically, it has been prevalent in tropical regions across several continents, including Europe, Africa, Asia, and the Americas. In humans, Leishmania parasites replicate intracellularly and characteristically manifest as either visceral or cutaneous forms of the illness(Maxfield & Crane, 2024).

2.2.2 Structure of leishmania

Leishmania species are unicellular eukaryotes characterized by a distinct nucleus and various organelles, including kinetoplasts and flagella. Throughout their life cycle, they different between two structural forms(Pulvertaft & Hoyle, 1960).

The amastigote form is found within the mononuclear phagocytes and circulatory system of humans. It is an intracellular, nonmotile form that lacks external flagella. Instead, a short flagellum is embedded at the anterior end but does not extend outward. The organism is oval-shaped, measuring approximately 3–6 μm in length and 1–3 μm in width. The kinetoplast and basal body are located near the anterior end. In contrast, the promastigote form is present in the alimentary tract of sandflies. It is an extracellular, motile form, significantly larger and more elongated than the amastigote. Its dimensions are roughly 5 μm in width and 15 to 30 μm

in length. This morphology resembles a spindle, narrowing at both ends, and contains a long anterior flagellum that is roughly the same length as the organism itself and reaches beyond the body. The kinetoplast and basal body are situated in the anterior end, ahead of the nucleus, which is positioned in the centre.

(https://www.ndvsu.org/images/StudyMaterials/Parasitology/Leishmaniosis.pdf).

Figure 1

Cellular Structures of Leishmania, Specifically Comparing the Promastigote and Amastigote Forms

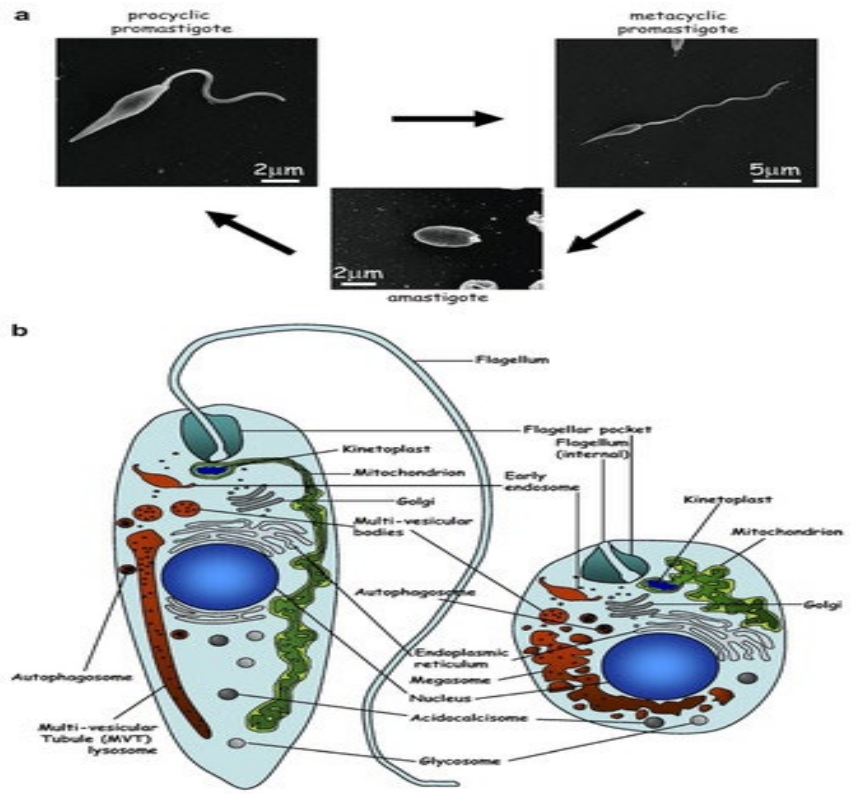

Source: (Besteiro, Williams, Coombs, & Mottram, 2007)

2.2.3 Taxonomy of leishmania

Taxonomy, originating from the Ancient Greek word's "taxis" ("arrangement") and "nomia" ("method"), is the scientific field dedicated to the naming, defining, and classification of biological organisms based on shared characteristics. These organisms are grouped into categories known as taxa (singular: taxon), each occupying a specific level within a taxonomic hierarchy. This hierarchical structure allows taxa at lower levels to be grouped into increasingly broader categories at higher levels. Accordingly, the classification of the leishmania organism, as outlined by the National Center for Biotechnology Information (NCBI), can be represented in the following table.

Table 1.

Displays A Comprehensive List of Various Species and Strains Within the Genus Leishmania, Including Known Hybrids, Species Complexes, And Laboratory Strains.

Scientific classification	
Domain	Eukaryota
Kingdom	Protista
Subkingdom	Protozoa
Phylum	Sarcomastigophora or Euglenozoa
Subphylum	Mastigophora
Class	Zoomastigophora
Order	Kinetoplastida
Family	Trypanosomatidae
Genus	leishmania
Species	*Leishmania aethiopica species complex* *Leishmania aethiopica* *Leishmania aethiopica L147* *Leishmania aethiopica x Leishmania donovani*

Leishmania aethiopica x Leishmania tropica

Leishmania aristidesi

Leishmania deanei

Leishmania donovani species complex

Leishmania chagasi

Leishmania donovani

Leishmania donovani archibaldi

Leishmania donovani BPK282A1

Leishmania donovani donovani

Leishmania donovani Ld 2001

Leishmania donovani Ld 39

Leishmania donovani complex GRE 1 dog

Leishmania donovani complex GRE 1 hare

Leishmania donovani complex GRE 2 dog

Leishmania donovani complex GRE 2 hare

Leishmania donovani complex GRE 3 dog

Leishmania donovani complex GRE 3 hare

Leishmania donovani complex GRE 4 hare

Leishmania donovani complex GRE 5 hare

Leishmania donovani complex GRE 6 hare

Leishmania donovani complex GRE 7 hare

Leishmania donovani complex Yangquan

Leishmania infantum

Leishmania infantum JPCM5

Leishmania donovani complex sp.

Leishmania donovani complex sp. CR-2013

Leishmania donovani complex sp. DYL-

Leishmania donovani complex sp. KA-2011

Leishmania donovani complex sp. KP-2013

Leishmania hertigi

Leishmania cf. infantum/mexicana

Leishmania major species complex
Leishmania major
Leishmania major strain Friedlin
Leishmania major strain LV39c5
Leishmania major strain SD 75.1
Leishmania cf. major
Leishmania major x Leishmania donovani
Leishmania major x Leishmania infantum
Leishmania martiniquensis
Leishmania mexicana species complex
Leishmania amazonensis
Leishmania mexicana
Leishmania mexicana mexicana
Leishmania mexicana
MHOM/GT/2001/U1103
Leishmania mexicana venezuelensis
Leishmania pifanoi
Leishmania mexicana complex sp.
Leishmania tropica species complex
Leishmania tropica
Leishmania tropica L590
Leishmania tropica complex sp.
Leishmania tropica complex sp. CR-2013
Leishmania (Leishmania) sp

"Source: (https://www.ncbi.nlm.nih.gov/datasets)"

2.2.4 Etiologic agent

Leishmaniasis is a disease caused by a protozoan belonging to the family *Trypanosomatidae*, order *Kinetoplastida*, and genus *Leishmania*. It has two main developmental stages: the amastigote and the promastigote.

The amastigote stage resides within the lysosomal vacuoles of phagocytic cells, while the promastigote is an extracellular form that adheres to the microvilli of the insect vector. Transmission occurs via sandflies, which vary by region. In the Old World, the primary vectors are species from the genera *Phlebotomus* and *Sergentomyia*. In contrast, *Lutzomyia* species are chiefly responsible for spreading the disease in the New World (Claborn, 2010). Adult sandflies are tiny insects, measuring less than 3.5 mm in length about one-third the size of a small mosquito. Due to their vulnerability to dehydration, they thrive in humid environments, which influences the spread of the diseases they carry. These flies are nocturnal and spend the daytime hidden in burrows, under rocks, or in other sheltered spots. When at rest, they exhibit a distinctive "V" shape across their backs and have a noticeable thoracic hump that causes their head to tilt downward. Both male and female sandflies feed on plant juices for carbohydrates, but only females require a blood meal. It is during this blood feeding that the female can transmit protozoan parasites to a human host(Wijerathna & Gunathilaka, 2020).

2.2.5 Vector

Phlebotomines are small blood-feeding flies belonging to domestic *Psychodidae*. They are noteworthy public health concern due to their role as vectors of leishmania parasites and bartonella bacteria. The dense coating of hair on the thorax and wings, as well as the veined wings, make these insects easy to identify. Tropical and subtropical regions are home to the majority of the species in the *Phlebotominae* subfamily. While the group includes six genera, the most important genus in the Americas is *Lutzomyia*, as illustrated in Figure 2. These flies' range in size from 1.5 mm to 3.5 mm, are yellowish in color, and are covered in fine hairs across their entire body, including their wings. Both males and females feed on sugary plant substances and floral nectar to survive; however, only the

females are capable of transmitting diseases, as they require blood meals to develop their eggs(Rogers, Chance, & Bates, 2002).

Sand flies become active at sundown, continuing their activity through the early night hours and at dawn. During daylight, they remain hidden in sheltered places like cracks, tree hollows, landfills, sewers, and abandoned buildings. In the Mediterranean region, they are more active on warm nights with temperatures above 16 °C. Due to their small size, they cannot fly in strong winds exceeding 1 m/s, and rainfall also delays their flight. Despite their limited flying ability, they can travel distances of up to 2 kilometers. They are highly attracted to light, and higher humidity levels contribute to their increased survival(Merritt, Courtney, & Keiper, 2009) .Sandflies typically inhabit rural areas or urban spots with vegetation, such as gardens and parks. While they primarily bite outdoors, they can also live inside homes. They locate their hosts by detecting body odors carried by air currents. Phlebotomine sandflies are usually active from the first warm days of May until September or October. During the winter, they remain in the Quaternary larval stage. However, due to rising temperatures linked to climate change, their activity is increasing, making it possible to encounter active sandflies year-round in the Mediterranean basin(Dostálová & Volf, 2012).

Figure 2

Shows Sandfly, Particularly the Genus Phlebotomus, is a Small, Bloodsucking Insect Known for Its Role as A Vector for Leishmania Parasites, Which Cause Leishmaniasis

Source: (Wijerathna & Gunathilaka, 2020)

2.2.6 Reservoir

The parasite is naturally present in reservoirs, which are vertebrate animals that enable vectors to contract the infection and continue the cycle of transmission. Although each *Leishmania species* typically has a primary reservoir in a particular location, other local animals may also contract the disease and serve as incidental or secondary hosts. Although they may or may not exhibit outward signs, a variety of domestic and wild mammals, including rodents, edentates, marsupials, carnivores, and primates, can contract "Leishmania". Humans are the primary reservoir for some Old World Leishmani species, however both domestic and wild animals can act as reservoirs. In the Old World, this is true for both cutaneous leishmaniasis caused by "*L. tropica*" and visceral leishmaniasis caused by "*L. donovani*".(Shaw, Marinho-Júnior, Courtenay, & Brandão-Filho, 2023). In the Americas' New World, leishmaniasis primarily

presents as a zoonotic disease. Known reservoirs include marsupials (such as Didelphis spp.), Sloths (*Choloepus* spp. and *Bradypus* spp.), the silky anteater (*Tamandua tetradactyla*), the crab-eating fox (*Cerdocyon thous*), and various rodent species (including *Rattus* spp., *Proechimys* spp., *Nectomys* spp., and *Oryzomys* spp.) have been identified as potential hosts. Among domestic animals, the dog is considered the primary reservoir for *Leishmania infantum*, as illustrated in Figures 3 through 6(Roque & Jansen, 2014).

The interaction between reservoirs and parasites is intricate, multifaceted, context-dependent, and constantly evolving. As such, it forms a dynamic biological unit that can shift with environmental changes. Therefore, only animals that consistently ensure both the transmission and persistence of various *Leishmania* species in nature are classified as reservoirs. The mere detection of *Leishmania* infection in an animal does not, by itself, constitute adequate suggestion to identify it as a reservoir(Roque & Jansen, 2014).

Figure 3

The Opossum. (Didelphis Albiventris), a Species Within the Genus Didelphis, Is Commonly Found to Be Infected with Leishmania Spp

Source: (Smith, 2007)

Figure 4

Thrichomys Pachyurus, a Caviomorph Rodent Species, Is Considered a Potential Reservoir for Leishmania Spp

Source: *(Kassahun et al., 2015)*.

Figure 5

The Crab-Eating Fox, also Known as the Forest Fox (Cerdocyon Thous) in Portuguese, is the Wild Canid Species Most Commonly Infected with Leishmania Infantum

Figure 6

Domestic dog (Canis lupus familiaris) exhibiting skin lesions indicative of a possible Leishmania infantum infection

Source:*(Ataide, Tavares, Nicola, Pereira, & Ribeiro, 2012).*

2.3 Life cycle of *Leishmania spp*

Leishmaniasis is a vector-borne disease diffused by sandflies and caused by obligate intracellular protozoa of the genus leishmania. Approximately 21 of the 30 known mammal-infecting species can cause disease in humans. These include members of the *L. donovani* complex, *L. donovani*, *L. infantum*, and *L. chagasi* as well as species in the *L. mexicana* complex, such as *L. mexicana*, *L. amazonensis*, and *L. venezuelensis*. Other significant species include *L. tropica*, *L. major*, *L. aethiopica*, and members of the subgenus *Viannia*, which includes *L. braziliensis*, *L. guyanensis*, *L. panamensis*, and *L. peruviana*. Although these species are morphologically similar, they can be distinguished

through isoenzyme analysis, molecular techniques, or the use of monoclonal antibodies.

Figure 7

The Life Cycle of the Leishmania Parasite, Illustrating the Stages it Undergoes in both Sandflies and Humans

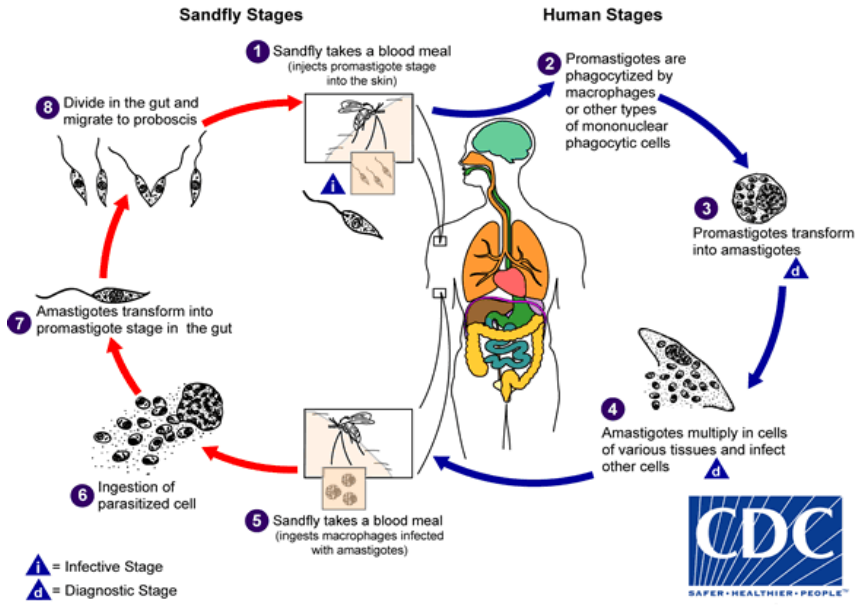

Source:(CDC, 2024).

Transmission to Humans: An infected female sandfly bite initiates the infection. Through the bite, the fly injects promastigotes a motile form of the Leishmania protozoa into the skin. Entry into Immune Cells: Subsequently, promastigotes are engulfed by macrophages, a type of immune cell, through phagocytosis. Transformation Inside Cells: Once inside, the promastigotes transform into the amastigote form. Multiplication in Tissues: Thereafter, amastigotes multiply within macrophages in various body tissues. Transmission to Flies: Eventually, when another sand fly bites an infected human or animal, it ingests blood containing macrophages filled with amastigotes. Transformation in the Fly Inside the fly, the ingested amastigotes transform back into

promastigotes. Maturation and Migration: Meanwhile, these promastigotes multiply, develop, and migrate to the fly's proboscis (mouthparts). Cycle Repeats; Consequently, the infected sand fly is now ready to transmit the parasite to another host during its next bite, thus continuing the cycle(Dostálová & Volf, 2012).

2.4 Distribution of leishmaniases in the world

Leishmaniasis-causing parasites are existing in 88 nations universal, mainly in regions of South and Central America, Africa, Asia, and southern Europe. Despite this widespread occurrence, over 90% of life-threatening cases are concentrated in just six countries: Brazil, Ethiopia, Sudan, South Sudan, India, and Bangladesh. While some explore has examined the disease's distribution within different countries, a comprehensive global indication of leishmaniasis distribution is still lacking(Pigott et al., 2014).

Figure 8

The Global Distribution of Leishmaniasis, Highlighting Areas Affected by The Disease. It Indicates That 12 million People Currently Infected with Leishmaniasis and 350 million People at Risk of Infection. Whereas Green Suggests Visceral Leishmaniasis, Red Suggests Cutaneous and Mucocutaneous Leishmaniasis, and Also Purple Suggests Visceral Combined with Cutaneous and Mucocutaneous Leishmaniasis

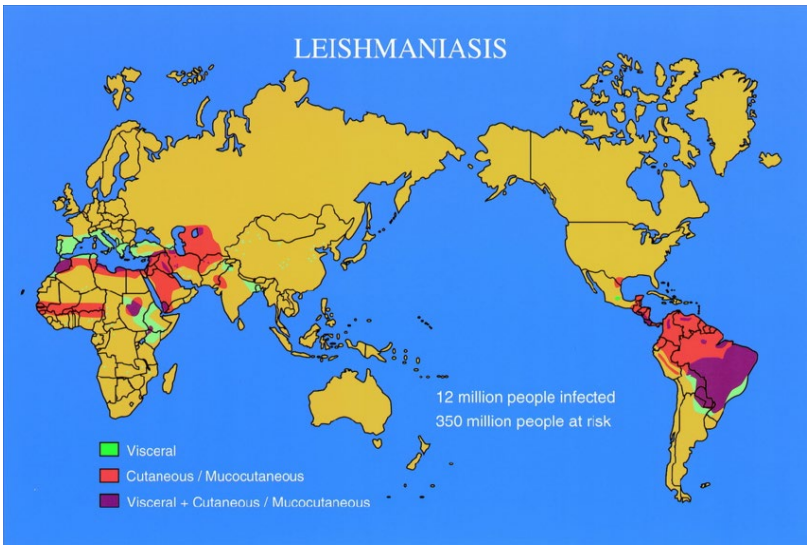

Source:(Bowles et al., 2015).

Pigott et al. aimed to produce detailed maps showing the distribution of leishmaniasis and the factors contributing to its spread. Similar methods had previously been applied to mapping dengue fever, another tropical disease. Using computer modelling, they generated these maps by analyzing environmental data from locations with confirmed leishmaniasis cases. The resulting distribution patterns will be explored later in relation to the various types of leishmaniasis.

2.5 Epidemiological aspects

Leishmaniasis is prevalent in 88 countries across tropical, subtropical, and temperate regions, putting over 350 million people at risk(Alvar et al., 2012). Approximately 12 million people are affected by leishmaniasis globally, with an estimated 0.2 to 0.4 million new cases of visceral leishmaniasis and 0.7 to 1.2 million new cases of cutaneous leishmaniasis reported each year(Murray, Berman, Davies, & Saravia, 2005). Poor nutrition, population displacement, subpar living circumstances, decreased immunity, and restricted access to basic resources are some of the reasons linked to the disease, which primarily affects

impoverished people in Africa, Asia, and Latin America(Alvar, Yactayo, & Bern, 2006). More than 90% of visceral leishmaniasis (VL) cases worldwide are concentrated in just six countries: Bangladesh, Brazil, Ethiopia, India, South Sudan, and Sudan(Alvar et al., 2012). Cutaneous leishmaniasis is widely distributed across the Americas, the Mediterranean basin, and western Asia. Ten countries, Afghanistan, Algeria, Brazil, Colombia, Costa Rica, Ethiopia, Iran, Peru, North Sudan, and Syria are account for approximately 75% of the global CL cases(Murray et al., 2005; Rostami, Saghafipour, & Vesali, 2013).

Infection is primarily caused by over 20 species of *Leishmania* parasites, which are transmitted by around 30 species of phlebotomine sand flies. In the Americas (New World), transmission is carried out by female sand flies of the genus *Lutzomyia*, while in other regions of the world (Old World), the genus *Phlebotomus* is responsible. These sand fly vectors are typically most active during the evening and nighttime hours, from dusk to dawn(Murray et al., 2005). Climate and other environmental changes could lead to an expansion of the geographic range of sand fly vectors, potentially increasing the regions of the world where leishmaniasis occurs(Sutherst, 2004). Leishmaniasis is typically transmitted through the bite of an infected female sand fly, which feeds on various mammalian reservoirs such as rodents, marsupials, edentates, monkeys, and wild or domestic canines. In endemic regions, humans become infected incidentally(Quinnell & Courtenay, 2009). VL can also be transmitted through intravenous drug use, blood transfusions, organ transplants, congenital infection, and laboratory accidents, though these routes of transmission are considered relatively rare(Dey & Singh, 2006).

Anthroponotic transmission is a key feature of the *L. tropica* complex (Old World) and the *L. donovani* complex, particularly in the Indian subcontinent(Bern, Maguire, & Alvar, 2008). *L. donovani* is present in South Asia-specifically in India, Bangladesh, and Nepal-as well as in East

African countries such as Sudan, Ethiopia, Kenya, and Somalia. In areas where the disease is primarily spread from person to person "anthroponotic transmission", promptly and effectively treating infected individuals can aid in limiting the parasite's spread. The clinical manifestation of the disease can occur in people of any age. However, in regions where transmission remains consistently high, older individuals may experience lower incidence rates due to immunity developed over time (Bern et al., 2006). In East Africa, *L. donovani* is linked to both anthroponotic and zoonotic forms of transmission(Dereure et al., 2003).

On the contrary, *L. infantum* (synonym to *L. chagasi*) occurs in the Mediterranean, the Middle East, Afghanistan, Iran, Pakistan and Brazil, although sporadic cases have been reported in Central Asia, China, Mexico and Central and Latin America(Ready, 2010). Notably, children and immunosuppressed adults are at higher risk of clinical disease due to *L. infantum* than immunocompetent adults(Van Griensven, Carrillo, López-Vélez, Lynen, & Moreno, 2014). Transmission of *L. infantum* infection is considered predominantly zoonotic, with domestic dog being the major reservoir(Chitimia et al., 2011; Ready, 2010).

L. infantum is a latent public health threat, as evidenced by the high frequency of asymptomatic human carriers in southern Europe. Although the majority of immunocompetent people won't experience any symptoms following this parasite infection, clinically serious illness could arise as a result of possible immunosuppression or acquired immunosuppression (Michel, Pomares, Ferrua, & Marty, 2011; Om Prakash Singh, Hasker, Sacks, Boelaert, & Sundar, 2014). In this context, an increase of co-infections with human immunodeficiency virus (HIV) and Leishmania has been observed during the last 30 years(Jarvis & Lockwood, 2013). Cases of co-infection have been reported in the Mediterranean region, mainly in

France, Italy, Portugal and Spain. Moreover, VL is an emerging condition affecting HIV-infected patients living in many Asian (especially India) and African countries as well as in Latin America, particularly in Brazil(Alvar et al., 2008). The fields of transplantation medicine, rheumatology, oncology, and hematology have identified the majority of non-HIV-related immunosuppressive disorders linked to VL development (Van Griensven et al., 2014). Numerous cases of VL following organ transplantation have been identified in the past 20 years as a result of the rising number of organ transplants and advancements in immunosuppressive therapies(Bouchekoua, Trabelsi, Abdallah, & Khaled, 2014). Furthermore, there have been more reports of leishmaniasis in individuals with autoimmune rheumatic disorders who reside in endemic locations since tumor necrosis factor-alfa (TNF-alfa) inhibition was introduced into clinical practice.(Guedes-Barbosa et al., 2013). Additionally, a number of cases have been documented in patients receiving treatment with other immunomodulatory medications, such as cyclosporine, methotrexate, azathioprine, and steroids (Bogdan, 2012; Erre, Mesina, Tonelli, & Passiu, 2010). Therefore, prior to receiving immunosuppressive medication, patients residing in or returning from leishmaniasis-endemic areas are advised to have a serological screening.

2.6 Classification of leishmania based on tissue tropisms

A significant role is played by tissue tropism in determining the clinical manifestations of leishmaniasis. Based on tissue tropism, leishmania can be classified into three main categories as shown in table 2.

Table 2.

Represented Tissue Tropism and Associated Leishmaniasis Forms

Tissue Tropism	Species	Clinical Forms
Skin	*L. tropica*, *L. major*, *L. mexicana*	Cutaneous leishmaniasis (CL)
Mucocutaneous tissues	*L. braziliensis*	Mucocutaneous leishmaniasis (MCL)
Internal organs	*L. donovani*, *L. infantum*	Visceral leishmaniasis (VL)
Diffuse skin	*L. amazonensis*, *L. aethiopica*	Diffuse cutaneous leishmaniasis (DCL)
Skin (non-ulcerated, chronic lesions)	*L. infantum.*	Atypical cutaneous leishmaniasis (ACL)

Source: (Ait Maatallah, Akarid, & Lemrani, 2022).

2.6.1 Cutaneous leishmaniasis

Cutaneous leishmaniasis is the most prevalent form of leishmaniasis in humans. It is a skin infection caused by a single-celled parasite from the Trypanosomatida group, which includes kinetoplastid organisms characterized by having a single flagellum. This infection is transmitted through the bite of a phlebotomine sand fly. Around thirty species of Leishmania are known to cause cutaneous leishmaniasis(James WD, 2006). This disease is generally classified as a zoonosis (an infectious disease naturally transmitted from animals to humans), except for *Leishmania tropica*, which is typically an anthroponotic disease (an infectious disease primarily transmitted from humans to vertebrate animals)(Ahyun Hong et al., 2020).

2.6.1.1 ***Etiology and Epidemiology of cutaneous leishmaniasis***

Four species *L. major, L. tropica, L. aethiopica, and L. infantum* are responsible for causing Old World Cutaneous Leishmaniasis (OWCL). *L. major* causes rural, wet, and zoonotic cutaneous leishmaniasis, with desert rodents serving as its animal reservoirs. This species is endemic to desert regions of northern Africa, Central Asia, the Sudan, and the Middle East, where in some communities, local prevalence can be as high as 100%. Travelers to these areas may also be at risk. *L. tropica* typically causes urban, dry, and often anthroponotic cutaneous leishmaniasis, where humans are the primary host and may even act as a reservoir in some regions, such as Afghanistan. A recent outbreak in Israel identified rock hyraxes as a reservoir. *L. tropica* is endemic in urban areas across the Mediterranean basin, Central Asia, and the Middle East. *L. aethiopica* is found mainly in the rural mountain regions of Ethiopia and Kenya, with hyraxes (distant relatives of elephants) as the animal reservoirs. *L. infantum* is found in the Mediterranean basin, China, Central Asia, and the Middle East. While adults infected with *L. infantum* usually experience a mild, self-limited cutaneous disease, infants may develop visceral disease. Domesticated and wild canines are the primary animal reservoirs(Mann et al., 2021).

Figure 9

The Distribution of Cutaneous Leishmaniasis Across the Americas, Divided into Two Sections. Section a Illustrates the Prevalence and Absence of Cutaneous Leishmaniasis in Central and South America. The Color Coding Indicates Complete Absence (Light Green), Indeterminate (Light Yellow) and Complete Presence (Dark Purple). Section B Provides a Broader View of the Same Region, Focusing on the Intensity of Presence. The Gradient from High (Dark Pink) to Low (Light Green) Signifies Varying Levels of Risk and Occurrence, Emphasizing Areas with Higher Prevalence

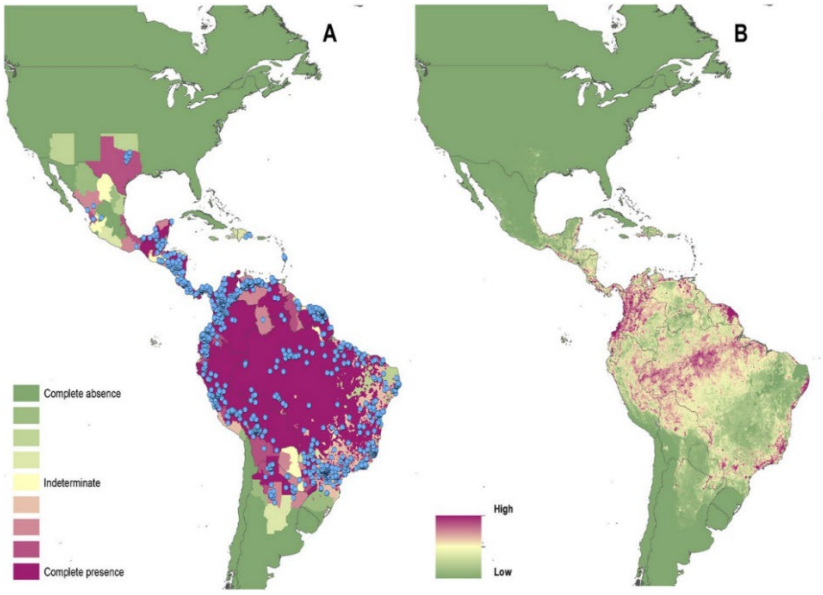

Source:(Pigott et al., 2014).

Figure 10

The Predicted Distribution of Cutaneous Leishmaniasis in The Old World is as Follows: (A) a Consensus Map Illustrating the Evidence for the Disease's Presence, Ranging from Green (Indicating Complete Consensus on Absence, −100%) to Purple (Representing Complete Consensus on Presence, +100%). Blue Spots Mark the Occurrence Points or Centroids of Occurrences Within Small Polygons, while (B) a Predicted Risk Map of Cutaneous Leishmaniasis, With Colour Shading from Green (Indicating Low Probability of Presence) to Purple (Signifying High Probability of Presence

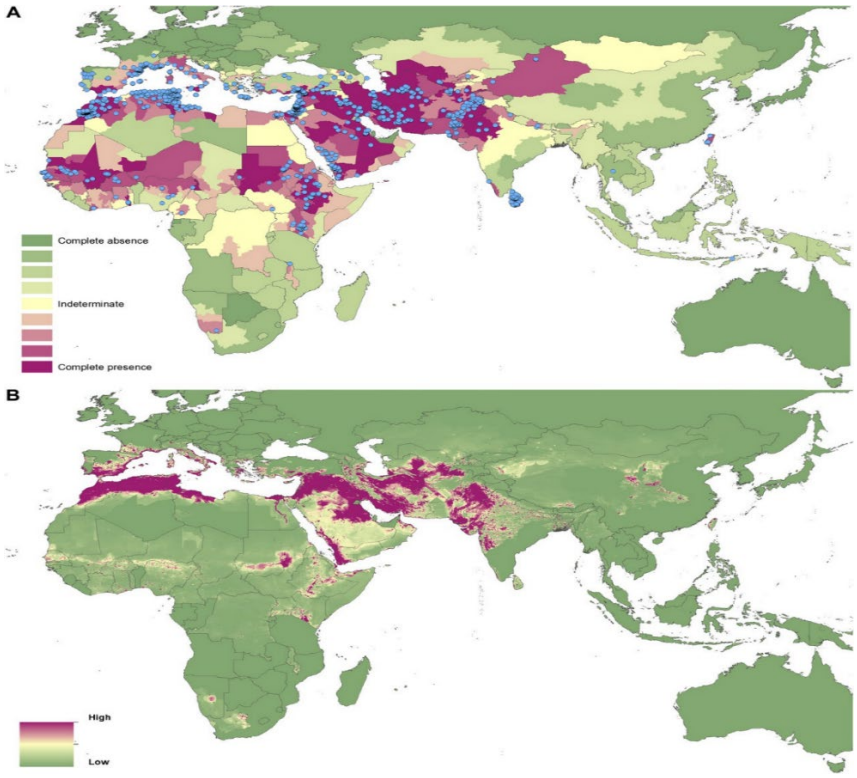

Source:(Pigott et al., 2014).

2.6.1.2 Transmission

Leishmania parasites that cause CL are transmitted through the bites of infected female phlebotomine sand flies. CL also can occur after accidental occupational (laboratory) exposures to Leishmania parasites. Transmission risk is greatest from dusk to dawn because sand flies typically feed (bite) at night and during twilight hours. Although sand flies are less active during the hottest part of the day, they can bite if they are disturbed, for instance when people brush against tree trunks or other sites where sand flies are resting. Vector activity might easily be overlooked because sand flies are small and silent, and their bites can go unnoticed. Travelers with potentially increased risk for CL include adventure travelers, bird watchers, construction workers, ecotourists, military

personnel, missionaries, Peace Corps volunteers, and people doing research or humanitarian work outdoors at night or twilight. Even short-term travelers in leishmaniasis-endemic areas have developed CL, however. Immigrants and refugees from endemic areas also might present with CL(Mary Kamb, 2024).

2.6.1.3 Clinical Manifestations of cutaneous Leishmaniases

Cutaneous leishmaniasis can exhibit a wide range of dermatologic presentations, from small, local skin lesions to extensive nodules or plaques that may involve multiple zones of the body. Approximately 10% of cases persist asymptomatic. Clinically, the condition can resemble other dermatologic illnesses such as leprosy, squamous cell carcinoma, or various fungal and skin infections(Bilgic-Temel, Murrell, & Uzun, 2019).

Cutaneous leishmaniasis is obvious by skin lesions that may appear as either bolted or open sores, typically developed on exposed areas of the skin within weeks or months after infection. In some cases, lesions may not appear until months or even years later, often triggered by trauma such as skin injuries or surgical procedures. The appearance and size of the sores can change over time. Initially, lesions often present as small, red papules or nodular plaques that gradually progress to open ulcers with raised edges and a central crater, sometimes covered by crusts or scales. While these sores are usually painless, they may become painful if secondarily infected with bacteria. Additional symptoms can include satellite lesions, swelling of nearby lymph nodes (regional lymphadenopathy), and nodular lymphangitis. Although most sores eventually heal on their own, the healing process can take months or years and typically leaves behind scars(Mary Kamb, 2024).

Figure 11

Skin Lesions Associated with Cutaneous Leishmaniasis may Appear in Various Forms, Including: (A) an Ulcerated, Crusted Nodule; (B) an Ulcerated Lesion; and (C) a Verrucous Lesion

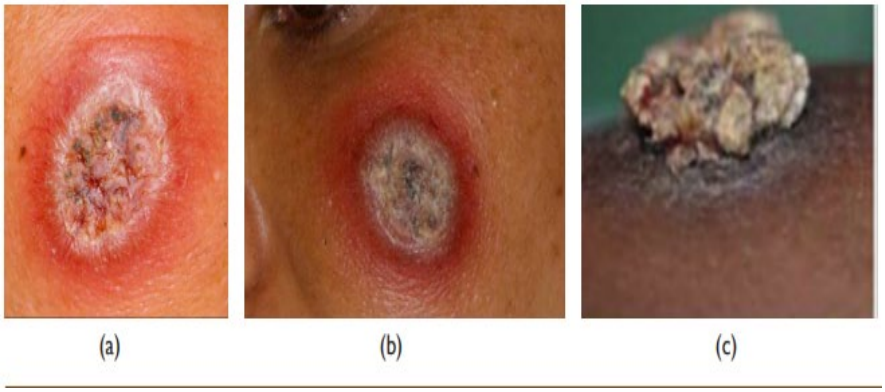

Source:(CDC, 2024)

2.6.1.4 Extensive cutaneous infection caused by Leishmania

The distributed form of cutaneous leishmaniasis (CL) is relatively uncommon, but in certain geographic regions, it holds significant clinical relevance due to its higher incidence. This form of the disease is primarily caused by species such as *L. braziliensis*, *L. panamensis*, *L. amazonensis*, *L. guyanensis*, and *L. mexicana*. Clinically, it presents with numerous popular lesions resembling acne, distributed across various parts of the body. In some cases, patients may develop several hundred lesions. The disease typically begins through unity or more primary lesions that exhibit the classic features of granulomatous abscesses by elevated borders. Following the initial presentation, a rapid and often acute dissemination phase occurs likely due to the spread of the parasite via the bloodstream or lymphatic system. This metastatic process can progress quickly, sometimes within 24 hours, resulting in new lesions far from the original site of infection as revealed in Figure 12 (Pan American Health Organization, 2019).

Figure 12

(A) Disseminated Cutaneous Leishmaniasis: Numerous Inflammatory Papules and Acneiform Lesions Extensively Distributed Across the Trunk. (B) Disseminated Cutaneous Leishmaniasis: Multiple Erythematous, Edematous, Ulcerated, and Pruritic Papules Present on the Trunk, with Similar Lesions Observed in Other Anatomical Regions

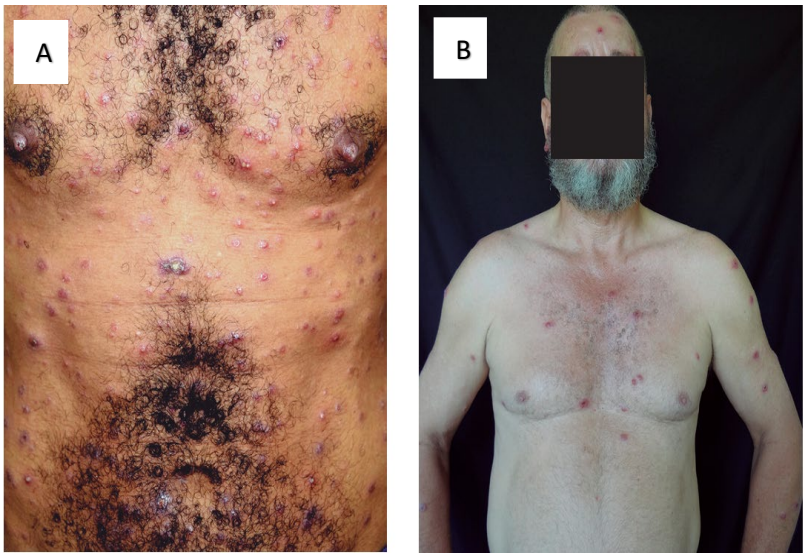

(Pan American Health Organization, 2019; Jaime Soto et al., 2022)

2.6.2 mucocutaneous leishmaniasis

Mucosal leishmaniasis, also known as mucocutaneous leishmaniasis, accounts for roughly 4% of all leishmaniasis cases described in the Americas, with a assortment that can vary from 0% to 16% dependent on the country. In some regions, such as Paraguay, the quantity can be meaningfully higher. The development of this clinical form is influenced by factors including the infecting *Leishmania* species, host genetics, and immune response. The most commonly implicated species is *L. braziliensis*, although other species such as *L. panamensis* and *L. guyanensis* have also been associated with ML/MCL. This illness typically rises as a difficulty due to metastatic spread of the parasite via hematogenous or lymphatic routes from a distant cutaneous lesion. Less

normally, it result from direct extension to facial mucous membranes or from a sandfly bite directly on the mucosa(Pan American Health Organization, 2019).

In general, ML or MCL have a habit of develop months or even years after a person has improved from CL. Most mucosal involvement arises within the first two years following the healing of skin lesions. Therefore, it is crucial to examine patients with suspected ML for characteristic CL scars. In some cases, ML may present concurrently with active skin lesions, while in others, there may be no visible scars or documented history of prior CL(Pan American Health Organization, 2019).

The condition typically begins in the mucous membrane of the nasal septum, which is also the most frequently affected site. Early signs include a feeling of nasal blockage, itching or discomfort, the formation of sero-hematic crusts, nasal discharge that may contain mucus and blood, or occasional nosebleeds. Inflammation characterized by redness, swelling, and tissue infiltration causes enlargement of the nasal tip and nasal ala, which can sometimes spread to the cheeks beyond the nasolabial folds. As the disease advances, it may perforate the cartilaginous portion of the nasal septum and damage surrounding tissues, leading to pronounced facial deformities. This includes a thickened, drooping nasal tip, and in some cases, excessive nasal growth that resembles “a tapir’s snout” an analogy commonly used in areas where the disease is widespread. The disease may also spread to the palate, particularly affecting the soft palate and pharynx with infiltrative, proliferative lesions. As the uvula becomes infiltrated, it enlarges and may eventually be lost due to tissue destruction as seen Figures 13 to 14. Additionally, between 5% and 15% of affected role through ML experience dysphonia. This typically begins as a bitonal voice and may progress to complete loss of voice (aphonia) if the larynx is

affected, significantly impairing the patient's ability to communicate(Jaime Soto et al., 2022).

In severe cases, the patient's overall condition deteriorates, often accompanied by significant weight loss. In fatal instances, emaciation, respiratory failure, or secondary infections may occur. Pneumonia resulting from broncho aspiration is a common terminal event. Mucosal and mucocutaneous forms of the disease do not resolve on their own; instead, they tend to progress, potentially leading to severe tissue damage and disfigurement, which can greatly impact the patient's value of lifecycle. Cases that persist for many years, involve extensive mucosal damage, or relapse after treatment must remain classified as severe. Long-term follow-up is essential, as relapses can occur even after apparent recovery(Diniz, da Rocha Costa, & Gonçalves, 2011). Since post-treatment declines are common, it is crucial to accurately recognize symptoms related to sequelae to avoid the unnecessary use of anti-Leishmania medications. Structural and functional damage to the nose impairs the ability to humidify and warm inhaled air, resulting in persistent "dryness, irritative cough", itching, pain, and the formation of scabs. Bacterial super-infections of paranasal sinuses are also frequently observed. Additionally, some patients experience swallowing difficulties due to facial sequelae, such as uvula amputation or synechiae in the soft palate and nasopharynx(Pan American Health Organization, 2019).

Figure 13

Mucosal Leishmaniasis with Nasal Involvement: Frontal and Lateral Views Showing Destruction of the Nasal Septum

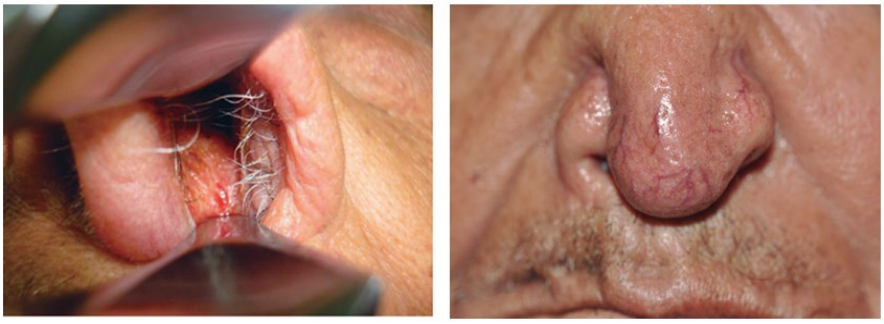

Source:(James WD, 2006).

Figure 14

Mucosal Leishmaniasis can Lead to Significant Sequelae, Including the Loss of Nasal Architecture Due to the Destruction of the Columella and Parts of the Nasal Septum, Resulting in Severe Impairment of Nasal Function

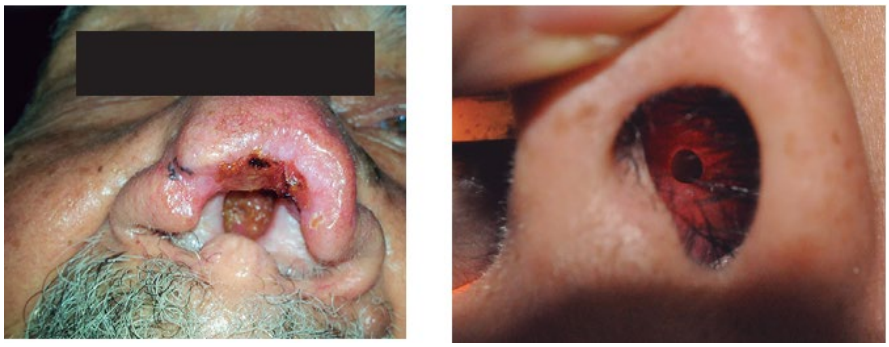

Source:(Jaime Soto et al., 2022).

2.6.3 Visceral leishmaniasis

The furthermost severe form of leishmaniasis is visceral leishmaniasis (VL). Following infection, the parasites spread to hematopoietic organs and tissues, including the liver, spleen, bone marrow, and lymph nodes, along with the macrophages they infiltrate. They multiply there, infect neighboring macrophages, and cause the

clinical signs and symptoms of visceral leishmaniasis. Usually, the incubation period lasts between two weeks and two months. Malnutrition and immunosuppressive diseases, such as HIV/AIDS, are often linked to VL, which primarily affects children and adolescents under five. VL can be fatal if it is not treated properly and quickly(Cota, de Sousa, & Rabello, 2011).

Figure 15

Illustrations two Sections, A) the Evidence Consensus for Disease Presence is Represented on a Spectrum from Green, Indicating Complete Agreement on Absence (-100%), to Purple, Indicating Complete Agreement on Presence (+100%). Blue Spots Denote Observed Occurrence Points or Centroids of Smaller Geographic Areas. B) the Predicted Risk of Visceral Leishmaniasis Is Shown Using a Color Gradient from Green (Indicating Low Likelihood of Presence to Purple (Indicating High Likelihood of Presence

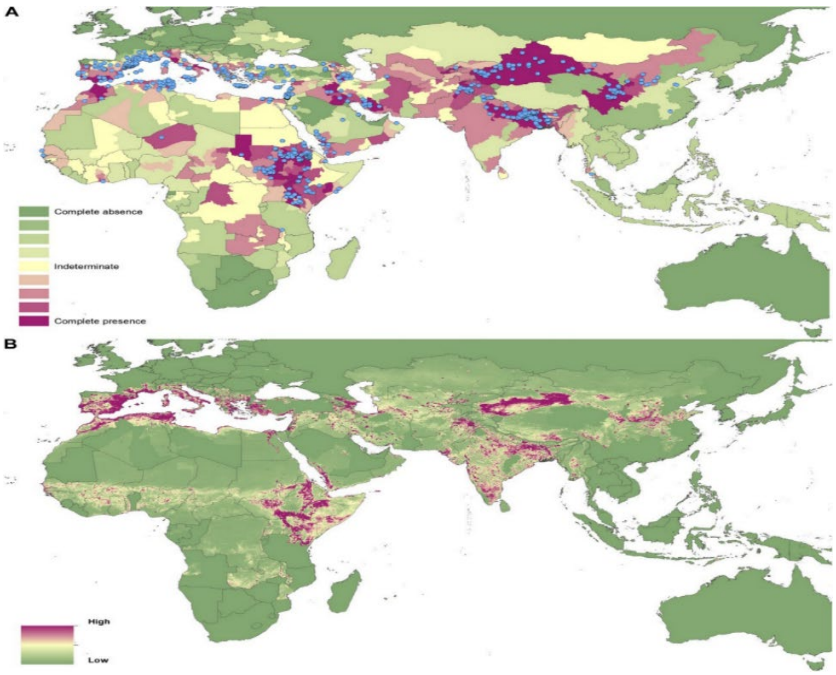

Source:(Pigott et al., 2014).

Infection by *Leishmania infantum* can often be asymptomatic, with not any noticeable clinical signs or symptoms. Epidemiological studies direct that most entities infected with the parasite keep on asymptomatic.

As a result, these cases do not necessitate reporting to the surveillance system and do not warranty treatment. However, when symptoms appear, they can range in harshness from mild to severe. The primary stages of the disease may be effortlessly mistaken for other infectious conditions. Common signs and symptoms include persistent or irregular fever, mild splenomegaly observed in furthermost patients, and hepatomegaly. Lymphadenopathy is similarly frequent, typically presenting as prevalent, firm, transportable, and non-tender lymph nodes. Other symptoms include mucocutaneous whiteness due to severe anemia and gradual, progressive weight loss as figure16 (C. H. N. Costa et al., 2010).

Figure 16

Visceral Leishmaniasis Affects Mostly Internal Organs, Particularly the Liver and Spleen, in Adults and Children

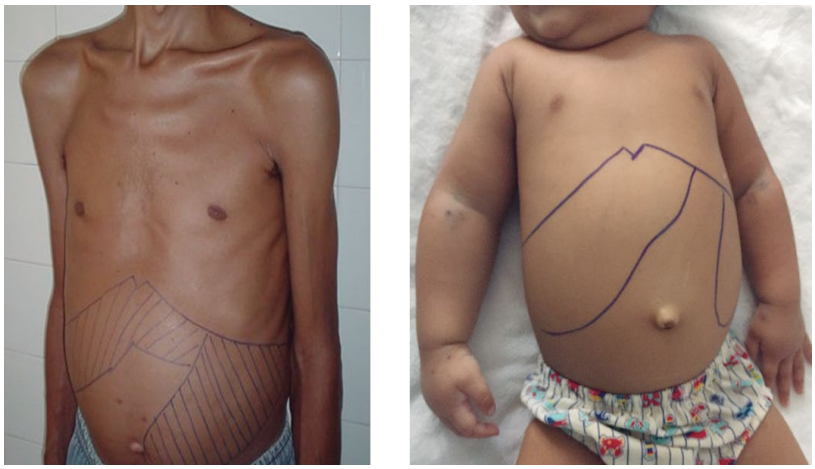

Source:(C. H. N. Costa et al., 2010).

During the evolutionary phase, the following symptoms are commonly practical: determined fever accompanied by broad-minded weight harm, general decline in health, loss of appetite, and increasingly noticeable mucocutaneous pallor. Additionally, there is often an increase in abdominal volume and enlargement of both the liver and spleen

(hepatosplenomegaly). As the condition progresses, secondary signs and symptoms may develop rapidly. These include respiratory complications, often due to severe immunosuppression, this increases patients' susceptibility to opportunistic bacterial or viral infections. They may also experience nonspecific gastrointestinal symptoms, including diarrhea, which can manifest as dysenteric syndromes and may be associated with recurring infections from pathogens such as *Entamoeba histolytica*, *Shigella*, or *Salmonella*(Pan American Health Organization, 2019).

Bleeding can become severe and life-threatening. The underlying causes are primarily linked to a reduced platelet count in the blood, bone marrow infection through parasites, and platelet confiscation in an engorged spleen. As a result, anorexia is commonly observed in affected patients. Less frequent symptoms include jaundice, edema in advanced stages, and neurological changes such as a red-hot impression in the feet and cerebellar ataxia. Laboratory findings often show leukopenia, hypoalbuminemia, thrombocytopenia, and hypergammaglobulinemia, all of which increase the patient's vulnerability to bleeding and opportunistic contagions. These complications can significantly worsen the disease and may lead to death. During this critical phase, the risk of fatal outcomes rises, underscoring the need for meticulous clinical evaluation. Special attention should be given to the tactual exploration of the liver and spleen, as these findings are crucial for raising investigative doubt(Romero & Boelaert, 2010).

2.6.3.1 Concurrent infection with visceral leishmaniasis and HIV

In individuals by HIV, contagion via *L. infantum* is more usually observed in adult males. It acts as an opportunistic disease, diffusion throughout the body as CD4 lymphocyte counts decline. This systemic

spread allows the parasite to be detected in blood, healthy skin, bronchial aspirates, and extra sites. Clinical estimation of VL in this population exposes that there is no consistent clinical shape linked to co-infection. When symptoms are existing, atypical manifestations for instance pleural involvement, gastrointestinal tract compromise, and a higher rate of relapses are more frequently observed. These factors contribute to an increased risk of mortality. Appropriate diagnosis is crucial. As such, completely patients diagnosed with VL should undergo HIV testing. An evaluation for potential visceral leishmaniasis should be conducted in individuals with HIV/AIDS who show cytopenia combined with splenomegaly (with or without fever) or cytopenia combined with hepatomegaly (also with or without fever)(Cota et al., 2011).

2.6.4 Diffuse cutaneous leishmaniasis

Numerous nations, including Brazil, Venezuela, Mexico, the Dominican Republic, Peru, and Colombia, have reported cases of diffuse cutaneous leishmaniasis (DCL). It can be caused by numerous Leishmania species, such as "*L. amazonensis*, *L. mexicana*, *L. venezuelensis*, *L. pifanoi*, and *L. braziliensis"*(Zerpa & Convit, 2009). DCL is a severe and anergic form of the disease, noticeable by the host's helplessness to mount an effective immune response. This immunosuppression may result from moreover the parasite's direct accomplishment or an underlying immune deficiency. DCL is distinguished by prevalent, parasite-laden lesions. Initially, it presents as papules or plaques confined to a localized area of the skin. However, within a few months, these lesions often spread to other regions of the body. The lesions are mostly nodular and plaque-like in appearance, closely resembling those seen in lepromatous leprosy as seen in figure 17. Treatment typically yields only temporary improvement, with relapses occurring frequently(Convit et al., 1989).

Figure 17

On the thighs and legs, diffuse cutaneous leishmaniasis manifests as nodular and tumorous growths. The lesions have a vegetative look and ulcerated areas.

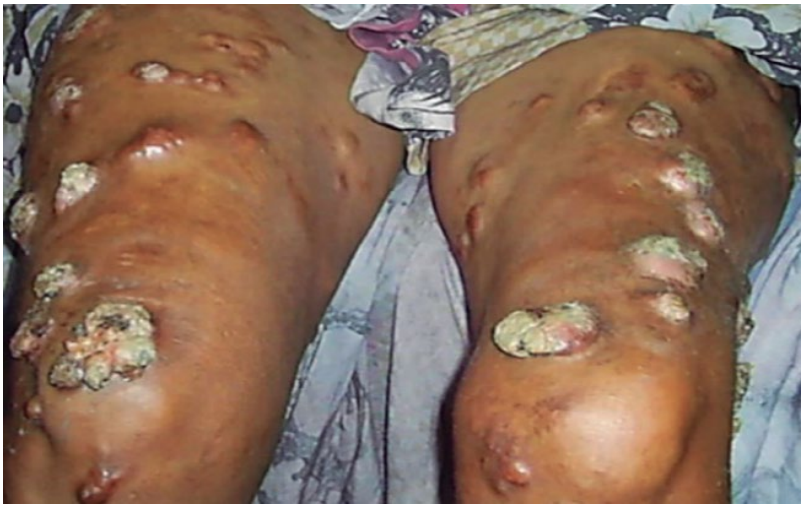

Source:(J. M. L. Costa et al., 1995).

2.6.5 Atypical cutaneous leishmaniasis

In Central America and Venezuela, a different of cutaneous leishmaniasis known as atypical cutaneous leishmaniasis (ACL) has been acknowledged. This form is characterized by localized; non-ulcerative, chronic skin lesions caused by *L. infantum*. Cases of ACL have be located in "Nicaragua, Honduras, Costa Rica, El Salvador, and Venezuela"(Pan American Health Organization, 2019).

Figure 18

Atypical Presentation of Cutaneous Leishmaniasis: a Single, Non-Ulcerated Lesion

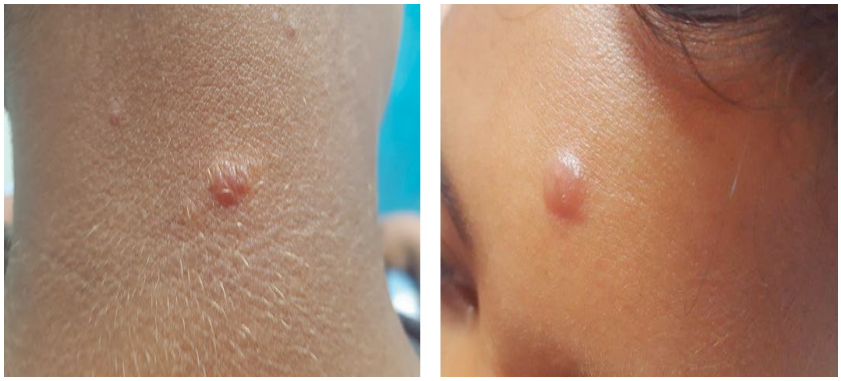

Source:(Pan American Health Organization, 2019).

2.7 Environmental and socioeconomic risk factors associated with cutaneous leishmaniasis

Human alterations to tropical landscapes have led to increased interactions between people and Leishmania vectors(Valero, Prist, & Uriarte, 2021). The growth and spread of human populations have contributed to the increased occurrence of the disease in settlements near forests, where conditions favor the development of phlebotomine sand flies(Casanova et al., 2013). Rural-to-urban migration and the growth of human settlements in peri-urban areas have intensified interactions between disease vectors, humans, and domestic animals. This increased connectivity among human habitats supports the life cycle and spread of leishmaniasis vectors(Thomaz-Soccol et al., 2018). As a consequence, sand flies have altered their transmission cycle to urban environments by relying on domestic animals instead of reservoirs found in densely vegetated areas(A. Hong & Zampieri, 2020).

The transmission cycle of cutaneous leishmaniasis in Neotropical regions persists mainly in areas with dense vegetation for example forests

or vegetation surrounding rural and peri-urban zones because the vector species and reservoirs of the Leishmania parasite responsible for the cutaneous form are closely tied to natural habitats and depend on the occurrence of vegetation. In contrast, visceral leishmaniasis, caused primarily by *Leishmania infantum*, is transmitted by the synanthropic vector *Lutzomyia longipalpis* and involves domestic dogs (*Canis familiaris*) as the main reservoir. As a consequence, VL principally affects human populations in urban and peri-urban environments(Kariyawasam et al., 2015).

Climate plays a crucial role in determining the distribution of vectors and pathogens. Factors such as temperature, precipitation, and comparative humidity influence the reproduction, development, behavior, and population dynamics of vector-borne diseases like leishmaniasis. The impact of climate conditions on leishmaniasis varies depending on the specific vector species, as each responds differently to environmental factors. Generally, sand flies—the primary vectors—require warm temperatures and consistent precipitation to maintain the humid conditions necessary for survival. However, excessive rainfall can be lethal to them, while drought conditions can hinder larval development(Desjeux, 2001). Neotropical sand flies are typically present throughout the year, but their population levels fluctuate with seasonal climate changes. In regions with distinct wet-dry or hot-cold seasons, sand flies often enter diapause during their early developmental stages (larvae and pupae) to survive unfavorable conditions until the environment becomes suitable for emergence (Pinheiro et al., 2016). However, optimal temperature and precipitation conditions differ among sand fly species and depend on their geographic distribution. Gaining a deeper understanding of how climate factors influence sand fly populations is crucial for predicting the risk of

leishmaniasis in the context of climate change(Carvalho, Rangel, & Vale, 2017).

Socioeconomic conditions play a significant role in influencing the risk of leishmaniasis. Poverty is commonly linked not only to limited access to healthcare services but also to living and working environments that facilitate disease transmission(Valero et al., 2021). In tropical regions, populations in rural and peri-urban areas often reside near vegetation, where the leishmaniasis transmission cycle can be sustained. Housing in these regions is frequently built with low-quality materials such as straw, mud, or bamboo, which provide suitable habitats for sandflies, the disease vectors(Oryan & Akbari, 2016). Additionally, inadequate infrastructure—such as the absence of sewage systems and garbage collection—leads to waste accumulation, which attracts potential animal reservoirs (e.g., domestic mammals) and creates humid conditions conducive to sandfly breeding. Agricultural work and livestock rearing further elevate the risk, as these activities increase human exposure to sandfly bites and draw sandflies toward cattle in search of a blood meal(Valero et al., 2021).

2.8 Leishmaniases Immunopathogenesis

The pathogenesis of visceral leishmaniasis (VL) is complex and not yet fully understood. During the progression of infection, significant alterations in gene expression can occur, including changes in microRNAs (miRNAs)(Ramos-Sanchez et al., 2022). In this context, investigated miRNA expression linked to immune and inflammatory pathways using a human monocytic THP-1 cell model infected with *Leishmania infantum* promastigotes, as well as plasma samples from VL patients. Their study identified miR-548d-3p as one of the few miRNAs consistently regulated in both the infected THP-1 cells and patient plasma. Furthermore,

inhibition of miR-548d-3p in THP-1 cells led to suppressed *Leishmania* growth, potentially due to the increased production of MCP-1/CCL2 and nitric oxide. These findings build on the authors' previous work highlighting the role of miR-548d-3p in cutaneous leishmaniasis caused by *L. (V.) braziliensis*(Souza et al., 2021).

Using a quantitative proteomics approach, a total of 4,048 proteins were identified, among which 254 were found to be upregulated and 196 downregulated in atypical cutaneous leishmaniasis strains compared to typical strains. The atypical strains exhibited increased expression of proteins involved in the early stages of mammalian host infection, which may enhance parasite survival within macrophages, as well as proteins linked to resistance to antimony-based therapy.(Esteves et al., 2022). Lesions in patients with ATL exhibit elevated appearance of IL-32γ. Both *L. amazonensis* and *L. braziliensis* stimulate the production of this cytokine in human macrophages(Gomes et al., 2017). Lipophosphoglycan (LPG) is a key multivirulence factor prominently displayed on the surface of Leishmania promastigotes, playing a crucial role in mediating host-parasite interactions(Silveira et al., 2022). The study investigated the ability of lipophosphoglycans (LPGs) from *L. amazonensis* and *L. braziliensis* to stimulate IL-32 production in human peripheral blood mononuclear cells (PBMCs). The results showed that both types of LPGs induced the expression of the IL-32γ isoform, which was associated with increased levels of IL-1β and IL-6. This response was found to be dependent on the activation of TLR4 and NOD receptors. The authors highlight the importance of identifying the parasite-derived molecules and host receptors involved in IL-32γ induction, as this could contribute to better control of Leishmania infections and the development of new therapeutic approaches for the disease(de Menezes, Brodskyn, Gonçalves, & Bacellar, 2022).

Th17 cells are believed to play a crucial role in defending against various extracellular and intracellular pathogens. They have also been shown to modulate the balance between pro-inflammatory and anti-inflammatory cytokines (25). Interleukin-17 (IL-17), primarily produced by Th17 cells, has complex and not yet fully understood effects. In the context of different clinical forms of leishmaniasis, Th17/IL-17 responses may contribute to both protective immunity and disease progression(Tomiotto-Pellissier et al., 2018). To investigate the role of transcription factors (TFs) and genes involved in Th17 cell induction during Leishmania–macrophage interactions, the authors employed gene regulatory networks (GRNs). They analyzed the infection dynamics and their correlation with the modulation of the Th17 immune response in cutaneous leishmaniasis using transcriptome sequencing data from macrophages infected with *Leishmania major* and *Leishmania amazonensis*, complemented by experimentally validated findings from the literature. Their analysis revealed that genes associated with the Th17 pathway were overexpressed in macrophages infected with both Leishmania species. In the early stages of infection, several genes related to immune regulation were upregulated, including those encoding the transcription factor STAT2, as well as IL-2 and CXCL12(Gonçalves et al., 2022).

2.9 Laboratory Diagnosis of Leishmaniases

The spectrum of clinical leishmaniasis is broad, often leading to confusion with other diseases. Consequently, early diagnosis is crucial for timely administration of specific treatments. Early detection can effectively control the disease's progression, alleviate symptoms, reduce mortality in cases of visceral leishmaniasis (VL), and enhance the quality of life for patients. This is especially important for those suffering from

cutaneous leishmaniasis (CL), mucosal leishmaniasis (ML), or mucocutaneous leishmaniasis (MCL), who often face social stigma due to the physical and psychological effects of the disease.

Different diagnostic methods are used depending on the clinical form of leishmaniasis. Direct visualisation of the parasite is ideal for diagnosis. However, clinical evaluation, backed by particular immunological (indirect) testing, should also be considered because it is not always possible to observe or isolate the parasite. The primary leishmaniasis diagnostic techniques currently in use concentrate on detecting amastigotes in samples taken from tissues, lymph nodes, mucous membranes, or skin lesions. Tests for identifying anti-Leishmania antibodies in serum or whole blood have also been developed for mucosal and visceral types.

2.10 Technical Procedures for Sample Collection

Microscopic examination of slides, including tissue and fluid aspirates, biopsy impression smears, and skin scrapings, is commonly used for diagnosing leishmaniasis. In vitro culture and PCR testing are also utilized for detecting the disease and identifying its species. Note that PCR does not require additional specimens beyond those already collected for culture. Serological testing, including the K39 test, can detect antibodies against the *L. donovani* species complex and is typically used for diagnosing visceral leishmaniasis.

Figure 19

A Clinical Classification of Leishmaniasis, Highlighting its Various Manifestations and Diagnostic Methods. It Provides an Overview of the Disease's Clinical Signs and Symptoms, Along with Corresponding Guidelines for Sample Collection Required for Laboratory Diagnosis

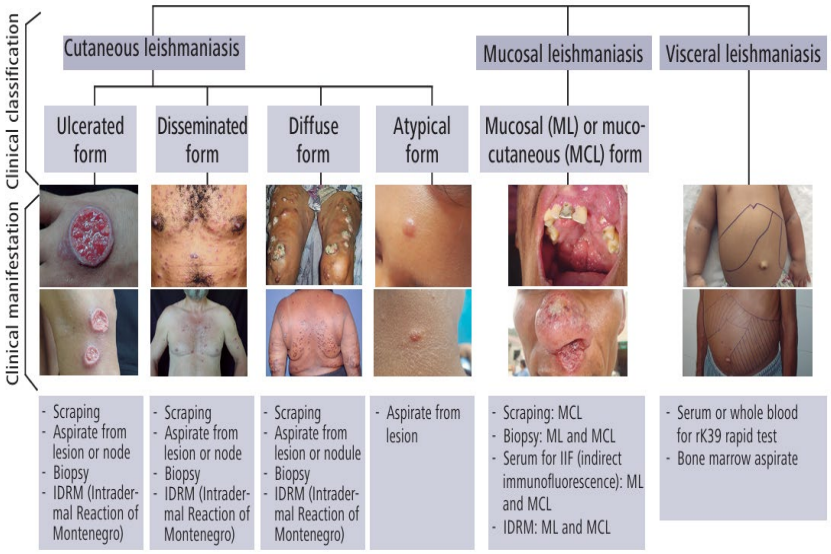

Source:(Pan American Health Organization, 2019).

2.10.1 Identification of Cutaneous, Mucosal, and Mucocutaneous Types of Leishmaniasis in a Laboratory

Direct diagnostic techniques are used to visually identify the parasite in the patient's sample. These techniques could entail taking samples via aspirating material from lymph nodes and lesions, scraping, or biopsy. Polymerase chain reaction (PCR), culture, histological study, and parasitological or direct examination are examples of diagnostic methods. The location of the lesion, the species or strains of parasites involved, the

length of the lesion, the examiner's experience, the techniques used for sample collection and processing, and any previous treatments-conventional or empirical can all affect how sensitive parasitological or direct examinations are. According to research, samples obtained from the active edges of a lesion, for example, have a sensitivity of 90.4%, while samples obtained from the base of an ulcer have a lesser sensitivity of 78.3%(Montalvo et al., 2008).

Due to the need for advanced laboratory infrastructure and highly trained personnel, methods such as isolation, culture, and molecular diagnosis of leishmania are not widely used in routine health services. Therefore, it is essential that these diagnostic techniques be made accessible for cases through specialized reference research laboratory.

Leishmaniasis can be indirectly diagnosed by using serological testing to detect anti-Leishmania antibodies, primarily of the IgG class, or by using the delayed-type hypersensitivity skin test, also known as the Montenegro or Leishmanin test, to assess the cellular immune response. Nevertheless, this skin test is not available for purchase in the region.

Due to its poor sensitivity and variable specificity, serological testing for cutaneous leishmaniasis (CL) has limited diagnostic usefulness. In situations of mucosal leishmaniasis (ML), it can still be a useful diagnostic tool. The enzyme-linked immunosorbent assay (ELISA) and indirect immunofluorescence assay (IIF) are the most commonly utilised serological methods in public health contexts; the specificity of both methods is largely reliant on the kind of antigen employed. Antibody-based examinations may support diagnosis when clinical signs are consistent with suspected cases of ML or MCL. However, a positive serological result alone is not sufficient to justify treatment should only be

initiated when clinical symptoms of the disease are also present(Pan American Health Organization, 2019).

2.10.2 Laboratory analysis of visceral leishmaniasis (VL)

In order to reduce mortality and avoid problems related to visceral leishmaniasis, it is imperative that the disease be diagnosed and treated promptly. Beginning with a thorough medical history and physical examination, the initial tentative diagnosis is based on clinical presentation and epidemiological context. Patients who have a fever that lasts more than a week, together with pallor and possibly hepatosplenomegaly, are usually suspected of having VL. In these situations, diagnostic testing ought to be undertaken, either to detect antibodies specific to Leishmania (such as rK39) or to examine the parasite in clinical specimens(Maia et al., 2012).

A number of considerations should be made when choosing diagnostic techniques, including the degree of invasiveness of the process, the degree of medical skill needed to collect and analyse the sample, and the quality control procedures required to guarantee diagnostic precision. Typically, quick immunochromatographic serological assays that use the recombinant rK39 antigen that have been validated for regional use are used to detect visceral leishmaniasis (VL) at the primary care level. However, not every case of VL can be identified with certainty at this stage. Therefore, it is still the responsibility of the clinician to make sure that patients with suspected but unconfirmed VL are transferred as soon as possible to higher-level healthcare facilities for additional assessment, even while efforts to increase the precision and dependability of current diagnostic techniques should continue(Peixoto, de Oliveira, & Romero, 2015). In the geographic area that includes the Americas, VL-HIV combination is becoming more common and now makes up around 8% of

all newly reported VL cases. Consequently, it is essential to conduct HIV testing in all confirmed cases of VL. It is crucial to remember that additional medical centres usually conduct standard histopathological and serological investigations for HIV and VL. Meanwhile, more advanced diagnostic methods such as immunohistochemical analysis, culture, PCR, and the development or evaluation of innovative testing techniques are generally conducted in reference laboratories or research institutions(Alves et al., 2024).

Table 3.

Describes the Several Types of Leishmaniasis Diagnostic Techniques, Including Parasitological, Protein-Based, DNA-Based, and Immunological Techniques. It Contains Details about Their Application in Various Clinical Forms, Including Visceral Leishmaniasis (VL) And Cutaneous Leishmaniasis (CL)

	The Diagnostic Approach	**Form of Clinical**	**The Need for Culture**	**Discrimination by Species**	**Reference(s)**
Parasitological methods	Biopsy, punch, scraping, smear or imprinting followed by microscopic examination	CL	No	No (only genus *Leishmania*)	(C. M. Sandoval Pacheco et al., 2018; Suárez et al., 2015)
	Bone marrow, lymph aspirations of the nodes, spleen, or liver, followed by microscopic analysis	VL	No	No (only genus *Leishmania*)	(Babiker, Davidson, Mazinda, Kipngetich, & Ritmeijer, 2007)
	Culture in vitro	VL, CL	Yes	No (only genus *Leishmania*)	(Schuster & Sullivan, 2002)

	Inoculation in animals (mice or hamsters)	VL, CL	No	No (only genus *Leishmania*)	(de Vries, Reedijk, & Schallig, 2015)
	Xenodiagnoses	VL	No	No (only genus *Leishmania*)	(O. P. Singh, Hasker, Boelaert, Sacks, & Sundar, 2020)
Protein-based methods	MLEE	VL, CL	Yes	Yes (almost all currently identified species)	(Cupolillo, Grimaldi, & Momen, 1994)
	Monoclonal-antibodies	VL, CL	Yes	"Yes, nearly all species are endemic to the Americas, with the exception of *L. (L.) major*, *L. (L.) donovani*, and *L. (L.) tropica*.")	(Grimaldi & McMahon-Pratt, 1996; Jaffe & Rachamim, 1989)
	MALDI-TOF, MS	VL, CL	Yes	"Yes, all species are native to the Americas, Europe, Asia, and Africa."	(Cassagne et al., 2014; Lachaud et al., 2017)

	KAtex	VL	No	No (only genus *Leishmania*)	(Salam, Khan, & Mondal, 2011)
DNA-based methods	PCR-RFLP	VL, CL	No	"Yes, applicable to most species, though it depends on the target involved."	(Akhoundi et al., 2017) (Van der Auwera & Dujardin, 2015)
	DNA sequencing	VL, CL	No	"Yes, for nearly all species-it varies based on the target."	(Akhoundi et al., 2017) (Van der Auwera & Dujardin, 2015)
	Real-time PCR	VL, CL	No	"Generally, yes, for the majority of species, but it can vary depending on the target."	(de Almeida, Koru, Steurer, Herwaldt, & da Silva, 2017; Weirather et al., 2011)
	PCR-HRM	VL, CL	No	"Yes, nearly all species are native to the Americas, Europe, Asia, and Africa."	(Müller et al., 2018; Zampieri et al., 2016)
	MLST	VL, CL	No	Yes (completely species)	(Boité, Mauricio, Miles, & Cupolillo, 2012;

					Tsukayama, Lucas, & Bacon, 2009)
	LAMP	VL, CL	No	Yes, although restricted to certain species.	(M. G. Khan et al., 2012; Verma et al., 2017)
Immunological-based methods	*Leishmania* skin test	CL (negative for DCL)	No	"Only the genus Leishmania is included."	(Goto & Lindoso, 2010)
	ELISA (rK39)	VL	No	No (only the Leishmania genus).	(Braz et al., 2002; D. P. Singh, Goyal, Singh, Sundar, & Mohapatra, 2010)
	ELISA (other recombinant antigens)	VL, CL	No	"Only the genus Leishmania is included."	(Celeste et al., 2014; D. Kumar, Kumar, Chakravarty, & Sundar, 2011; Mohapatra, Singh, Sen, Bharti, & Sundar, 2010)
	IFAT	VL, CL	No	No (only genus *Leishmania*)	(Bangert et al., 2018; Pedras, de Gouvêa Viana,

				de Oliveira, & Rabello, 2008)
DAT	VL	No	No (only genus *Leishmania*)	(Bangert et al., 2018; Cunningham et al., 2012; Pedras et al., 2008)
ICT (rK39)	VL	No	"Only the genus Leishmania is included."	(Bangert et al., 2018; Cunningham et al., 2012; Pedras et al., 2008)
Dipstick test [*L. donovani* promastigote antigens]	VL	No	No (only genus *Leishmania*)	(Ejazi et al., 2019; Saha et al., 2011)
Western blot	VL, CL	No	"Only the genus Leishmania is included."	(Mary, Lamouroux, Dunan, & Quilici, 1992; Santos-Gomes, Gomes-Pereira, Campino, Araújo, & Abranches, 2000)

Source: (J. Q. Reimão & Coser, 2020)

2.11 Treatment

2.11.1 Management of Cutaneous Leishmaniasis

The treatment of cutaneous leishmaniasis varies depending on the causative species and the geographic origin of the infection. In cases where the risk of mucosal involvement is low, topical paromomycin may be an appropriate option. For patients with only one or a few small lesions provided they are not located on the face or over joints close observation without pharmacologic intervention may be a suitable approach(CDC, 2024). For more invasive lesions such as those unresponsive to topical treatment, those with metastatic spread to lymph nodes, or large, disfiguring, or multiple skin lesions, particularly on the face, near mucosal surfaces, or around joints systemic treatments like sodium stibogluconate or pentamidine may be used.

2.11.1.1 Oral miltefosine

The treatment of New World cutaneous leishmaniasis has shown varying degrees of success. In a randomized controlled trial conducted in Brazil, miltefosine alone proved significantly more effective than parenteral stibogluconate in older children and adults. In Colombia, miltefosine achieved a 91% cure rate for infections caused by *L. panamensis*, comparable to the results seen with antimony therapy. However, in Guatemala, miltefosine cured only 53% of infections caused by *L. (V.) braziliensis*, a rate substantially lower than historical cure rates with antimony treatment(CDC, 2024; Machado et al., 2010).

A study conducted in Bolivia found that oral miltefosine, administered for 28 days, achieved an 82% cure rate, while intramuscular

meglumine antimonate resulted in an 88% cure rate for *L (Viannia) braziliensis*. However, the tolerance for oral miltefosine was significantly better than that of the intramuscular meglumine antimonate, to the extent that local physicians refused to continue using the intramuscular treatment for the control group(J. Soto & Toledo, 2007).

2.11.1.2 Topical paromomycin

Topical paromomycin has been found to be effective in treating cutaneous leishmaniasis caused by *L. major* and *L. mexicana*. These species are less likely to lead to visceral or mucocutaneous disease, making topical paromomycin a suitable alternative that minimizes systemic side effects often seen with parenteral treatments. However, topical therapy is not recommended for treating New World species known to progress to mucocutaneous disease(CDC, 2024).

In a randomized, double-blind, parallel-group controlled trial involving 375 patients from an endemic region in Tunisia, Ben Salah et al. demonstrated the effectiveness of topical paromomycin cream, with or without gentamicin, in treating ulcerative cutaneous leishmaniasis. Patients were treated with 15% paromomycin, 15% paromomycin combined with 0.5% gentamicin, or a vehicle control (which contained neither paromomycin nor gentamicin). After 20 days of treatment, the cure rates were 82% for paromomycin alone, 81% for paromomycin-gentamicin combination, and 58% for the vehicle control(Jaime Soto et al., 2022). An ointment containing 15% paromomycin and 12% methylbenzethonium chloride demonstrated an even higher cure rate of 87% after 20 days of topical treatment for cutaneous *L. major*. However, its effectiveness against infections caused by *L. tropica* has been disappointing(El-On, Livshin, Even-Paz, Hamburger, & Weinrauch, 1986).

2.11.1.3 Management of Visceral Leishmaniasis

Be cautious of complications associated with reticuloendothelial system failure, which can lead to bleeding or neutropenia, increasing the risk of infections such as pneumonia or diarrhea. In cases of severe bleeding or anemia, transfusions may be necessary. Antibiotics should be used to address concurrent infections(CDC, 2024). Pentavalent antimonial compounds are typically effective in treatment, but in regions with high resistance to this therapy (such as India) or where other benefits exist (e.g., improved toxicity profile or shorter treatment duration), alternative parenteral agents may be considered, even for first-line treatment.

Liposomal formulations of amphotericin B, which selectively target macrophage-rich organs, have largely replaced deoxycholate formulations. Though liposomal amphotericin B is more expensive and may be cost-prohibitive in poorer countries, it offers advantages such as reduced nephrotoxicity and the ability to administer in shorter treatment courses. Despite the traditional use of multiple doses of amphotericin B deoxycholate for treating visceral leishmaniasis, a randomized trial suggests that a single dose of liposomal amphotericin B may be equally effective and more cost-effective(Sundar, Chakravarty, Agarwal, Rai, & Murray, 2010).

Oral miltefosine is Food and Drug Administration (FDA) approved for the treatment of visceral, cutaneous, and mucocutaneous leishmaniasis. Sitamaquine, another oral therapy, is currently being researched for the treatment of visceral leishmaniasis. This 8-aminoquinoline, initially discovered by the Walter Reed Army Research Institute, is now undergoing phase 3 clinical trials in Kenya and India(Seifert, 2011).

2.11.1.4 Surgical Intervention

Surgical excision is generally not recommended for managing leishmaniasis due to risks such as relapse (exacerbation of dormant disease), recurrence at the excision site, and cosmetic disfigurement. However, surgical intervention may be required in specific cases, such as adjunctive splenectomy for patients with treatment-resistant disease or orofacial surgery for those with severe mucocutaneous leishmaniasis.

2.12 Prevention

Currently, no vaccines or medications are available to prevent infection. Travelers can reduce the risk of Cutaneous Leishmaniasis by taking personal protective measures to avoid contact with and bites from sand flies (refer to Section 4, Chapter 6, Mosquitoes, Ticks & Other Arthropods). It is recommended that travelers limit outdoor activities, especially between dusk and dawn when sand flies are most active. Wearing protective clothing and applying insect repellent to exposed skin and under clothing (e.g., shirt sleeves, pant legs) as directed by the manufacturer is essential. Travelers should also sleep in air-conditioned or well-screened areas. Spraying sleeping areas with insecticide may offer some protection, and the use of fans or ventilators can help deter sand flies, as they are weak fliers(Mary Kamb, 2024).

Sand flies are tiny, measuring about 2–3 mm (less than 1/8 inch), and can easily pass through the gaps in regular mosquito nets. While fine mesh nets are available, they may not be as comfortable in hot climates. To improve the effectiveness of mosquito nets, they can be treated with a pyrethroid-based insecticide, such as permethrin. This treatment can also be applied to bed sheets, clothing, curtains, and window screens(Mary Kamb, 2024).

2.13 Artificial Neural Networks

2.13.1 Introduction

Over the past decade, the term Artificial Intelligence (AI) has increasingly appeared in scientific literature, including journals focused on image processing and medical physics. Interestingly, AI is not a new concept it began to take shape in the 1940s, with the term itself being introduced by John McCarthy in 1956. At its core, AI involves computer algorithms designed to replicate aspects of human intelligence, such as learning and problem-solving. The recent surge in AI's capabilities is largely due to significant advancements in computational power and the exponential growth of available data. In particular, AI systems powered by machine learning (ML) have achieved remarkable progress in computer vision. The medical field has embraced these advancements, leveraging AI to enhance the analysis of medical images, streamline various clinical processes, and support decision-making. As a result, numerous studies using AI and ML techniques have reported promising outcomes across a broad spectrum of medical applications(R. Singh, Wu, Wang, & Kalra, 2020; C. Wang, Zhu, Hong, & Zheng, 2019; T. Wang et al., 2021). Tasks such as disease diagnosis, image segmentation, and outcome prediction are undergoing a transformative shift driven by recent advancements in artificial intelligence. Machine learning tools have now reached a level of maturity that meets clinical standards, enabling collaboration between research teams, clinicians, and industry to develop practical AI-driven solutions for healthcare. As we move closer to the widespread clinical integration of AI, it is increasingly essential for all medical professionals

to understand the fundamentals of this technology. Equipping the medical physics community with a strong foundation in AI and machine learning including their evolution and current capabilities will not only enhance the quality of research but also support newcomers entering the field and inspire innovative research directions(Barragán-Montero et al., 2021).

2.13.2 Artificial intelligence, Machine Learning, and Deep Learning

Artificial Intelligence (AI) broadly encompasses any technique or algorithm designed to replicate human intelligence. Historically, two main approaches have shaped the development of AI: computationalism and connectionism. Computationalism takes a top-down perspective, aiming to replicate formal reasoning and logic through predefined rules and axioms. This method resembles traditional computing, where information is stored and manipulated as symbols. In contrast, connectionism adopts a bottom-up strategy, drawing inspiration from the brain's architecture. It models intelligence through networks of simple, interconnected units similar to biological neurons that learn and adapt based on experience(Barragán-Montero et al., 2021; Bekheet & Sallah, 2024).

Accurate disease diagnosis regularly depends on advanced image acquisition systems and precise image interpretation. In recent years, technologies like computed tomography (CT) and magnetic resonance imaging (MRI) have seen significant improvements, enabling the capture of in height resolution medicinal pictures ranging from radiological scans (e.g., X-rays, CT, and MRI) to microscopic images such as histologic slides. Interpreting these images demands both expertise and meticulous attention to detail, as the volume of data can be overwhelming(Kim et al., 2022). For instance, diagnosing cancer typically involves analyzing cellular structures under a microscope. A single sample may contain millions of cells, and pathologists examine these for cytological and

architectural abnormalities(Zhao, Shuai, Ma, Liu, & Wu, 2022). However, due to the small size of some cells, even skilled pathologists can make misclassifications, which may lead to delayed or incorrect diagnoses contributing to higher mortality rates(Mazo, Bernal, Trujillo, & Alegre, 2018). Consequently, Accurate, computerised evaluation of medical images systems driven by reliable and effective machine learning algorithms are desperately needed.

In addition to providing more precise diagnoses and quicker diagnostic procedures, automated medical image analysis helps reduce the workload of radiologists and pathologists. Because they allow systems to learn from data, identify patterns, and make well-informed predictions or judgements, machine learning and deep learning techniques are frequently used in this field. Medical research and healthcare services have been significantly impacted by these technologies. However, the calibre of feature extraction techniques has a significant impact on how well machine learning algorithms perform in picture analysis. The automation potential may be limited because choosing the most pertinent features frequently still calls for specialised knowledge(Lu, Lu, & Zhang, 2019).

Images are usually processed by machine learning algorithms in two steps. First, important characteristics are found and extracted from the image using a manually created feature extraction technique. Following, a classification algorithm analyzes these features to categorize the image. This two-step approach makes the use of machine learning in medical image analysis both complex and time-consuming(Lu et al., 2019).

Deep learning algorithms have demonstrated superior performance over traditional machine learning algorithms in medical image analysis tasks. Their ability to automatically extract relevant features from images makes them particularly well-suited for automated medical diagnostics. In

image processing, deep learning models can be trained on vast datasets containing millions of images, enabling them to accurately identify and classify objects within medical images(Nguyen, Lin, Lin, & Cao, 2018; Vuola, Akram, & Kannala, 2019). The two main categories of deep learning are supervised and unsupervised learning. In medical image processing, supervised learning has proven to be particularly effective, frequently attaining performance levels on par with those of human experts. A ground truth dataset and prior knowledge of the anticipated results are prerequisites for this method. Learning the underlying relationships and structure in the input data is the main goal of supervised learning in order to precisely anticipate the related outputs(Ker, Wang, Rao, & Lim, 2017).

Unlike supervised learning, unsupervised learning identifies patterns in data without relying on labeled examples. It uncovers the underlying structure within a dataset using statistical techniques like clustering and density estimation. These algorithms are versatile and can be applied beyond tasks like classification, detection, and segmentation they are also useful for image compression, dimensionality reduction, denoising, super-resolution, and reconstruction(Ghahramani, 2003).

2.13.3 Medical Imaging Processing Workflows

As illustrated in Figure 20, medical image processing activities are often divided into three categories: classification, detection, and segmentation. Deep learning approaches can automate these processes, which are often completed by clinicians by hand, to cut down on processing time and enable predictive modelling for illness detection, including recognising cancer cells(Ker et al., 2017). Computer-aided diagnosis (CAD), another name for categorisation, is the process of grouping items according to predetermined criteria. Binary classification (differentiating between benign and malignant instances) or multi-class

classification (differentiating between lesion types or severity levels) may be used in this approach. Classification, for example, can be used to categorise cancer cells into distinct classes, such as mild, moderate, or severe, or to distinguish between normal and malignant cells(Montagnon et al., 2020). Detection, involves identifying the locations of objects within an image by drawing bounding boxes around them. For instance, detection can be used to identify tissue heterogeneities, such as anomalous lesions, by marking their regions with bounding boxes.

Figure 20

Utilising Deep Learning Methods for Important Medical Tasks: A) Categorisation, B) Identification, and C) Division

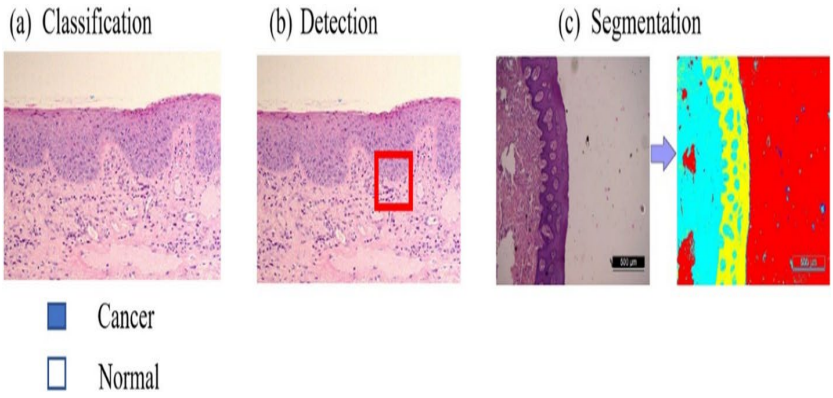

Source:(Das et al., 2018).

2.13.4 Architectures in Supervised Deep Learning

Convolutional neural networks (CNNs) are widely regarded as the leading architecture for supervised deep learning tasks, especially in image classification, detection, and segmentation(Talo, 2019) and The performance of CNNs in image classification has exceeded that of humans(Ker et al., 2017). These include the ability to extract features automatically from large datasets, require fewer parameters compared to

fully connected (dense) networks, and incorporate local connectivity and parameter sharing.

Local connectivity means that each hidden unit in a CNN is linked to a small region (receptive field) of the input image, rather than to the entire image. Parameter sharing refers to the practice of using the same set of weights (filters or kernels) across different parts of the image, reducing the number of parameters. In contrast, a dense network connects each neuron in one layer to every neuron in the subsequent layer, resulting in a large numeral of weights and in height computational charge due to the calculations of linear activations. By reducing both memory and parameter requirements, CNNs enhance computational efficiency(Aljuaid & Anwar, 2022). Convolutional, rectified linear activation function, normalisation, pooling, dropout, and fully connected layers make up a CNN.

Figure 21

A Neural Network Architecture Used for Image Classification. It Includes the Following Components: Input Image, Convolution Layer, Relu Layer, Pooling Layer, Fully Connected Layer, and Output Classes

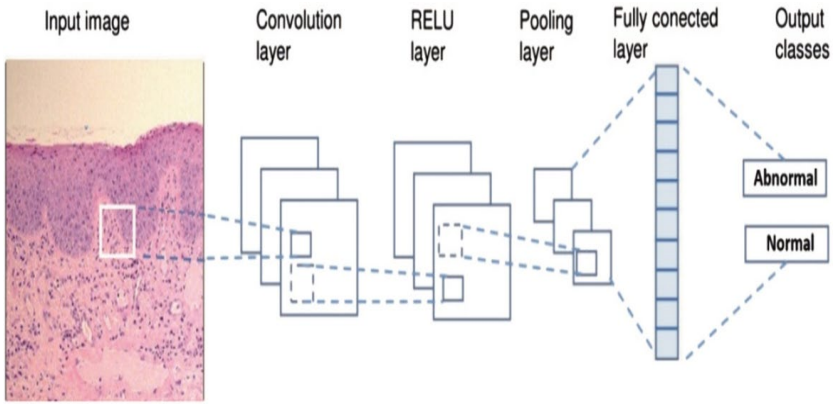

Source:(Ker et al., 2017).

2.13.5 Convolutional Layer Unit

The convolutional layer is the core building block of a Convolutional Neural Network (CNN), designed to automatically learn and extract key features from an input image. This is achieved through a convolution process a linear that calculates the blotch invention between a conventional of weights (known as kernel) and local regions of the input image (receptive fields). Each convolutional layer can use multiple filters, allowing it to generate multiple feature maps. Unlike traditional linear neural networks, Multidimensional arrays are usually used to arrange the weights in a CNN; 2D is used for greyscale images and 3D for colour images. Each filter captures a specific pattern or feature and is smaller than the input image, allowing it to slide across overlapping regions to detect these features throughout the entire image(Aljuaid & Anwar, 2022).

The filter is applied in the upper-left corner of the input data, starting the convolution process. The stride length is then used to determine how many steps it takes to travel horizontally to the right. The filter shifts downward by the same stride length and starts scanning from the left side again after it reaches the far-right edge. This pattern continues until the entire input is covered. The result of this operation is a feature map, as illustrated in Figure 22.

Figure 22

By generating the dot product between an 8 × 8 input image and a 3 × 3 filter, the layer of convolution extracts features from an input image, producing a 6 × 6 feature map. The filter's purpose in this instance is to identify vertical line features

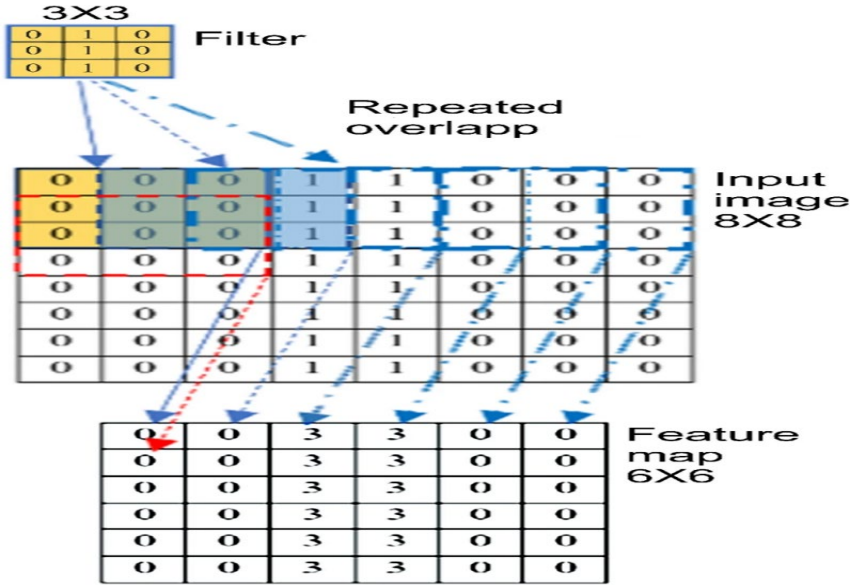

Source:(Fang, 2018).

The interaction between a filter and the input image in CNN result in a feature plot that typically minor than the original image. For instance, applying a 3 × 3 filter to an image with 64 pixels can produce a feature map containing just 36 pixels as shown in Figure 22. To address this size reduction, padding is used. Padding involves adding extra pixels with a value of zero around the image's edges, allowing every pixel the opportunity to appear at the center of the filter and helping preserve spatial dimensions.

CNNs often consist of multiple convolutional layers stacked together to learn increasingly complex patterns. The productivity from the initial convolutional layer, which captures low-level structures, can be combined with features from subsequent layers to build a richer representation. These combined low-level features form more complex, multi-feature

maps that can represent shapes. As the network deepens, the layers begin to capture higher-level, more abstract features—eventually recognizing specific patterns like faces or animals. In this way, early convolutional layers detect basic elements such as edges, dots, and corners, while deeper layers focus on complex structures and complete objects(Aljuaid & Anwar, 2022; Fang, 2018; Ker et al., 2017).

2.13.6 Rectified Linear Activation Function Unit Layer

The rectified linear unit (ReLU) is employed as an activation function in many convolutional neural networks, typically serving as the second layer following the convolutional layer. Introduced by Krizhevsky et al. in 2012, the ReLU function transforms its input by setting any negative values to zero and retaining all positive values. This behavior can be concisely captured by the mathematical expression.

$$f(x) = \max(0, x).$$

In this equation, for any input value xxx, the function outputs xxx if xxx is greater than zero; otherwise, it outputs zero.

The ReLU activation layer is commonly accustomed mitigate the vanishing gradient problematic, which occurs when a deep neural network struggles to propagate meaningful gradients from the output layer back to the earlier layers. Traditional S-shaped activation functions like sigmoid and tanh map input values to limited ranges (0, 1) for sigmoid and (-1, 1) for tanh. In deep networks, the derivatives of these functions can become very small during backpropagation, especially in the earlier layers. This leads to extremely slow or stalled weight updates, making it difficult for the model to learn effectively. ReLU helps avoid this issue by maintaining

stronger gradients and promoting faster convergence(Krizhevsky, Sutskever, & Hinton, 2012).

Figure 23

Graphically, Relu Appears as a Ramp Function: It Stays at Zero for all Negative Inputs and Increases Linearly Matching the Identity Function for All Positive Inputs

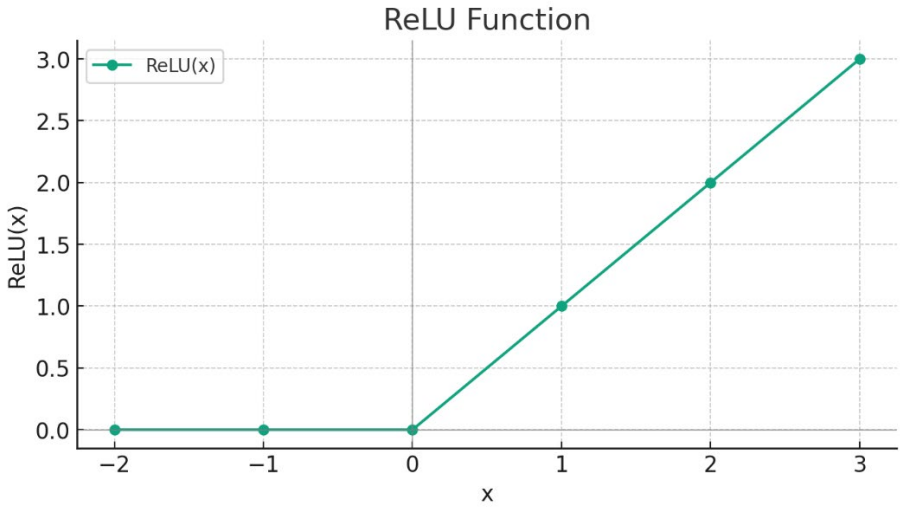

Source:(Krizhevsky et al., 2012).

2.13.6.1 Regularization Unit

Normalization helps scale miserable activation features to a limited range (e.g., 0 to 1), which prevents unbounded activation functions like ReLU from producing excessively large output values. This not only stabilizes the learning process but also speeds up the training of CNNs. Several normalization techniques exist, including local response normalization.(Krizhevsky et al., 2012), batch normalization(Ioffe, 2015), weight normalization(Salimans & Kingma, 2016), Layer normalization(Salimans & Kingma, 2016), group normalization, and weight standardization(Qiao, Wang, Liu, Shen, & Yuille, 2019). The first two are the most adapted in deep learning(Krizhevsky et al., 2012) and in

medical images processing(Beevi, Nair, & Bindu, 2019; Lu et al., 2019; Nguyen et al., 2018; Talo, 2019).

Figure 24

In-Layer Normalization Techniques for Training Very Deep Neural Networks

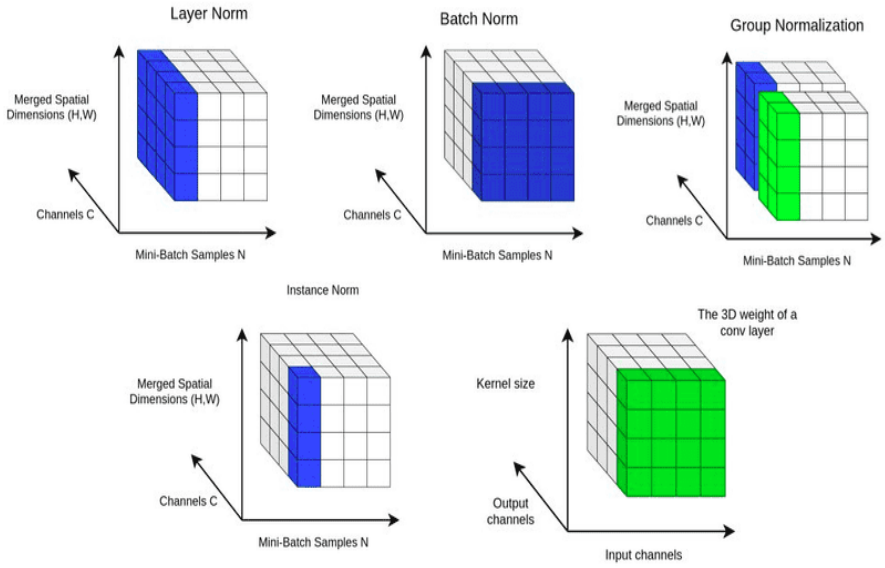

Source:(Adaloglou, 2020).

Limited Reply Normalization (LRN) is inspired by the neurobiological perception of adjacent inhibition, where an animated neuron suppresses the commotion of its neighboring neurons. This mechanism enhances local contrast and helps emphasize prominent features. In neural networks, LRN is used to improve generalization by normalizing the responses across adjacent neurons. It is typically applied after the activation function and works by using the local maximum activation value as a reference for normalization. Mathematically, LRN is defined as:

$$b_{x,y}^{i} = \frac{a_{x,y}^{i}}{\left(K + \alpha \sum_{j=\max\left(0,\frac{i-n}{2}\right)}^{\min\left(N-1,\frac{i+n}{2}\right)} \left(a_{x,y}^{j}\right)^{2}\right)^{\beta}},$$

Let i stand for the filter's output, which is also known as the feature map. The pixel intensity at position (x, y) in the feature map before to normalisation is represented by the value $a_{x,\gamma}$. N is the total number of feature maps, while n is the number of nearby maps taken into account. In the normalisation procedure, the established hyperparameters k, α (alpha), and β (beta) are employed.

By standardising each layer's inputs for each mini-batch, batch normalisation reduces internal covariate shift. The term "internal covariate shift" describes how adjustments to the weights in earlier layers during training result in modifications to the distribution of input characteristics. This shift can slow down convergence in deep learning models, as it necessitates a smaller learning rate, careful weight initialization, and makes training more challenging, especially when using saturating nonlinear activation functions(Ioffe, 2015).

Batch normalisation applies two learnable parameters to scale and shift the normalised values after normalising each minibatch according to the standard normal distribution. The batch normalization process is illustrated in Figure 25. While the distributions of the input features may change during training, batch normalization ensures that these changes are consistent in terms of mean and variance.

Figure 25

It Is Possible to Apply the Batch Normalisation Algorithm Before the Activation Function and After Each Convolutional Layer

Input: Values of x over a mini-batch: $\mathcal{B} = \{x_{1...m}\}$;
Parameters to be learned: γ, β
Output: $\{y_i = \mathrm{BN}_{\gamma,\beta}(x_i)\}$

$$\mu_{\mathcal{B}} \leftarrow \frac{1}{m}\sum_{i=1}^{m} x_i \qquad \text{// mini-batch mean}$$

$$\sigma^2_{\mathcal{B}} \leftarrow \frac{1}{m}\sum_{i=1}^{m}(x_i - \mu_{\mathcal{B}})^2 \qquad \text{// mini-batch variance}$$

$$\widehat{x}_i \leftarrow \frac{x_i - \mu_{\mathcal{B}}}{\sqrt{\sigma^2_{\mathcal{B}} + \epsilon}} \qquad \text{// normalize}$$

$$y_i \leftarrow \gamma\widehat{x}_i + \beta \equiv \mathrm{BN}_{\gamma,\beta}(x_i) \qquad \text{// scale and shift}$$

Source:(Ioffe, 2015).

2.13.6.2 Pooling Layer

Subsequently the ReLU layer, the pooling layer follows, which diminishes the spatial dimensions of the input illustration(Ker et al., 2017). Feature maps capture the exact positions of features in the input image, so even a small shift in a feature's location can result in a different feature representation. By reducing the spatial size, the pooling layer enhances the model's ability to recognize objects regardless of their exact location, making the feature representation more invariant to translation(Sun, Song, Jiang, Pan, & Pang, 2017).

The pooling layer carries out a pooling process that resembles a convolution operation(Sun et al., 2017). It computes the dot product

between a pooling filter and a fixed-size section of the feature maps, known as the pooling window. This pooling filter slides over the feature map, beginning at the top-left corner and moving rightward and downward by the stride length until it covers the whole map. Unlike convolution filters, pooling filters do not contain any learnable parameters. Common types of pooling operations include average pooling, max pooling, and global pooling.

Figure 26

Convolutional Neural Networks are a Modern Technique Widely Used in Computer Vision Applications, Where Pooling Plays a Crucial Role as an Integral Component of Deep CNN Architectures

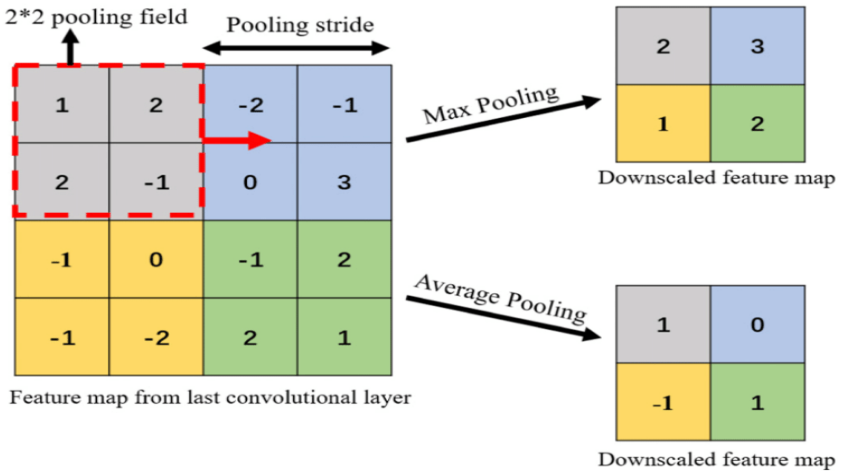

Source:(Yu, Wang, Chen, & Wei, 2014).

While max pooling chooses the highest value from the window's elements, average pooling determines the mean of the values within the pooling window. Conversely, global pooling reduces a feature map to a single value, usually indicating the strongest activation(Ker et al., 2017).

2.13.6.3 Dropout Unit

Dropout is a regularisation technique that lowers the model's complexity in order to solve the overfitting problem(Hinton, 2012). When

a CNN or other deep learning model is trained on an inappropriate dataset, it is said to be overfitting, which results in poor generalisation and reduced performance(Nguyen et al., 2018). It occurs when the model learns to memorize the noise in the training data rather than learning meaningful patterns. By randomly deactivating specific activation nodes during each training iteration based on the designated dropout rate, dropout helps to mitigate this. The forward pass and back-propagation do not include these inactive nodes(Beevi et al., 2019).

2.13.6.4 Fully Connected Layer

The fully connected layer, usually the last layer in a convolutional neural network, is in charge of label prediction for the input image. One kind of linear layer is a fully connected layer(Ker et al., 2017). A linear layer consists of an input layer, one or more hidden layers, and an output layer. In a linear layer, every neuron in a given layer is connected to every neuron in the subsequent layer(Ma & Lu, 2017). The computation for each linear layer is accomplished via the next formula:

$$g\left(wx + \mathrm{bias}\right),$$

Wherever *g* is a stimulation function (ReLU), *w* be situated a weight vector, and *x* is an input route.

For each class label, the output layer of the fully connected layer computes a probability score, which ranges from 0 to 1, using an activation function, like soft-max.

Figure 27

A Fully Connected Layer in a Deep Network

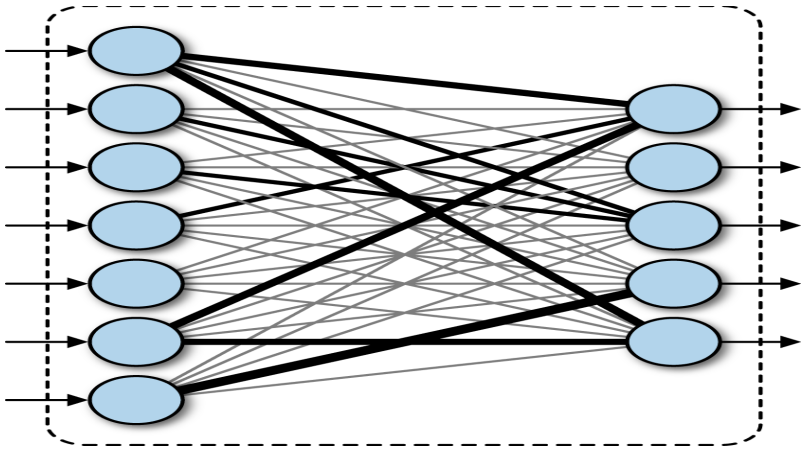

Source:(Ma & Lu, 2017).

Figure 28

A Multilayer Deep Fully Connected Network

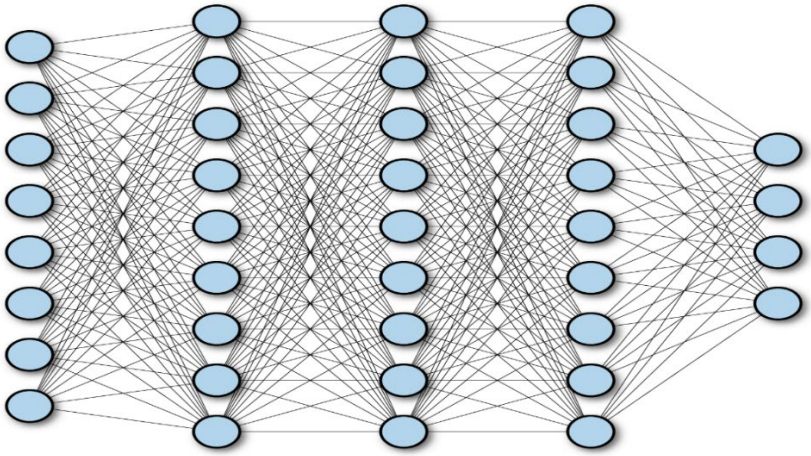

Source:(Ma & Lu, 2017).

2.13.7 Related work

In this study, focusing on the cutaneous leishmaniasis classification, microscopic images are mostly taken into consideration. In this section, studies in the literature are presented in detail.

2.13.7.1 Cutaneous leishmaniasis

The used microscopic images to analysis diverse cultures of cutaneous leishmania parasites. With diameters of roughly 1500–1300 pixels, the images caught and annotated the promastigote and amastigote stages of *Leishmania infantum*, *Leishmania major*, and *Leishmania braziliensis*. The work was a success in terms of creating parasite cultures, annotating images, and training the U-Net model. During training, a U-Net model was used for pixel-wise classification to solve class imbalances. Performance was evaluated using criteria such as precision, recall, and F1-score. The approach used to deal with class imbalance was critical for analysing pixel percentages per class and revealed information on image region distribution and representation The algorithm used accurately detected 82.3% of amastigote stages frequencies (Górriz et al., 2018). Using a dataset of 300 images gathered from 50 laboratory slides, this study attempted to develop an artificial intelligence-based technique to perform the automated diagnosis of leishmaniasis. These slides were obtained from patients at the Valfajr Clinic in Shiraz, Iran, and included 150 images from positive and 150 from negative leishmania slides. The Viola-Jones technique was used in the algorithm, which included three important steps: feature extraction, integral picture creation for quicker processing, and classification using Haar-like features. The classifier was trained using the AdaBoost algorithm after discriminative characteristics were chosen. The task of recognising amastigotes outside of macrophages

had a recall of 0.520 and a precision of 0.711 (Zare et al., 2022). The images have been captured with a smartphone at a microscopic magnification of 50 and exported in PNG format with an average resolution of 1320px x 1900px. The collection was 45 microscopic images in total. The resulting images were pre-processed, and pre-training was implemented for segmentation images of promastigotes and amastigotes forms for cutaneous leishmanials using the K-means algorithm, histogram thresholding, and the U-net structure. Individual precision and recall values for amastigotes phases were 61.07% and 87.90%, respectively (Limon Jacques, 2017).

2.13.7.2 Plasmodium parasites (malaria)

For the all-important work of identifying malaria by blood smear testing, 27,558 malaria blood smear images from the National Institute of Health (NIH) and expanded wielding rotation, zooming, and flipping then a two-stage technique was created. Initially, a U-Net method was used to precisely segment red blood cell clusters. Following that, faster R-CNN was used to recognize smaller cell objects inside these linked components. This technique was especially successful because of its versatility, with U-Net-derived cell-cluster masks guiding the detection process, resulting in higher true positive rates and lower false alarms. A unique CNN termed Attentive Dense Circular Net was introduced for the successful classification of malaria-infected red blood cells, inspired by residual and dense networks and including an attention mechanism. The revolutionary inclusion of attention mechanisms in ADCN allows it to focus on key features, resulting in a patient-level accuracy of 97.47% in the classification of infected RBCs(Kassim et al., 2020; Pattanaik, Mittal, Khan, & Panda, 2022). Pattanaik and colleagues introduced a novel approach, the Multi-Magnification Deep Residual Network (MM-

ResNet), tailored for the classification of malaria-infected blood smears captured using Android smartphones. Their study utilized a publicly available dataset consisting of 1182 field-stained images, encompassing three magnification levels: 200x, 400x, and 1000x. MM-ResNet is built upon convolutional layers, batch normalization, and ReLU activation functions, trained with a single pass through the data, reducing the data requirements. This model effectively mitigates the challenges posed by the low image quality, varying luminance, and noise inherent in smartphone-captured images, thanks to the utilization of residual connections and an abundance of filters. Remarkably, the proposed MM-ResNet achieved an impressive accuracy rate of 98.08% during five-fold cross-validation, demonstrating its efficacy in malaria blood smear classification across varying magnifications and challenging image conditions(Pattanaik et al., 2022).

2.13.7.3 Trypanosoma parasites

Traditional approaches for identifying Chagas disease's acute phase entail detecting *Trypanosoma cruzi* in peripheral blood slides using microscopy. An innovative approach analyses image tiles from these samples using MobileNet V2 convolutional layers, yielding 1,280-dimensional feature vectors that are input into a single-neuron classifier. Initial validation tests on a small 12-slide dataset achieved 96.4% accuracy but dipped to 72.0% on the 13th slide. Incorporating images from six additional slides, including thick blood samples, raised the accuracy to 95.4% on two further slides. Raster scans with overlapping windows efficiently reveal positive *Trypanosoma cruzi* occurrences in both blood smear and thick blood images, highlighting the method's potential to boost Chagas disease detection(Pereira et al., 2022). In this study, an innovative approach was developed for the automatic detection of the *Trypanosoma*

cruzi parasite in blood smears using machine learning techniques applied to mobile phone images. A total of 33 slides containing thin blood smears from Swiss mice infected with *T. cruzi* Y strain during the acute phase were analyzed. Images were standardized to 768 × 1,024 pixels^2 and parasites were segmented, with 100 × 100 pixels^2 regions around each parasite cropped based on manual annotations. Object features were extracted after converting from RGB to CIEL color space. To enhance performance and mitigate noise, Principal Component Analysis (PCA) was applied. Supervised learning classifiers such as Support Vector Machines (SVM), K-nearest neighbors (KNN), and Random Forest (RF) were employed due to their strong generalization with limited data. The dataset was split into training and test sets (4:1 ratio) and classified using the RF algorithm. The proposed method demonstrated significant precision (87.6%), sensitivity (90.5%), and an impressive "Area Under the Receiver Operating Characteristic (ROC) Curve" of 0.942. This research showcases the potential of automating image analysis through mobile devices, offering a cost-effective and efficient alternative to traditional optical microscope methods(Morais et al., 2022). A mobile bot application was created using deep learning to identify *Trypanosoma evansi* infection using 125 images of *T. evansi* obtained in an oil immersion field. In a one-stage learning technique, the YOLOv4-tiny model was used to categorise two particular parasite stages: "*Trypanosoma_evansi*_slender" and "*Trypanosoma_evansi*_stumpy." The addition of 20-degree rotational angles to the data resulted in remarkable performance metrics: 95% sensitivity, specificity, precision, accuracy, and F1 score with a misclassification rate of less than 5%. CIRA Bot, the simulation platform, produced equivalent results to computational trials, with an area under the ROC curve of 0.964 and a precision-recall curve of 0.962. This

breakthrough offers considerable potential for using thin-blood film evaluation to diagnose *T. evansi* infection(Jomtarak et al., 2023).

2.13.7.4 Cryptococcus neoformans

Web scraping was used in this study to collect data on microscopic images of both *C. neoformans* and non- *C. neoformans* using specified keywords such as "India-ink-stained smear of CSF," "*C. neoformans*," and others. These images were classified as positive or negative, yielding a dataset of 63 high-quality microscopic images for each category, which was later expanded to 1000 images. The study is supposed to recognise and classify *C. neoformans* images using a deep learning approach constructed on convolutional neural networks (CNN). Various frameworks and libraries were used to carry out model training, validation, testing, and evaluation. The VGG16 model, deemed cutting-edge, performed successfully, with an accuracy of 86.88% and a loss of 0.36203, respectively(Seyer Cagatan, Taiwo Mustapha, Bagkur, Sanlidag, & Ozsahin, 2022).

Chapter III

3 Materials and Methods

3.1 Framework of research

A prospective cohort research project was undertaken in the Al-Murqub regions (8,841.08 square kilometers) 32°19'12.7"N 13°57'39.2"E in the north-western part of Libya as presented in figure, which encompass five cities and roughly nine villages where ZCL is endemic. The samples have been collected in August, September, and October 2022. Zliten has indications of widespread Leishmania dissemination, as poses by cases reported there since 1980, but the other four cities and villages are thought to be new foci because cases there have only been reported since 2015, or less than 7 years prior to the current study. Furthermore, the Ethical Committee at Emhimid Almgarif polyclinic, situated in Al-Murqub district, provided approval to conduct the research (EMHC. REF. 1063. 08. 22).

Figure 29

This Image is a Satellite Map View of a Region in Northwestern Libya Centered on the Al Marqab District, with some Covered Colored Zones and Geographic Markers

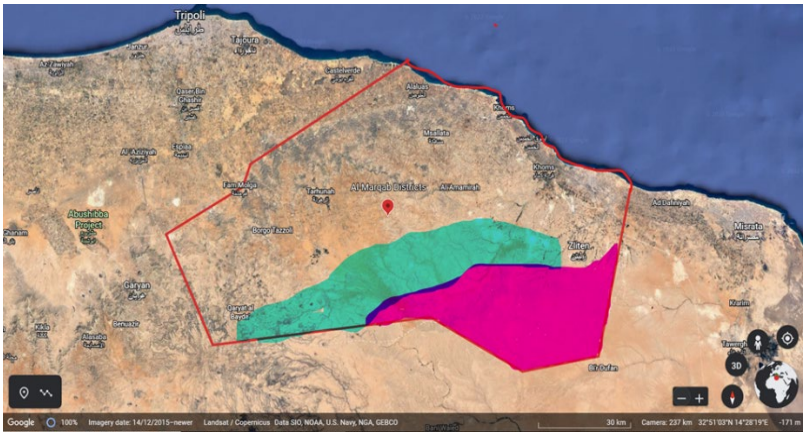

3.2 Slit-skin smear technique for infected leishmaniasis patients

The experiment followed to the Centers for Disease Control and Prevention (CDC) guidelines in carrying out the procedure. To begin, the skin was compressed to minimize bleeding before making a small upper dermal incision, just a few millimeters in length and depth. In the case of ulcerative lesions, the incision started at the active edge of the ulcer and extended several millimeters into the surrounding healthy skin. Tissue scrapings were then transferred onto a glass slide and left to air-dry.

Fixation was performed using 70% ethanol for two minutes, followed by another drying phase. Giemsa stain was applied to the slide, left to set temporarily, and then rinsed off with tap water. The prepared smear was examined under a microscope using immersion oil, and images of leishmanial amastigotes were captured using a mobile phone camera.

Figure 30

Cases of Cutaneous Leishmaniasis Observed among Patients Attending Emhimid Almgarif Polyclinic

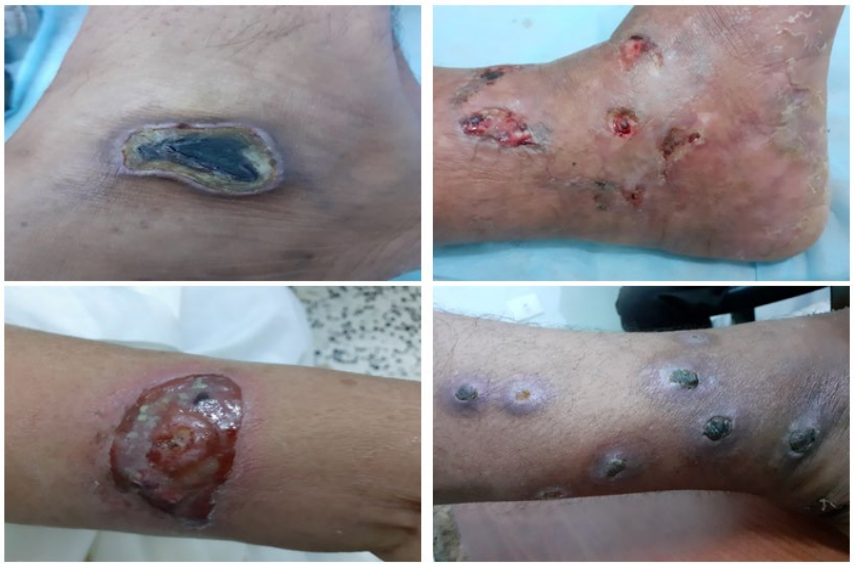

3.3 Non-infected images collection aimed at convolution neural network task

Dermatologists at Near East University Hospital prepared negative skin smears and negative blood smears. Afterwards, they were submerged in immersion oil and examined under a microscope. Hence, by using a phone camera, negative photos were gathered for use in the CNN model's classification task.

Figure 31

A Negative-Stained Microscopic Image of the Amastigote Stage of Cutaneous Leishmaniasis, Predominantly Featuring Various Red Blood Cells

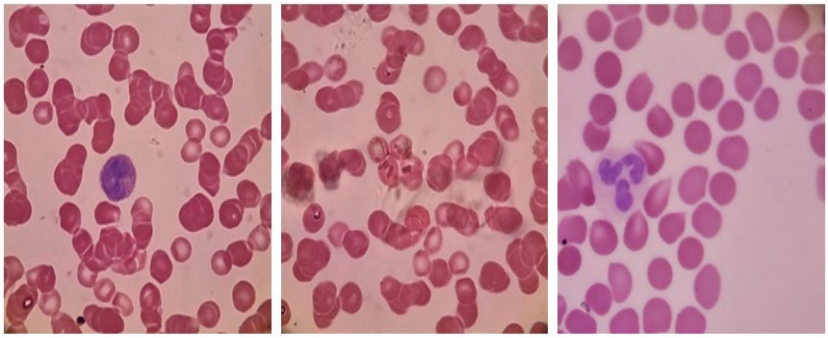

3.4 Image evaluation

Infectious disease and clinical microbiology physicians, in conjunction with a medical microbiologist, conducted the classification of all visual depictions, including both positive and negative representations images.

Figure 32

The Positive Amastigote Stage of Cutaneous Leishmaniasis, Characterized by Clusters of Amastigotes both Within Host Cells and in the Surrounding Extracellular Space

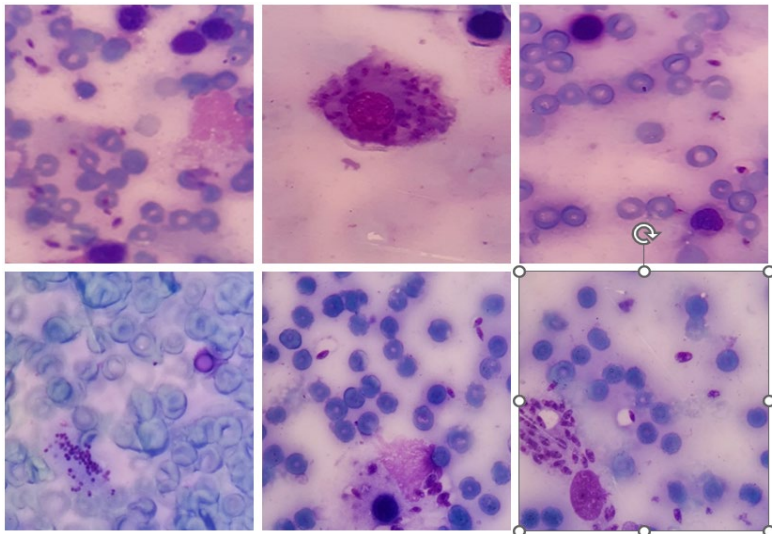

3.5 Images Classification used in the CNN into categories

In this work, a slit skin smear was conducted on leishmaniasis patients in order to produce positive images for the leishmanial parasite amastigote stage, which produced a total of 1,265 images. Moreover, negative images were prepared by dermatologists from negative skin lesions and blood smears of non-infected leishmaniasis patients, totaling 1431 images.

3.6 Study design

This study aimed to develop a cutaneous leishmania parasite diagnosis system using the images observed under a microscope. Considered pre-trained models, including MobileNet-v2, Xception, DenseNet-201, ResNet-101, and EfficientNet-b0, as shown below.

Figure 34

The Block Diagram of the Proposed System

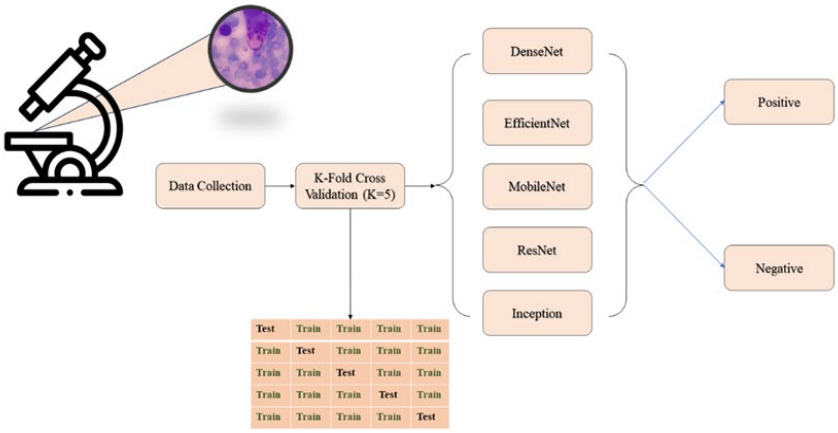

3.7 Pre-trained Models

The pre-trained models utilized in this study include MobileNet-v2, Xception, DenseNet-201, ResNet-101, and EfficientNet-b0. These models, originally trained on large-scale datasets, are well-regarded for their outstanding performance in various computer vision tasks. By leveraging their pre-trained weights, both training time and computational resources are significantly reduced, while model accuracy is enhanced. To further improve performance on the specific dataset used in this experiment, the models were fine-tuned accordingly.

3.7.1 DenseNet-201

DenseNet-201 is a deep convolutional neural network with 201 layers. It originates with a pre-trained version that has been trained on over a million images from the ImageNet dataset. This pre-trained model can classify images into 1,000 distinct categories, including everyday objects

like mice, keyboards, pencils, and a variety of animals. Through this extensive training, the network has learned rich and detailed feature representations across a wide array of image types. It expects input images to be sized at 224 by 224 pixels(Salim, Saeed, Basurra, Qasem, & Al-Hadhrami, 2023).

3.7.2 Xception

Xception is a 71-layer convolutional neural network that replaces traditional convolutions with depth-wise separable convolutions, allowing it to efficiently model both spatial and cross-channel correlations. A pretrained version of this model, trained on over a million images from the ImageNet database, is available and capable of classifying images into 1,000 distinct categories including everyday objects like keyboards, mice, and pencils, as well as various animals. Through this extensive training, Xception has learned robust and diverse feature representations. The network is designed to accept input images with a resolution of 299 by 299 pixels(Chollet, 2017).

3.7.3 MobileNet-v2

MobileNet-v2 is an efficient convolutional neural network architecture that utilizes depth wise separable convolutions, inverted residual blocks, and linear bottlenecks to optimize performance. It consists of 53 layers and is available as a pretrained model trained on the extensive ImageNet dataset, which includes over a million images. This pretrained version can classify images into more than 1,000 categories, such as keyboards, mice, pencils, and various animal species. The network is designed to work with input images sized at 224 by 224 pixels(Qayyum et al., 2023).

3.7.4 ResNet-101

ResNet-101 is a renowned model in the field of computer vision, designed to address challenges in image recognition tasks. It features a deep architecture comprising 104 convolutional layers, organized into 33 blocks. Out of these, 29 blocks are directly connected to their preceding counterparts, forming a hierarchical structure of interconnected layers. Extensive empirical studies have demonstrated that residual networks like ResNet-101 are easier to optimize and can effectively leverage increased depth to achieve higher accuracy. These conclusions have been validated through comprehensive experimentation on the ImageNet dataset, confirming ResNet-101's robustness and effectiveness in computer vision applications(A. Khan et al., 2022).

3.7.5 EfficientNet-b0

EfficientNet-B0 is widely recognized for its thoughtfully optimized and comprehensive network architecture. It achieves an impressive top-1 accuracy of 84.3% on the challenging ImageNet dataset, all while maintaining exceptional computational efficiency. Despite its performance, EfficientNet contains approximately 66 million parameters and performs nearly 37 billion floating-point operations per second (FLOPS). Compared to the most advanced CNNs, EfficientNet is about 8.4 times more compact and offers 6.1 times faster inference speed(Tan & Le, 2019).

3.8 Experimental Design

The configuration of the computer used to perform the experiments is 32 GB of RAM, an NVIDIA GeForce RTX 2080-Ti graphics processor, and an i9-9th Generation CPU. Each model is trained using the Adam

optimizer while maintaining a batch size of 10 and a learning rate of 0.001. Additionally, all models underwent training for a maximum of 30 epochs.

3.9 Performance Evaluation

We used Receiver Operating Characteristic curve analysis to evaluate the models' performances. The area under the curve was computed to determine the overall accuracy in both the training and validation datasets. Other performance indicators, such as sensitivity, specificity, precision, Matthew's correlation coefficient, Cohen's kappa, and F1-score, were examined to offer a more thorough assessment of the models' efficacy.

Accuracy is a metric that quantifies the proportion of right predictions to determine how accurately an algorithm predicts outcomes.

$$Accuracy = \frac{TP+TN}{TP+TN+FP+FN}$$

Sensitivity, often known as recall, assesses an algorithm's ability to recognise genuine positives within all positive cases.

$$Sensitivity = \frac{TP}{TP+FN}$$

Precision calculates the ratio of true positives compared to all predicted positives to determine the accuracy of an algorithm's positive predictions.

$$Precision = \frac{TP}{TP+FP}$$

Specificity, also known as the true negative percentage, is the number of actual negative observations correctly estimated by an algorithm out of all negative occurrences.

$$Specificity = \frac{TN}{TN+FP}$$

The F1 score is an indicator that combines precision and recall to provide a balanced evaluation of a model's accuracy for positive as well as negative predictions. The weighted harmonic mean of these two metrics is used to calculate it.

$$F1\ score\ = 2 \times \frac{Precision \times recall}{precision + recall}$$

The Matthews correlation coefficient estimates the effectiveness of a binary classification model on a scale of -1 to +1. A -1 score point to an inadequate classifier, while a +1 score indicates an accurate classifier. MCC is observed as a well-balanced metric since it considers both positive and negative results.

$$MCC\ = \frac{(TP \times TN) - (FP \times FN)}{\sqrt{(TP+FP)(TP+FN)(TN+FP)(TN+FN)}}$$

Cohen's kappa is a statistic used to quantify the level of agreement between a model's overall accuracy and the accuracy expected by chance. The kappa value, which is determined using Equation (10), falls between 0 and 1. A kappa value of 0 implies no agreement, whereas a kappa value of 1 shows complete agreement.

$$K = \frac{P_o - P_e}{1 - P_e}$$

Where P_o is the accuracy of the model (Equation (1)) and P_e is the hypothetical probability of chance agreement, computed as:

$$P_e = \frac{(TP+FN)(TP+FP) + (FP+TN)(FN+TN)}{(TP+TN+FP+FN)^2}$$

Chapter IV

4 Results

AI-based methods are transforming the healthcare sector by enhancing accuracy, efficiency, and reliability. With the use of supervised and unsupervised machine learning models, healthcare professionals can now perform intelligent, automated diagnoses. Over the past decade, numerous deep learning models—such as Convolutional Neural Networks (CNNs) and Artificial Neural Networks (ANNs)—have been developed and applied in healthcare to support disease diagnosis. In recent years, deep learning models have been widely applied for the detection of various diseases. This study focused on evaluating five pre-trained deep learning models for classifying microscopic images related to cutaneous leishmaniasis into positive and negative categories. The performance of each model was assessed using five-fold cross-validation, with the results reported as the average performance across all five folds.

4.1 Model Performance Monitoring During Training

The image below was captured during the training phase of our model for the detection of amastigote forms in cutaneous leishmaniasis. It illustrates the performance monitoring of five different architectures employed for the diagnosis of cutaneous leishmaniasis.

Figure 35

How Well the Model is Learning, Training Accuracy Fluctuates Likely Due to Mini-Batch Variation but High From 85% To 100%) And Validation Accuracy (Black Dots) is Fairly Stable around 85-90%, Indicating Decent Generalization

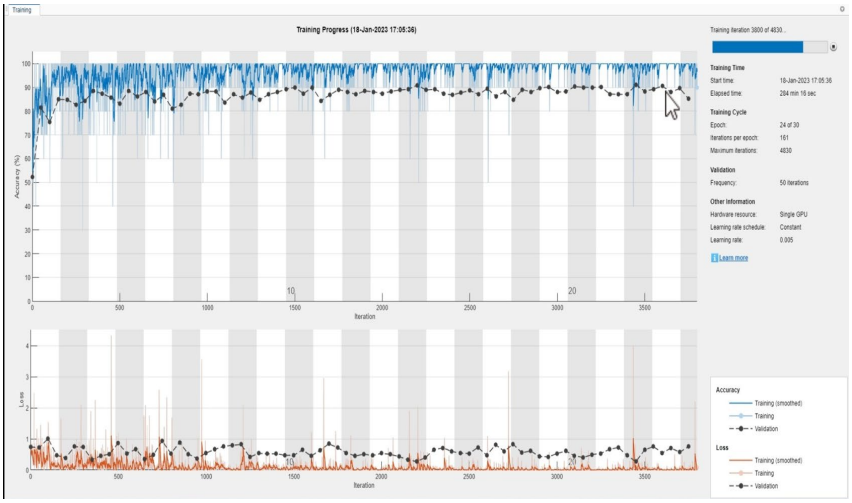

Top Graph shows Accuracy which was represented in blue line that training accuracy (per iteration) and light blue line was Flattened training accuracy (averaged to diminish noise). In addition, black dotted line presented Validation accuracy. On the other hand, bottom Graph shows the loss, whereas orange line represented training loss (per iteration) and light orange line represented smoothed training loss then black dotted line showed validation loss. Consequently, interpretation was high accuracy and low loss that mean model was performing well.

Table 4.

Expressions Epoch and Iteration Overview with Hardware and Hyperparameter Details

Training Details	
Training Iteration	3800 out of 4830 total iterations completed
Elapsed Time	284 minutes (about 4.7 hours)
Epoch	Currently on epoch 24 out of 30
Iterations per Epoch	161
Validation Frequency	Every 50 iterations
Learning Rate	0.005 (constant)
Hardware	Training is being performed on a single GPU

4.2 Deep Learning-Based Analysis of Microscopic Images in the Amastigote Stage of Cutaneous Leishmaniasis

Tables 1–5 demonstrate the results of the considered deep learning models when applied to microscopic images of the cutaneous leishmanial amastigote stage. The proportion of properly identified cases is measured by accuracy, whereas the F1-score combines precision and recall to provide a balanced assessment of model performance. The MCC and the Cohen's kappa coefficient were employed as assessment measures.

Table 5.

The Performance Metrics of the Densenet-201 Deep Learning Model Across Five Cross-Validation Folds, along with the Average of each Metric. It Assesses How Well the Model Performs on a Classification Task Using Several Key Evaluation Metrics

	DenseNet-201							
Folds	ACC	SV	SP	PPV	NPV	F1-Score	MCC	CK
Fold1	0.98886827	1	0.97902098	0.97683398	1	0.98828	0.977927	0.977683
Fold2	0.99074074	1	0.98233216	0.98091603	1	0.99037	0.981624	0.981455
Fold3	0.99072356	1	0.98251748	0.98062016	1	0.99022	0.981568	0.981399
Fold4	0.99072356	0.98479087	0.99637681	0.99615385	0.98566308	0.99044	0.981492	0.981431
Fold5	0.99628942	0.9916318	1	1	0.99337748	0.9958	0.992504	0.992476
Average	0.99146911	0.99528453	0.98804949	0.9869048	0.99580811	0.99102	0.98302	0.98289

Table 6.

A Performance Evaluation of the Efficientnet-B0 Model Using A 5-Fold Cross-Validation Method Across Multiple Metrics. each Row Corresponds to a Specific Fold (Fold1 to Fold5), with the Last Row Showing the Average of all Folds

	EfficientNet-b0							
Folds	ACC	SV	SP	PPV	NPV	F1-Score	MCC	CK
Fold1	0.99814471	1	0.9965035	0.99606299	1	0.99803	0.99628	0.99628
Fold2	0.99074074	1	0.98233216	0.98091603	1	0.99037	0.98162	0.98146
Fold3	0.99072356	0.98418972	0.9965035	0.996	0.98615917	0.99006	0.98143	0.98136
Fold4	0.9851577	0.99239544	0.97826087	0.97752809	0.99264706	0.98491	0.97042	0.97031
Fold5	0.98886827	0.9748954	1	1	0.98039216	0.98729	0.97764	0.97739
Average	0.990727	0.99029611	0.99072	0.99010142	0.99183968	0.99013	0.98148	0.98136

Table 7.

The Summarizes the Performance of the Mobilenet-V2 Model Across Five Different Data Folds Using Several Evaluation Metrics. Here's a Breakdown of the Content and What each Column Represents

	MobileNet-v2							
Folds	ACC	SV	SP	PPV	NPV	F1-Score	MCC	CK
Fold1	0.98144712	0.98418972	0.97902098	0.97647059	0.98591549	0.98031	0.9628	0.96277
Fold2	0.99074074	0.9844358	0.99646643	0.99606299	0.98601399	0.99022	0.98149	0.98143
Fold3	0.99257885	0.99604743	0.98951049	0.98823529	0.99647887	0.99213	0.98514	0.98511
Fold4	0.98144712	0.98479087	0.97826087	0.97735849	0.98540146	0.98106	0.96291	0.96288
Fold5	0.99072356	0.9832636	0.99666667	0.99576271	0.98679868	0.98947	0.98124	0.98118
Average	0.98738748	0.98654548	0.98798509	0.98677802	0.9881217	0.98664	0.97471	0.97467

Table 8.

The Cross-Validation Performance of the Resnet-101 Model Across Five Different Folds Using Various Classification Metrics. These Metrics Assess the Model's Ability to Correctly Identify and Distinguish Between Classes. Each Row Corresponds to a Single Fold (Fold1 Through Fold5), and the Final Row Shows the Average Performance Across all Folds

	ResNet-101							
Folds	ACC	SV	SP	PPV	NPV	F1-Score	MCC	CK
Fold1	0.97959184	0.96442688	0.99300699	0.99186992	0.96928328	0.97796	0.95929	0.95896
Fold2	0.98518519	1	0.97173145	0.96981132	1	0.98467	0.97077	0.97034
Fold3	0.98144712	0.98023715	0.98251748	0.98023715	0.98251748	0.98024	0.96275	0.96275
Fold4	0.99072356	0.99239544	0.98913043	0.98863636	0.99272727	0.99051	0.98144	0.98144
Fold5	0.98886827	0.9874477	0.99	0.9874477	0.99	0.98745	0.97745	0.97745
Average	0.9851632	0.98490143	0.98527727	0.98360049	0.98690561	0.98417	0.97034	0.97019

Table 9.

Summarizes the Performance Metrics of the Xception Model Evaluated Across Five Folds (Fold1 to Fold5) Using Cross-Validation. Here's a Breakdown of each Metric and What the Numbers Indicate

	Xception							
Folds	ACC	SV	SP	PPV	NPV	F1-Score	MCC	CK
Fold1	0.987012987	0.976284585	0.996503497	0.995967742	0.979381443	0.986028	0.974068	0.973898
Fold2	0.994444444	0.996108949	0.992932862	0.992248062	0.996453901	0.994175	0.988872	0.988865
Fold3	0.975881262	0.960474308	0.98951049	0.987804878	0.965870307	0.973948	0.951828	0.951504
Fold4	0.987012987	0.988593156	0.985507246	0.984848485	0.989090909	0.986717	0.97402	0.974013
Fold5	0.994434137	1	0.99	0.987603306	1	0.993763	0.988801	0.988738
Average	0.987757163	0.9842922	0.990890819	0.989694495	0.986159312	0.986926	0.975518	0.975404

4.3 Comparison of pre-trained model performances

Figure 36

The Performance Evaluation of CNN Architectures Based on Accuracy, Sensitivity and specificity of Five Different Deep Learning Models. Here's A Detailed Breakdown

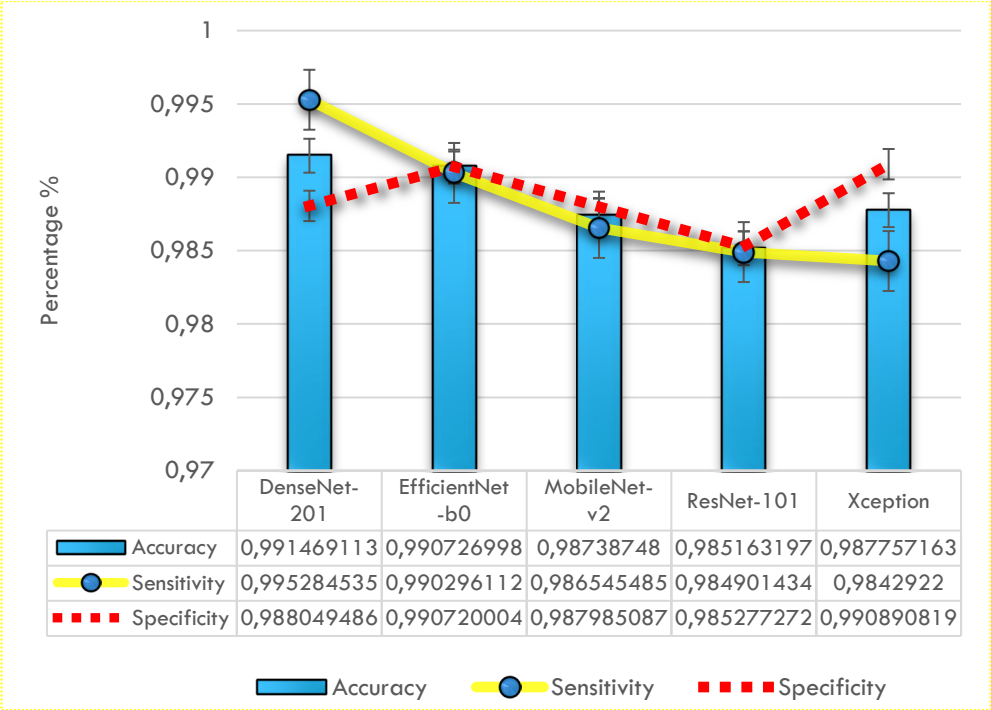

The bar chart illustrates a comparative analysis of classification accuracy, expressed as percentages, across five deep learning models: DenseNet-201, EfficientNet-B0, MobileNet-V2, ResNet-101, and Xception. The vertical axis represents accuracy values ranging from 97.8% to 99.4%, while the horizontal axis denotes the respective model names. Error bars are incorporated to reflect variability measures, such as standard deviation or confidence intervals, thereby providing insights into each model's stability and consistency.

Among the evaluated models, DenseNet-201 demonstrated the highest performance, achieving an accuracy of approximately 99.15%, followed closely by EfficientNet-B0 with an accuracy of around 99.07%. These two models exhibit superior classification performance relative to the others. Xception and MobileNet-V2 yielded moderate results, with accuracies of approximately 98.75% and 98.74%, respectively marginally lower than those of DenseNet-201 and EfficientNet-B0. In contrast, ResNet-101 recorded the lowest accuracy at approximately 98.52% and displayed one of the largest error bars, suggesting greater variability and potentially reduced reliability in the specific task under investigation.

The interpretation of the graph offers a clear comparative analysis of sensitivity performance among the evaluated models. Especially, DenseNet-201 demonstrates the highest sensitivity (~99.53%), indicating superior effectiveness in correctly identifying positive cases. A gradual decline in sensitivity is observed from DenseNet-201 to Xception. This overall trend suggests that DenseNet-201 and EfficientNet-b0 exhibit comparatively better sensitivity performance than MobileNet-v2, ResNet-101, and Xception. Despite the presence of variability, as illustrated by the error bars, all models maintain consistently high sensitivity values (>98%), underscoring their robustness in positive case detection.

The graph presents the specificity values of five distinct models, accompanied by error bars to indicate variability. Among these, EfficientNet-b0 and Xception exhibit the highest specificity, both marginally exceeding 99.0%, reflecting superior capability in accurately identifying negative cases. In contrast, ResNet-101 demonstrates the lowest specificity at 98.52%, implying a comparatively higher false positive rate. Despite this variation, all models maintain high specificity values (greater than 98.5%), underscoring their overall effectiveness.

Notably, Xception marginally outperforms EfficientNet-b0, suggesting it may be the most effective model in terms of specificity. Although the error bars reflect some degree of variability, the observed differences remain relatively minor, indicating consistent performance across all models.

Figure 37

The Positive Predictive Value (PPV), Negative Predictive Value (NPV) and F1 Scores a Metric Commonly Used in Medical Classification Tasks to Measure the Accuracy of Positive Predictions Across Five Different Deep Learning Models

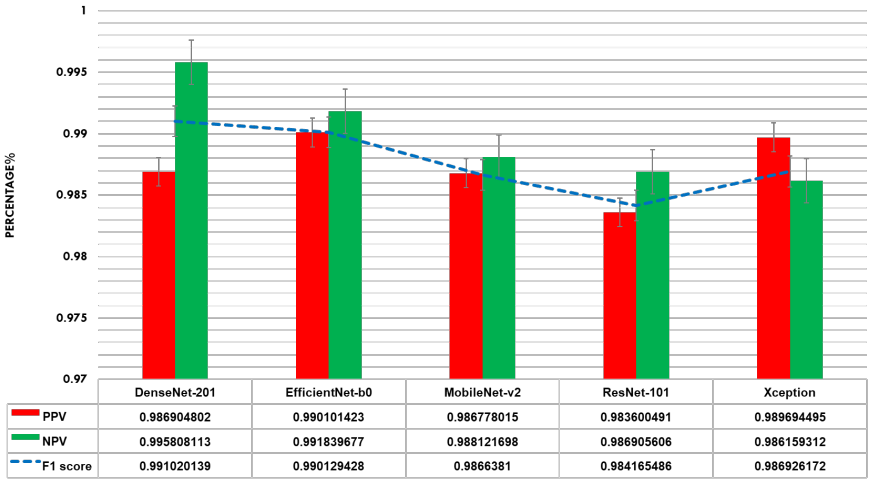

	DenseNet-201	EfficientNet-b0	MobileNet-v2	ResNet-101	Xception
PPV	0.986904802	0.990101423	0.986778015	0.983600491	0.989694495
NPV	0.995808113	0.991839677	0.988121698	0.986905606	0.986159312
F1 score	0.991020139	0.990129428	0.9866381	0.984165486	0.986926172

EfficientNet-B0 demonstrates the highest PPV, achieving approximately 99.01%, indicating greater precision in identifying true positive cases. In contrast, ResNet-101 records the lowest PPV at approximately 98.36%, reflecting a slightly lower precision in its positive predictions. Xception and DenseNet-201 also exhibit strong performance, both attaining PPVs exceeding 98.96%. Meanwhile, MobileNet-V2 shows comparable performance to DenseNet-201, although with a slightly lower PPV.

The reported values are relatively high, indicating that the models exhibit strong performance in accurately predicting negative outcomes.

Particularly, there is a progressive decline in NPV observed from DenseNet-201 to Xception, suggesting that DenseNet-201 demonstrates higher performance among the evaluated architectures. This comparison is particularly relevant in a diagnostic context, where high NPV is critical for reliably excluding disease. Therefore, the chart effectively highlights the comparative diagnostic utility of the models, with an emphasis on their capacity to correctly identify negative cases an essential consideration in clinical decision-making.

The best-performing model in this evaluation is DenseNet-201, achieving the highest F1 score of approximately 99.1%, thus demonstrating higher performance among the tested architectures. Closely following DenseNet-201 is EfficientNet-B0, which also accomplishes an F1 score near 99.1%. MobileNet-V2 exhibits slightly lower performance with an F1 score of approximately 98.7%, while ResNet-101 follows with a score of around 98.5%. On the other hand, the lowest-performing model is Xception, registering an F1 score of approximately 98.7%. Despite being the least effective in this comparison, Xception still maintains a high level of performance. Overall, the consistently elevated F1 scores across all models indicate their strength and effectiveness in addressing the classification task.

Figure 38

The Matthews Correlation Coefficient Values and of Cohen's Kappa, Ranging from Approximately 0.955 to 0.99. MCC is a Measure of the Quality of Binary Classifications, with Values Closer to 1 Indicating Better Performance

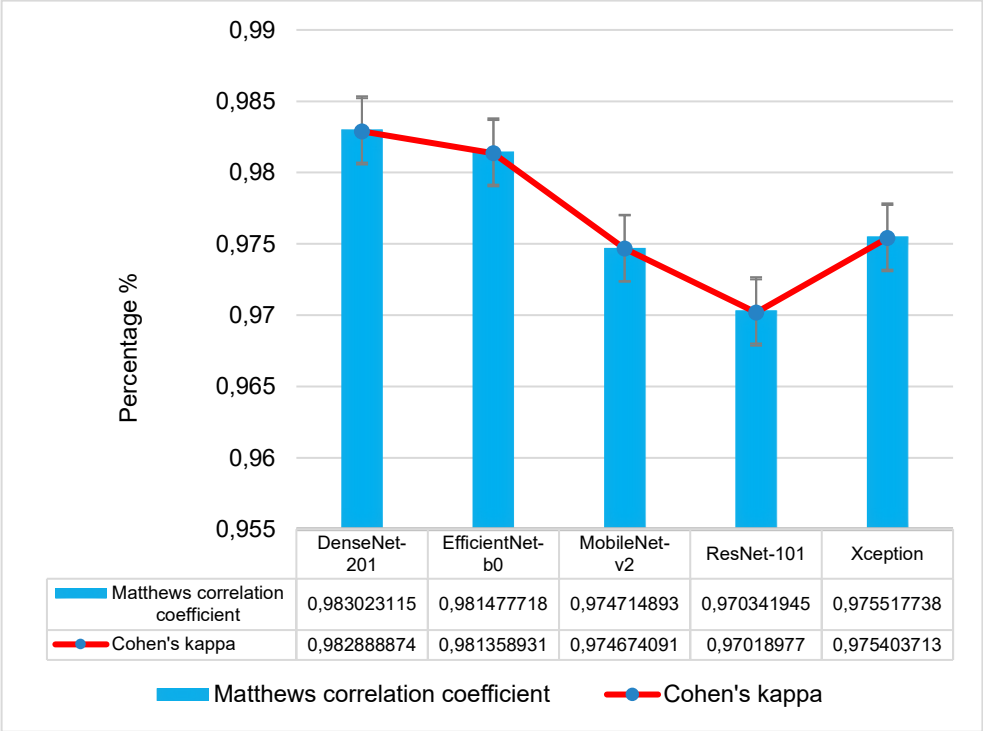

DenseNet-201 demonstrates the highest MCC among the models evaluated, indicating superior classification performance relative to the others. EfficientNet-B0 and MobileNet-V2 also exhibit strong performance, albeit slightly lower than that of DenseNet-201. In contrast, ResNet-101 and Xception yield comparatively lower MCC values, suggesting reduced effectiveness for the specific classification task under consideration. Overall, the comparative analysis, as illustrated in the accompanying graph, provides valuable insight into the relative efficacy of various neural network architectures, with MCC serving as a robust metric for performance evaluation.

DenseNet-201 demonstrates the highest Cohen's Kappa coefficient among the evaluated models, indicating superior agreement and overall classification performance. Conversely, the Xception model exhibits the lowest Kappa value, suggesting comparatively weaker performance. The inclusion of error bars facilitates the assessment of performance variability; models with narrower error bars are typically considered more consistent and reliable in their predictions.

4.4 Confusion Matrix Evaluation for Predictions from Five Pre-Trained Models

Figure 39

Explaining a Confusion Matrix That is a Useful Tool for Evaluating the Performance of a Classification Model, particularly in the Framework of Classifying Microscopic Images. In Our Case, we Have Confusion Matrices for Different Pre-Trained Models: Xception, Densenet 201, Resnet101, Efficientnet B0, and Mobilenet V2

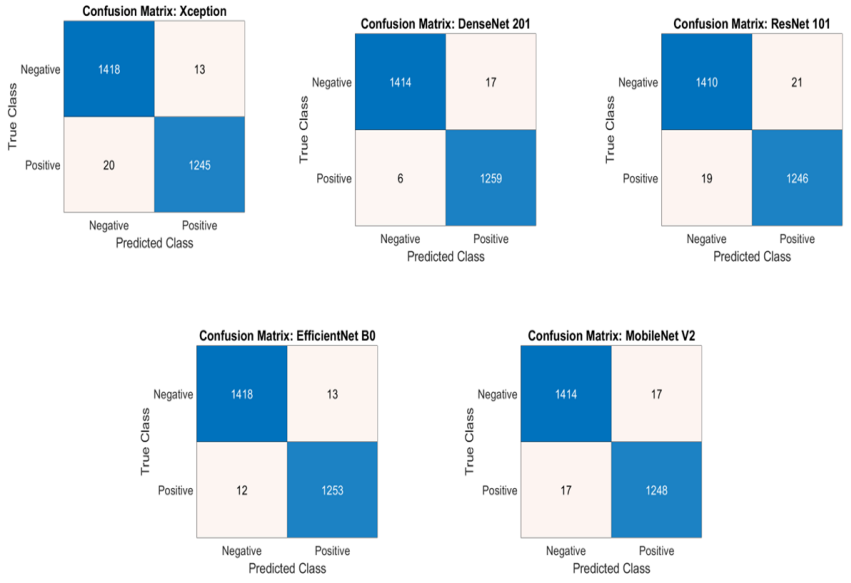

To understanding the Confusion Matrix where Each confusion matrix displays four key components:

- True Positives (TP) is correct predictions of the positive class.
- True Negatives (TN) is correct predictions of the negative class.
- False Positives (FP) incorrect predictions where the model predicted the positive class incorrectly.
- False Negatives (FN) incorrect predictions where the model predicted the negative class incorrectly.

The Xception model demonstrated advanced predictive performance, characterized by high accuracy and minimal misclassifications, indicating robust classification capabilities. Similarly, DenseNet-201 achieved performance metrics comparable to Xception, although with a slightly elevated number of false negatives, while still maintaining overall effectiveness. In contrast, ResNet-101 exhibited a balanced distribution between true positives and true negatives, with a low false positive rate but a relatively higher false negative rate, suggesting potential areas for improvement in the detection of positive cases. EfficientNet-B0 showed moderately lower performance, with a visible increase in false negatives, indicating a tendency to overlook certain positive cases. MobileNet-V2 displayed results comparable to EfficientNet-B0, achieving a reasonable balance yet highlighting further opportunities for enhancement. Overall, models such as Xception and DenseNet-201 outperformed others in the classification of microscopic images, evidenced by high true positive rates and low false positive rates. The confusion matrices provide valuable insights into each model's strengths and limitations, particularly emphasizing the importance of minimizing false negatives to enhance the accurate identification of positive cases.

4.5 Evaluation of ROC and AUC for Five Pretrained Models

Figure 40

A Series of Receiver Operating Characteristic (ROC) Curves for Different Neural Network Architectures: Xception, Densenet 201, Resnet 101, Efficientnet B0, and Mobilenet V2

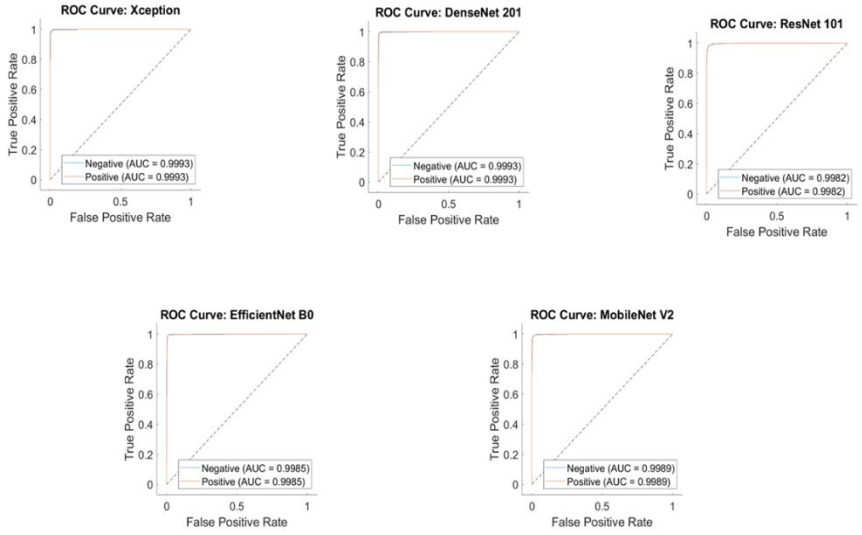

Receiver Operating Characteristic Curve (ROC)

- False Positive Rate (FPR): the proportion of negative cases incorrectly classified as positive.
- True Positive Rate (TPR): also known as sensitivity or recall, the proportion of actual positive cases correctly identified.

Area Under the Curve (AUC)

The AUC value indicates the model's ability to distinguish between classes.

- AUC = 1: Perfect model.
- AUC = 0.5: No discrimination (random guessing).
- AUC < 0.5: Indicates a model that performs worse than random guessing.

Each model is associated with an Area Under the Curve (AUC) value, which approaches 1.0, indicative of high discriminative performance. The Receiver Operating Characteristic (ROC) curves are plotted relative to the diagonal reference line (dashed), which represents the performance of a random classifier. The greater the deviation of a model's curve from this diagonal, the stronger its classification capability. All models exhibit strong performance in distinguishing between positive and negative cases, as evidenced by their corresponding AUC values. These values assist as a quantitative metric for comparing the relative effectiveness of the models.

4.6 Grad-CAM-Based Visualization of Cutaneous Leishmania Amastigote Stages: Positive and Negative Classification

Figure 41

Compares the Visualisations of the Negative and Positive Cutaneous Leishmania Amastigote Stages Using Grad-CAM (Gradient-Weighted Class Activation Mapping). Convolutional Neural Networks (Cnns) are Frequently Interpreted Using Grad-CAM, Which Highlights the Areas of the Input Image that are Crucial to the Model's Prediction

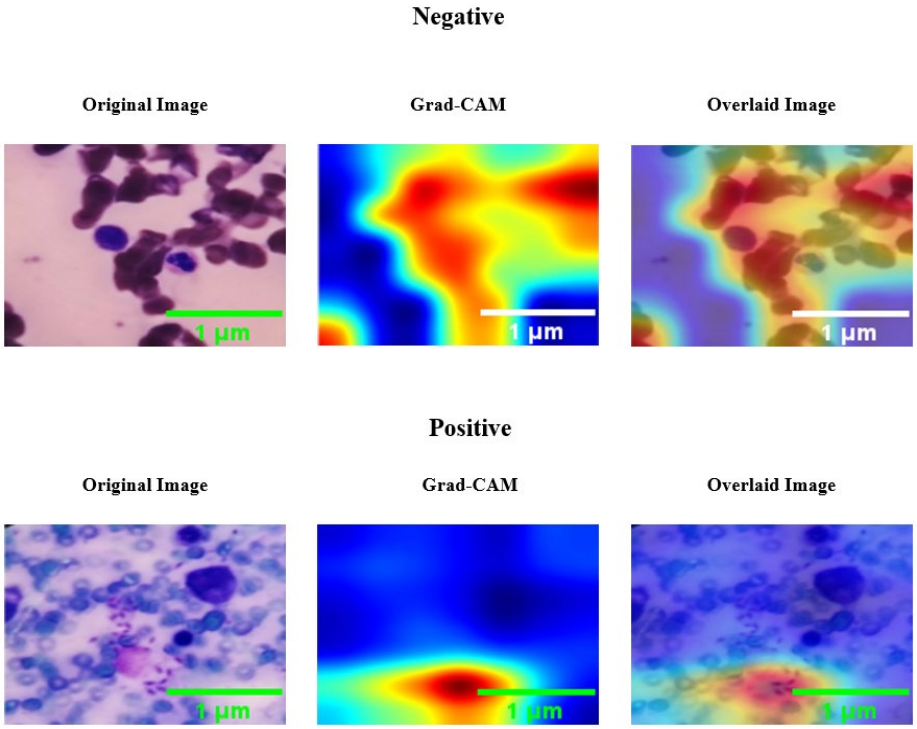

The top row represented a negative case, whereas the original image That was the raw microscopic image used as input to the model. It showed cutaneous leishmania's amastigote stage under magnification, with a scale bar indicating 1 µm for reference. Correspondingly, Grad-CAM was represented as a heatmap where the areas the model focused on to predict a negative result and red/yellow areas were of high importance (strong model attention). Therefore, blue areas showed low importance (little

attention). Furthermore, the overlaid image represented the Grad-CAM heatmap, which was overlaid on the original image to visualise which parts of the image influenced the model's prediction. The model likely paid attention to a specific cluster of cells or features to decide it was a negative case.

The bottom row characterised a positive case, while the original image showed another raw microscopic image, but this time corresponding to a positive case of cutaneous leishmania's amastigote stage. In addition, Grad-CAM presented a heatmap highlighting the model's focus for predicting a positive result. The red area in the bottom center shows where the model found significant features suggesting a positive diagnosis. Moreover, the overlaid image combined the Grad-CAM with the original image to help interpret the model's reasoning. The model focuses on different cellular regions compared to the negative case.

Chapter V

5 Discussion

When we compared our findings to those of prior research on the amastigote stage of CL, Górriz's research focused on the promastigote and amastigote stages of *Leishmania infantum*, *Leishmania major*, and *Leishmania braziliensis*, and they used the U-Net model to train. A model had a precision of 0.757, which means that 75.7% of the predicted amastigote of cutaneous leishmania occurrences were right. With a recall of 0.823, the model correctly detected 82.3% of the actual amastigote occurrences(Górriz et al., 2018). Zare et al. created The Viola–Jones approach algorithm with an adaboost optimiser algo-rithm using a dataset of 300 images of positive and negative cutaneous leishmaniasis. The results showed that detecting macrophages infected with leishmania parasites had a 65% recall and 50% precision, and identifying amastigotes outside of macrophages had a 52% recall and 71% precision(Zare et al., 2022). Limon Jacques captured microscopic images with a smartphone at a magnification of 50 were pre-processed and subjected to pre-training using the K-means algorithm, histogram thresholding, and the U-net structure for segmenting promastigotes and amastigotes forms in cutaneous leish-maniasis. The precision and recall values for amastigotes stages were 61.07% and 87.90%, individually, based on the segmentation data. However, the precision and re-call scores for promastigotes were 91.0% and 47.14%, respectively(Limon Jacques, 2017).

In the study conducted by Maqsood et al. experimental evaluations are per-formed on the benchmark NIH Malaria Dataset, and the results reveal that the pro-posed Xception model is 0.9494% accurate and 0.9494% F1-score in detecting malaria from the microscopic blood smears. Meanwhile, Densenet-201 achieved 0.9054% ac-curacy and 0.9052% F1-score(Maqsood, Farid, Khan, & Grzegorzek, 2021). Biswal

et al. conducted an experiment with the Mo-bileNet-v2 neural network model on a Kaggle dataset of 12,444 augmented images ex-hibiting diverse blood cell types classified into four separate classes. Pre-processing processes included data refining and image resizing to a consistent size of 128 × 128 pixels. In the study, two adaptive optimization methods, Adam and stochastic gradi-ent descent (SGD), were used. The Adam optimiser produced an accuracy of 0.920, while the SGD optimiser provided an accuracy of 0.90, reflecting how well the model performed in categorizing the blood cell images(Biswal, Mallick, Panda, Chae, & Mishra, 2023). The research was carried out by Hiremath an investigation was conducted to assess the efficacy of various models for the classification of histopathological breast cancer images into benign and malig-nant categories at different magnification levels, specifically at 40×, 100×, 200×, and 400×. The models employed for this task included EfficientNet-b0 and EfficientNet with HSV colour transformation. The research utilised an openly accessible dataset sourced from Kaggle, comprising a total of 7909 images, with 2480 representing benign cases and 5429 representing malignant cases. The performance evaluation of Effi-cientNet-b0 was based on the accuracy metric, resulting in classification accuracy rates of 86%, 88%, 88%, and 83% for the respective magnification levels(Hiremath, 2022). Xu and his colleagues analyse a dataset consisting of 4011 IVCM images captured from a total of 48 eyes. These eyes were categorised into different groups, including 35 eyes with keratitis, 7 eyes with dry eyes, and 6 eyes with pterygium. The original IVCM im-ages were standardised to a resolution of 224 × 224 pixels. Deep Transfer Learning was conducted using various neural network models, with one of them being Residual Network-101. The findings revealed that ResNet-101 exhibited a notable level of accuracy, achieving a score of 0.9283(Xu et al., 2021).

In the study conducted by Sanghvi et al. DenseNet201-based deep learning approach to detect COVID-19 and pneumonia from chest x-ray images. It leveraged a freely available Kaggle database containing 15,153 images classified into three categories: COVID-19 positive (3,616), viral pneumonia positive (1,345), and normal (10,192). In detecting pneumonia, the model achieved 99.1% accuracy, 98.5% sensitivity, and 98.95% specificity(Sanghvi et al., 2023). When we applied to predicting cutaneous leishmaniasis cases, our model demonstrated 99.14% accuracy, 98.52% sensitivity, and 98.80% specificity.

The EfficientNet-B0 architecture was utilised due to its balance of computational efficiency and performance. The dataset used in work comprises 40 microbial classes, drawn from a subset of the DIBaS dataset and supplemented with additional images collected by the authors to form a unified dataset. The EfficientNet-B0 model demonstrated higher performance, achieving a training accuracy of 100% and a loss value of 0.0897 while requiring only 140 iterations for conjunction(Tripathi, Kumar, Sharif, Chand, & Santosh, 2024). In comparative evaluations, our proposed model attained a training accuracy of approximately 99.07%, indicating its strong potential for the accurate diagnosis of cutaneous leishmaniasis. In 2024 Nirupama and his colleague presented novel model for skin disease classification using advanced deep learning methodologies. The proposed architecture incorporates the MobileNet-V2 infrastructure and is trained on four diverse and widely known datasets: the PH2 dataset, the MNIST AM10000 skin cancer dataset, the DermNet dataset, and the ISIC skin cancer dataset. Experimental results demonstrate that the proposed model significantly outperforms several baseline approaches, including traditional machine learning techniques, achieving an overall classification accuracy of 98.6%(Nirupama & Virupakshappa, 2024). While, our model achieved a training accuracy of

approximately 98.73%, confirming its robust ability to accurately diagnose cutaneous.

Yadav et al presented a modified ResNet-101 architecture specifically optimised for the classification of breast cancer in ultrasound images. The dataset utilised comprises 780 ultrasound images, categorised into three classes: normal, benign, and malignant. The proposed model demonstrates outstanding classification performance, achieving precision, recall, F1-score, and accuracy values of 0.9855, 0.9677, 0.9756, and 0.9743, respectively(Yadav, Kolekar, & Zope, 2024). Furthermore, our model achieved a training of precision, recall, F1 score, and accuracy of approximately 0.9863, 0.9846, 0.9841 and 0.9851, respectively. confirming its robust ability to accurately diagnose cutaneous leishmaniasis and its broader applicability in dermatology diagnostics.

A study investigated the complex relationship between microorganisms and ecosystems, with a particular focus on the accurate classification of parasitic organisms. The study provided an in-depth exploration of the integration of swarm intelligence techniques with deep learning (DL) algorithms, specifically targeting the challenging task of parasite identification. The research was supported by a robust dataset of 34,298 images representing ten distinct parasite species(Hosen et al., 2024). Furthermore, a comprehensive comparative analysis of four state-of-the-art pre-trained convolutional neural network (CNN) architectures was conducted to guide model selection. Among the evaluated models, XceptionNet demonstrated advanced performance, achieving a remarkable accuracy of 0.9489 and an F1 score of 0.9492. Additionally, our model established progressive performance, achieving an extraordinary accuracy of 0.9877 and an F1 score of 0.9869, respectively.

confirming its strong ability to accurately diagnose cutaneous leishmaniasis.

6 Conclusion

Considering the use of ultra-thin skin smear pictures, the study demonstrated the appealing potential of deep learning more especially, convolutional neural networks, in improving the diagnosis accuracy of cutaneous leishmaniasis. With the highest accuracy and F1 score of almost 99.15% and 99.1%, respectively, DenseNet201 was among the most effective of the five pre-trained models that were assessed: EfficientNetB0, ResNet101, MobileNetV2, Xception, and DenseNet201. The robustness and dependability of these designs in categorising CL infections were further supported by EfficientNetB0, which came in second with similarly strong performance.

By visualising areas crucial for a positive diagnosis and boosting confidence in automated decision-making systems, the Grad-CAM application offered helpful details about model comprehensibility. These results provide confidence in the incorporation of CNN-based diagnostic tools into clinical procedures, especially in areas with limited resources or afflicted by conflict, such as northern Libya, where prompt and precise diagnosis is essential. By introducing more and more varied datasets and investigating current-time diagnostic applications in field situations, future research could improve these models even further.

Finally, both DenseNet-201 and EfficientNet-B0 demonstrated high accuracy in accurately identifying specimens and strong agreement with actual classifications when tested on microscopic images of amastigote stage of the cutaneous leishmania spp. Both models demonstrated excellent classification performance, achieving a good balance between recall and precision. However, the requirements and constraints of the task in question should be considered when selecting the best model for practical applications.

7 Recommendations

Based on the results of this study, which showed that DenseNet-201 and EfficientNet-B0 performed better than other models in identifying cutaneous leishmaniasis from ultra-thin skin smear images, a number of suggestions are made to improve future research and possible practical uses. DenseNet-201 and EfficientNet-B0 in particular have demonstrated good accuracy and F1 scores, making them suitable for incorporation into clinical laboratory diagnostic procedures. Dermatologists and pathologists could benefit from the development of a decision-support system, particularly in areas with low resources.

Expanding the dataset to include additional samples from various demographics and geographical areas should be the goal of future research. This would increase the model's resilience and generalisability across different lesion presentations and picture quality. Through multimodal learning techniques, combining image data with patient characteristics (such as age, lesion duration, location, and travel history) may improve model performance and offer a more comprehensive diagnostic approach. Future research should investigate more sophisticated explainability methods to further test the model's reliability and enhance clinician adoption, even though Grad-CAM offered helpful insights into the model's decision-making process.

8 References

Adaloglou, N. (2020). In-layer normalization techniques for training very deep neural networks. *AI Summer. Доступно на: https://theaisummer. com/normalization/, Приступљено, 15*.

Ait Maatallah, I., Akarid, K., & Lemrani, M. (2022). Tissue tropism: Is it an intrinsic characteristic of Leishmania species? *Acta Tropica, 232*, 106512. doi: https://doi.org/10.1016/j.actatropica.2022.106512

Akhoundi, M., Downing, T., Votýpka, J., Kuhls, K., Lukeš, J., Cannet, A., . . . Sereno, D. (2017). Leishmania infections: Molecular targets and diagnosis. *Mol Aspects Med, 57*, 1-29. doi: 10.1016/j.mam.2016.11.012

Al Jawaldeh, A., Osman, D., Tawfik, A., & Organization, W. H. (2014). Regional Office for the Eastern Mediterranean. *Food and nutrition surveillance systems: Technical guide for the development of a food and nutrition surveillance system for countries in the Eastern Mediterranean Region [homepage on the Internet].[cited 2022 June 15]. Available from: https://apps. who. int/iris/handle/10665/119995*.

Aljuaid, A., & Anwar, M. (2022). Survey of Supervised Learning for Medical Image Processing. *SN Computer Science, 3*(4), 292. doi: 10.1007/s42979-022-01166-1

Alvar, J., Aparicio, P., Aseffa, A., Den Boer, M., Canavate, C., Dedet, J.-P., . . . Moreno, J. (2008). The relationship between leishmaniasis and AIDS: the second 10 years. *Clinical microbiology reviews, 21*(2), 334-359.

Alvar, J., Vélez, I. D., Bern, C., Herrero, M., Desjeux, P., Cano, J., . . . Team, W. L. C. (2012). Leishmaniasis worldwide and global estimates of its incidence. *PloS one, 7*(5), e35671.

Alvar, J., Yactayo, S., & Bern, C. (2006). Leishmaniasis and poverty. *Trends in parasitology, 22*(12), 552-557.

Alves, N. O., Oshiro, J. A., Silva, Y. C., Pacher, G. C., Casaril, A. E., Rizk, Y. S., . . . Oliveira, A. G. (2024). VL-HIV co-infection with Leishmania containing skin lesions resembling para-kala-azar dermal leishmaniasis. *PLoS neglected tropical diseases, 18*(8), e0012438. doi: 10.1371/journal.pntd.0012438

Aoki, J. I., Muxel, S. M., Zampieri, R. A., Müller, K. E., Nerland, A. H., & Floeter-Winter, L. M. (2019). Differential immune response modulation in early Leishmania amazonensis infection of BALB/c and C57BL/6 macrophages based on transcriptome profiles. *Scientific reports, 9*(1), 19841.

Aronson, N., Herwaldt, B. L., Libman, M., Pearson, R., Lopez-Velez, R., Weina, P., . . . Magill, A. (2016). Diagnosis and treatment of leishmaniasis: clinical practice guidelines by the Infectious Diseases Society of America (IDSA) and the American Society of Tropical Medicine and Hygiene (ASTMH). *Clinical Infectious Diseases, 63*(12), e202-e264.

Ataide, E., Tavares, A. P., Nicola, P., Pereira, L., & Ribeiro, L. (2012). Gymnophthalmid and tropidurid lizards as prey of the crab-eating fox, Cerdocyon thous (Linnaeus, 1766) (Carnivora: Canidae). *Herpetology Notes, 5*, 463-466.

Babiker, Z. O., Davidson, R., Mazinda, C., Kipngetich, S., & Ritmeijer, K. (2007). Utility of lymph node aspiration in the diagnosis of visceral leishmaniasis in Sudan. *Am J Trop Med Hyg, 76*(4), 689-693.

Bangert, M., Flores-Chávez, M. D., Llanes-Acevedo, I. P., Arcones, C., Chicharro, C., García, E., & Ortega, S. (2018). Validation of rK39 immunochromatographic test and direct agglutination test for the diagnosis of Mediterranean visceral leishmaniasis in Spain. *12*(3), e0006277. doi: 10.1371/journal.pntd.0006277

Barragán-Montero, A., Javaid, U., Valdés, G., Nguyen, D., Desbordes, P., Macq, B., . . . Lee, J. A. (2021). Artificial intelligence and machine learning for medical imaging: A technology review. *Physica Medica, 83*, 242-256. doi: https://doi.org/10.1016/j.ejmp.2021.04.016

Beevi, K. S., Nair, M. S., & Bindu, G. (2019). Automatic mitosis detection in breast histopathology images using convolutional neural network based deep transfer learning. *Biocybernetics and Biomedical Engineering, 39*(1), 214-223.

Bekheet, M., & Sallah, M. (2024). Cardiac Fibrosis Automated Diagnosis Based on FibrosisNet Network Using CMR Ischemic Cardiomyopathy. *14*(3). doi: 10.3390/diagnostics14030255

Bern, C., Amann, J., Haque, R., Chowdhury, R., Ali, M., Kurkjian, K. M., . . . Secor, W. E. (2006). Loss of leishmanin skin test antigen sensitivity and potency in a longitudinal study of visceral leishmaniasis in Bangladesh. *American Journal of Tropical Medicine and Hygiene, 75*(4), 744-748.

Bern, C., Maguire, J. H., & Alvar, J. (2008). Complexities of assessing the disease burden attributable to leishmaniasis. *PLoS neglected tropical diseases, 2*(10), e313.

Besteiro, S., Williams, R. A., Coombs, G. H., & Mottram, J. C. (2007). Protein turnover and differentiation in Leishmania. *Int J Parasitol, 37*(10), 1063-1075.

Bilgic-Temel, A., Murrell, D. F., & Uzun, S. (2019). Cutaneous leishmaniasis: a neglected disfiguring disease for women. *International journal of women's dermatology, 5*(3), 158-165.

Biswal, R., Mallick, P. K., Panda, A. R., Chae, G. S., & Mishra, A. (2023). *White Blood Cell Classification Using Pre-Trained Deep Neural Networks and Transfer Learning.* Paper presented at the 2023 1st International Conference on Circuits, Power and Intelligent Systems (CCPIS).

Bogdan, C. (2012). Leishmaniasis in rheumatology, haematology and oncology: epidemiological, immunological and clinical aspects and caveats. *Annals of the rheumatic diseases, 71*(Suppl 2), i60-i66.

Boité, M. C., Mauricio, I. L., Miles, M. A., & Cupolillo, E. (2012). New insights on taxonomy, phylogeny and population genetics of Leishmania (Viannia) parasites based on multilocus sequence analysis. *PLoS Negl Trop Dis, 6*(11), e1888. doi: 10.1371/journal.pntd.0001888

Bouchekoua, M., Trabelsi, S., Abdallah, T. B., & Khaled, S. (2014). Visceral leishmaniasis after kidney transplantation: Report of a new case and a review of the literature. *Transplantation reviews, 28*(1), 32-35.

Bowles, D. E., Gibson, S., Linthicum, K., Johnson, R. N., Linton, Y.-M., & White, G. B. (2015). *Sand Flies: Significance, Surveillance, and Control in Contingency Operations*.

Braz, R. F., Nascimento, E. T., Martins, D. R., Wilson, M. E., Pearson, R. D., Reed, S. G., & Jeronimo, S. M. (2002). The sensitivity and specificity of Leishmania chagasi recombinant K39 antigen in the diagnosis of American visceral leishmaniasis and in

differentiating active from subclinical infection. *Am J Trop Med Hyg, 67*(4), 344-348. doi: 10.4269/ajtmh.2002.67.344

Cao, G., Song, W., & Zhao, Z. (2019). *Gastric cancer diagnosis with mask R-CNN.* Paper presented at the 2019 11th international conference on intelligent human-machine systems and cybernetics (IHMSC).

Carvalho, B. M., Rangel, E. F., & Vale, M. M. (2017). Evaluation of the impacts of climate change on disease vectors through ecological niche modelling. *Bull Entomol Res, 107*(4), 419-430. doi: 10.1017/s0007485316001097

Casanova, C., Andrighetti, M. T., Sampaio, S. M., Marcoris, M. L., Colla-Jacques, F. E., & Prado, A. P. (2013). Larval breeding sites of Lutzomyia longipalpis (Diptera: Psychodidae) in visceral leishmaniasis endemic urban areas in Southeastern Brazil. *PLoS Negl Trop Dis, 7*(9), e2443. doi: 10.1371/journal.pntd.0002443

Cassagne, C., Pratlong, F., Jeddi, F., Benikhlef, R., Aoun, K., Normand, A. C., . . . Piarroux, R. (2014). Identification of Leishmania at the species level with matrix-assisted laser desorption ionization time-of-flight mass spectrometry. *Clin Microbiol Infect, 20*(6), 551-557. doi: 10.1111/1469-0691.12387

CDC. (2024). Clinical Care of Leishmaniasis. US Centers for Disease Control and Prevention. 2024, from https://www.cdc.gov/leishmaniasis/hcp/clinical-care/index.html

Celeste, B. J., Arroyo Sanchez, M. C., Ramos-Sanchez, E. M., Castro, L. G. M., Lima Costa, F. A., & Goto, H. (2014). Recombinant Leishmania infantum heat shock protein 83 for the serodiagnosis of cutaneous, mucosal, and visceral leishmaniases. *Am J Trop Med Hyg, 90*(5), 860-865. doi: 10.4269/ajtmh.13-0623

Chambers, S. T. (2011). Control of the Leishmaniases: Report of a Meeting of the WHO Expert Committee on the Control of Leishmaniases: NEW ZEALAND MEDICAL ASSOC C/O BRENNAN EDWARDES, DEPT SURGERY, CHRISTCHURCH ….

Chitimia, L., Muñoz-García, C., Sánchez-Velasco, D., Lizana, V., Del Río, L., Murcia, L., . . . Jiménez-Montalbán, P. (2011). Cryptic Leishmaniosis by Leishmania infantum, a feature of canines only? A study of natural infection in wild rabbits, humans and dogs in southeastern Spain. *Veterinary parasitology, 181*(1), 12-16.

Chollet, F. (2017). *Xception: Deep learning with depthwise separable convolutions.* Paper presented at the Proceedings of the IEEE conference on computer vision and pattern recognition.

Claborn, D. M. (2010). The biology and control of leishmaniasis vectors. *Journal of global infectious diseases, 2*(2), 127-134.

Convit, J., Castellanos, P. L., Ulrich, M., Castés, M., Rondón, A., Pinardi, M. E., . . . Valecillos, L. (1989). Immunotherapy of localized, intermediate, and diffuse forms of American cutaneous leishmaniasis. *Journal of Infectious Diseases, 160*(1), 104-115.

Copeland, N. K., & Aronson, N. E. (2015). Leishmaniasis: treatment updates and clinical practice guidelines review. *Current Opinion in Infectious Diseases, 28*(5), 426-437.

Cordeiro, L. V., de Andrade Júnior, F. P., & de Oliveira, E. (2019). Antimony Resistance in Leishmania Parasites may be Related to an Increased Virulence. *Ponte, 3*(5), 529-530.

Costa, C. H. N., Werneck, G. L., Costa, D. L., Holanda, T. A., Aguiar, G. B., Carvalho, A. S., . . . Santos, L. S. (2010). Is severe visceral leishmaniasis a systemic inflammatory response syndrome? A

case control study. *Revista da Sociedade Brasileira de Medicina Tropical, 43*, 386-392.

Costa, J. M. L., Saldanha, A. C. R., Silva, C. d. M. P. e., Branco, M. d. R. F. C., Barrai, A., Carvalho, E. M., & Bittencourt, A. L. (1995). Spontaneous regional healing of extensive skin lesions in diffuse cutaneous Leishmaniasis (DCL). *Revista da Sociedade Brasileira de Medicina Tropical, 28 1*, 45-47.

Cota, G. F., de Sousa, M. R., & Rabello, A. (2011). Predictors of visceral leishmaniasis relapse in HIV-infected patients: a systematic review. *PLoS neglected tropical diseases, 5*(6), e1153.

Cunningham, J., Hasker, E., Das, P., El Safi, S., Goto, H., Mondal, D., . . . Boelaert, M. (2012). A global comparative evaluation of commercial immunochromatographic rapid diagnostic tests for visceral leishmaniasis. *Clin Infect Dis, 55*(10), 1312-1319. doi: 10.1093/cid/cis716

Cupolillo, E., Grimaldi, G., Jr., & Momen, H. (1994). A general classification of New World Leishmania using numerical zymotaxonomy. *Am J Trop Med Hyg, 50*(3), 296-311. doi: 10.4269/ajtmh.1994.50.296

Das, D. K., Bose, S., Maiti, A. K., Mitra, B., Mukherjee, G., & Dutta, P. K. (2018). Automatic identification of clinically relevant regions from oral tissue histological images for oral squamous cell carcinoma diagnosis. *Tissue and Cell, 53*, 111-119.

de Almeida, M. E., Koru, O., Steurer, F., Herwaldt, B. L., & da Silva, A. J. (2017). Detection and Differentiation of Leishmania spp. in Clinical Specimens by Use of a SYBR Green-Based Real-Time PCR Assay. *J Clin Microbiol, 55*(1), 281-290. doi: 10.1128/jcm.01764-16

de Menezes, J. P. B., Brodskyn, C., Gonçalves, R., & Bacellar, O. (2022). Editorial: Immunology and immunopathogenesis of human leishmaniasis. *Front Cell Infect Microbiol, 12*, 1055221. doi: 10.3389/fcimb.2022.1055221

de Vries, H. J., Reedijk, S. H., & Schallig, H. D. (2015). Cutaneous leishmaniasis: recent developments in diagnosis and management. *Am J Clin Dermatol, 16*(2), 99-109. doi: 10.1007/s40257-015-0114-z

Dereure, J., El-Safi, S. H., Bucheton, B., Boni, M., Kheir, M. M., Davoust, B., . . . Dessein, A. (2003). Visceral leishmaniasis in eastern Sudan: parasite identification in humans and dogs; host-parasite relationships. *Microbes and infection, 5*(12), 1103-1108.

Desjeux, P. (2001). The increase in risk factors for leishmaniasis worldwide. *Transactions of the Royal Society of Tropical Medicine and Hygiene, 95*(3), 239-243. doi: https://doi.org/10.1016/S0035-9203(01)90223-8

Dey, A., & Singh, S. (2006). Transfusion transmitted leishmaniasis: a case report and review of literature. *Indian Journal of Medical Microbiology, 24*(3), 165-170.

Diniz, J. L. C. P., da Rocha Costa, M. O., & Gonçalves, D. U. (2011). Mucocutaneous Leishmaniasis: clinical markers in presumptive diagnosis. *Brazilian journal of otorhinolaryngology, 77*(3), 380-384.

Dostálová, A., & Volf, P. (2012). Leishmania development in sand flies: parasite-vector interactions overview. *Parasites & Vectors, 5*, 1-12.

Ejazi, S. A., Ghosh, S., Saha, S., Choudhury, S. T., Bhattacharyya, A., Chatterjee, M., . . . Moreno, J. (2019). A multicentric evaluation of dipstick test for serodiagnosis of visceral leishmaniasis in

India, Nepal, Sri Lanka, Brazil, Ethiopia and Spain. *9*(1), 9932. doi: 10.1038/s41598-019-46283-9

El-On, J., Livshin, R., Even-Paz, Z., Hamburger, D., & Weinrauch, L. (1986). Topical treatment of cutaneous leishmaniasis. *J Invest Dermatol, 87*(2), 284-288. doi: 10.1111/1523-1747.ep12696697

Erre, G., Mesina, P., Tonelli, N., & Passiu, G. (2010). Visceral Leishmaniasis among immunosuppressed patients with rheumatic diseases. *Clinical and experimental rheumatology, 28*(4), 590-591.

Espinosa, O., Serrano, M. G., Camargo, E., Teixeira, M. M. G., & Shaw, J. J. (2018). An appraisal of the taxonomy and nomenclature of trypanosomatids presently classified as Leishmania and Endotrypanum. *Parasitology, 145*(4), 430-442.

Esteves, B. B., Melo-Braga, M. N., Gorshkov, V., Verano-Braga, T., Larsen, M. R., Gontijo, C. M. F., . . . Andrade, H. M. (2022). Characterization of Differentially Abundant Proteins Among Leishmania (Viannia) braziliensis Strains Isolated From Atypical or Typical Lesions. *Frontiers in Cellular and Infection Microbiology, 12*. doi: 10.3389/fcimb.2022.824968

Fang, T. (2018). *A novel computer-aided lung cancer detection method based on transfer learning from GoogLeNet and median intensity projections.* Paper presented at the 2018 IEEE international conference on computer and communication engineering technology (CCET).

Gabriel, Á., Valério-Bolas, A., Palma-Marques, J., Mourata-Gonçalves, P., Ruas, P., Dias-Guerreiro, T., & Santos-Gomes, G. (2019). Cutaneous leishmaniasis: the complexity of host's effective immune response against a polymorphic parasitic disease. *Journal of immunology research, 2019*(1), 2603730.

Ghahramani, Z. (2003). Unsupervised learning *Summer school on machine learning* (pp. 72-112): Springer.

Gomes, R. S., Silva, M. V. T., Dos Santos, J. C., de Lima Silva, L. L., Batista, A. C., Machado, J. R., . . . Ribeiro-Dias, F. (2017). IL-32γ promotes the healing of murine cutaneous lesions caused by Leishmania braziliensis infection in contrast to Leishmania amazonensis. *Parasit Vectors, 10*(1), 336. doi: 10.1186/s13071-017-2268-4

Gonçalves, L. O., Pulido, A. F. V., Mathias, F. A. S., Enes, A. E. S., Carvalho, M. G. R., de Melo Resende, D., . . . Ruiz, J. C. (2022). Expression Profile of Genes Related to the Th17 Pathway in Macrophages Infected by Leishmania major and Leishmania amazonensis: The Use of Gene Regulatory Networks in Modeling This Pathway. *Frontiers in Cellular and Infection Microbiology, 12*. doi: 10.3389/fcimb.2022.826523

Górriz, M., Aparicio, A., Raventós, B., Vilaplana, V., Sayrol, E., & López-Codina, D. (2018). *Leishmaniasis parasite segmentation and classification using deep learning.* Paper presented at the Articulated Motion and Deformable Objects: 10th International Conference, AMDO 2018, Palma de Mallorca, Spain, July 12-13, 2018, Proceedings 10.

Goto, H., & Lindoso, J. A. (2010). Current diagnosis and treatment of cutaneous and mucocutaneous leishmaniasis. *Expert Rev Anti Infect Ther, 8*(4), 419-433. doi: 10.1586/eri.10.19

Grimaldi, G., & McMahon-Pratt, D. (1996). Monoclonal antibodies for the identification of New World Leishmania species. *Mem Inst Oswaldo Cruz, 91*(1), 37-42. doi: 10.1590/s0074-02761996000100006

Gu, J., Wang, Z., Kuen, J., Ma, L., Shahroudy, A., Shuai, B., . . . Cai, J. (2018). Recent advances in convolutional neural networks. *Pattern recognition, 77*, 354-377.

Guedes-Barbosa, L. S., da Costa, I. P., Fernandes, V., da Mota, L. M. H., de Menezes, I., & Scheinberg, M. A. (2013). *Leishmaniasis during anti-tumor necrosis factor therapy: report of 4 cases and review of the literature (additional 28 cases).* Paper presented at the Seminars in arthritis and rheumatism.

Gunjan, V. K., Singh, N., Shaik, F., & Roy, S. (2022). Detection of lung cancer in CT scans using grey wolf optimization algorithm and recurrent neural network. *Health and Technology, 12*(6), 1197-1210.

Guo, J., Li, C., Sun, Z., Li, J., & Wang, P. (2022). A deep attention model for environmental sound classification from multi-feature data. *Applied Sciences, 12*(12), 5988.

Hawash, Y. A., Ismail, K. A., Abdel-Wahab, M. M., & Khalifa, M. (2018). Diagnosis, treatment and clinical features of cutaneous Leishmaniasis in Saudi Arabia. *The Korean journal of parasitology, 56*(3), 229.

Hay, R. J., & Asiedu, K. (2018). Skin-related neglected tropical diseases (skin NTDs)—a new challenge (Vol. 4, pp. 4): MDPI.

Hinton, G. (2012). Improving neural networks by preventing co-adaptation of feature detectors. *arXiv preprint arXiv:1207.0580*.

Hiremath, N. V. (2022). *Breast Cancer Detection and Classification using EfficientNet B0 and EfficientNet B0-HSV.* Dublin, National College of Ireland.

Hong, A., & Zampieri, R. A. (2020). One Health Approach to Leishmaniases: Understanding the Disease Dynamics through Diagnostic Tools. *9*(10). doi: 10.3390/pathogens9100809

Hong, A., Zampieri, R. A., Shaw, J. J., Floeter-Winter, L. M., & Laranjeira-Silva, M. F. (2020). One health approach to leishmaniases: understanding the disease dynamics through diagnostic tools. *Pathogens, 9*(10), 809.

Hosen, M. D., Mohiuddin, A. B., Sarker, N., Sakib, M. S., Al Sakib, A., Dip, R. H., . . . Haque, R. (2024). *Parasitology unveiled: Revolutionizing microorganism classification through deep learning.* Paper presented at the 2024 6th International Conference on Electrical Engineering and Information & Communication Technology (ICEEICT).

https://www.ncbi.nlm.nih.gov/datasets.

https://www.ndvsu.org/images/StudyMaterials/Parasitology/Leishmaniosis.pdf.

Ioffe, S. (2015). Batch normalization: Accelerating deep network training by reducing internal covariate shift. *arXiv preprint arXiv:1502.03167*.

Jaffe, C. L., & Rachamim, N. (1989). Amastigote stage-specific monoclonal antibodies against Leishmania major. *Infect Immun, 57*(12), 3770-3777. doi: 10.1128/iai.57.12.3770-3777.1989

James WD, B. T. (2006). Andrews' Diseases of the Skin: clinical Dermatology. *Saunders Elsevier* (pp. p. 423.).

Jarvis, J. N., & Lockwood, D. N. (2013). Clinical aspects of visceral leishmaniasis in HIV infection. *Current Opinion in Infectious Diseases, 26*(1), 1-9.

Jomtarak, R., Kittichai, V., Kaewthamasorn, M., Thanee, S., Arnuphapprasert, A., Naing, K. M., . . . Chuwongin, S. (2023). *Mobile Bot Application for Identification of Trypanosoma evansi Infection through Thin-Blood Film Examination Based on Deep*

Learning Approach. Paper presented at the 2023 IEEE International Conference on Cybernetics and Innovations (ICCI).

Kak, G., Raza, M., & Tiwari, B. K. (2018). Interferon-gamma (IFN-γ): Exploring its implications in infectious diseases. *Biomolecular concepts, 9*(1), 64-79.

Kariyawasam, K. K., Edirisuriya, C. S., Senerath, U., Hensmen, D., Siriwardana, H. V., & Karunaweera, N. D. (2015). Characterisation of cutaneous leishmaniasis in Matara district, southern Sri Lanka: evidence for case clustering. *Pathog Glob Health, 109*(7), 336-343. doi: 10.1179/2047773215y.0000000032

Kassahun, A., Sadlova, J., Dvorak, V., Kostalova, T., Rohousova, I., Frynta, D., . . . Votypka, J. (2015). Detection of Leishmania donovani and L. tropica in Ethiopian wild rodents. *Acta Tropica, 145*, 39-44. doi: https://doi.org/10.1016/j.actatropica.2015.02.006

Kassim, Y. M., Palaniappan, K., Yang, F., Poostchi, M., Palaniappan, N., Maude, R. J., . . . Jaeger, S. (2020). Clustering-based dual deep learning architecture for detecting red blood cells in malaria diagnostic smears. *IEEE journal of biomedical and health informatics, 25*(5), 1735-1746.

Ker, J., Wang, L., Rao, J., & Lim, T. (2017). Deep learning applications in medical image analysis. *Ieee Access, 6*, 9375-9389.

Khan, A., Khan, M. A., Javed, M. Y., Alhaisoni, M., Tariq, U., Kadry, S., . . . Nam, Y. (2022). Human Gait Recognition Using Deep Learning and Improved Ant Colony Optimization. *Computers, Materials & Continua, 70*(2).

Khan, M. G., Bhaskar, K. R., Salam, M. A., Akther, T., Pluschke, G., & Mondal, D. (2012). Diagnostic accuracy of loop-mediated isothermal amplification (LAMP) for detection of Leishmania

DNA in buffy coat from visceral leishmaniasis patients. *Parasit Vectors, 5*, 280. doi: 10.1186/1756-3305-5-280

Kim, H. E., Cosa-Linan, A., Santhanam, N., Jannesari, M., Maros, M. E., & Ganslandt, T. (2022). Transfer learning for medical image classification: a literature review. *BMC medical imaging, 22*(1), 69.

Krizhevsky, A., Sutskever, I., & Hinton, G. E. (2012). Imagenet classification with deep convolutional neural networks. *Advances in neural information processing systems, 25*.

Kumar, A., Gadag, S., & Nayak, U. Y. (2020). The beginning of a new era: artificial intelligence in healthcare. *Advanced Pharmaceutical Bulletin, 11*(3), 414.

Kumar, D., Kumar, S., Chakravarty, J., & Sundar, S. (2011). A novel 12.6-kDa protein of Leishmania donovani for the diagnosis of Indian visceral leishmaniasis. *Vector Borne Zoonotic Dis, 11*(10), 1359-1364. doi: 10.1089/vbz.2011.0620

Lachaud, L., Fernández-Arévalo, A., Normand, A. C., Lami, P., Nabet, C., Donnadieu, J. L., . . . Piarroux, R. (2017). Identification of Leishmania by Matrix-Assisted Laser Desorption Ionization-Time of Flight (MALDI-TOF) Mass Spectrometry Using a Free Web-Based Application and a Dedicated Mass-Spectral Library. *J Clin Microbiol, 55*(10), 2924-2933. doi: 10.1128/jcm.00845-17

Li, S., Liu, Z.-Q., & Chan, A. B. (2014). *Heterogeneous multi-task learning for human pose estimation with deep convolutional neural network.* Paper presented at the Proceedings of the IEEE conference on computer vision and pattern recognition workshops.

Limon Jacques, S. M. (2017). *Image analysis and classification techniques for Leishmaniosis Detection.* Universitat Politècnica de Catalunya.

Lu, S., Lu, Z., & Zhang, Y.-D. (2019). Pathological brain detection based on AlexNet and transfer learning. *Journal of computational science, 30*, 41-47.

Ma, W., & Lu, J. (2017). An equivalence of fully connected layer and convolutional layer. *arXiv preprint arXiv:1712.01252*.

Mabrouk, A., Diaz Redondo, R. P., Dahou, A., Abd Elaziz, M., & Kayed, M. (2022). Pneumonia detection on chest X-ray images using ensemble of deep convolutional neural networks. *Applied Sciences, 12*(13), 6448.

Machado, P. R., Ampuero, J., Guimarães, L. H., Villasboas, L., Rocha, A. T., Schriefer, A., . . . Carvalho, E. M. (2010). Miltefosine in the treatment of cutaneous leishmaniasis caused by Leishmania braziliensis in Brazil: a randomized and controlled trial. *PLoS Negl Trop Dis, 4*(12), e912. doi: 10.1371/journal.pntd.0000912

Maia, Z., Lírio, M., Mistro, S., Mendes, C. M., Mehta, S. R., & Badaro, R. (2012). Comparative study of rK39 Leishmania antigen for serodiagnosis of visceral leishmaniasis: systematic review with meta-analysis. *PLoS Negl Trop Dis, 6*(1), e1484. doi: 10.1371/journal.pntd.0001484

Mann, S., Frasca, K., Scherrer, S., Henao-Martínez, A. F., Newman, S., Ramanan, P., & Suarez, J. A. (2021). A review of leishmaniasis: current knowledge and future directions. *Current tropical medicine reports, 8*, 121-132.

Maqsood, A., Farid, M. S., Khan, M. H., & Grzegorzek, M. (2021). Deep malaria parasite detection in thin blood smear microscopic images. *Applied Sciences, 11*(5), 2284.

Markell, E., John, D., & Krotoski, W. (1999). Toxoplasma gondii. Markell and Voges's Medical Parisitology: WB Saunders Co, Philadelphia, Pennsylvania.

Mary, C., Lamouroux, D., Dunan, S., & Quilici, M. (1992). Western blot analysis of antibodies to Leishmania infantum antigens: potential of the 14-kD and 16-kD antigens for diagnosis and epidemiologic purposes. *Am J Trop Med Hyg, 47*(6), 764-771. doi: 10.4269/ajtmh.1992.47.764

Mary Kamb, S. R., Paul Cantey,. (2024). Travel-Associated Infections & Diseases. from https://wwwnc.cdc.gov/travel/yellowbook/2024/infections-diseases/leishmaniasis-cutaneous

Maxfield, L., & Crane, J. S. (2024). Leishmaniasis *StatPearls*. Treasure Island (FL) ineligible companies. Disclosure: Jonathan Crane declares no relevant financial relationships with ineligible companies.: StatPearls Publishing

Mazo, C., Bernal, J., Trujillo, M., & Alegre, E. (2018). Transfer learning for classification of cardiovascular tissues in histological images. *Computer methods and programs in biomedicine, 165*, 69-76.

Melville, J., Alguri, K. S., Deemer, C., & Harley, J. B. (2018). *Structural damage detection using deep learning of ultrasonic guided waves.* Paper presented at the AIP conference proceedings.

Merritt, R. W., Courtney, G. W., & Keiper, J. B. (2009). Diptera:(Flies, Mosquitoes, Midges, Gnats) *Encyclopedia of insects* (pp. 284-297): Elsevier.

Michel, G., Pomares, C., Ferrua, B., & Marty, P. (2011). Importance of worldwide asymptomatic carriers of Leishmania infantum (L. chagasi) in human. *Acta Tropica, 119*(2-3), 69-75.

Modarres, C., Astorga, N., Droguett, E. L., & Meruane, V. (2018). Convolutional neural networks for automated damage recognition and damage type identification. *Structural Control and Health Monitoring, 25*(10), e2230.

Mohapatra, T. M., Singh, D. P., Sen, M. R., Bharti, K., & Sundar, S. (2010). Compararative evaluation of rK9, rK26 and rK39 antigens in the serodiagnosis of Indian visceral leishmaniasis. *J Infect Dev Ctries, 4*(2), 114-117. doi: 10.3855/jidc.544

Montagnon, E., Cerny, M., Cadrin-Chênevert, A., Hamilton, V., Derennes, T., Ilinca, A., . . . Tang, A. (2020). Deep learning workflow in radiology: a primer. *Insights into imaging, 11*, 1-15.

Montalvo, A. M., Monzote, L., Fraga, J., Montano, I., Muskus, C., Marín, M., . . . Dujardin, J. C. (2008). RFLP y RAPD para la tipificación de Leishmania neotropical. *Biomédica, 28*, 597-606.

Morais, M. C. C., Silva, D., Milagre, M. M., de Oliveira, M. T., Pereira, T., Silva, J. S., . . . Gazzinelli, R. (2022). Automatic detection of the parasite Trypanosoma cruzi in blood smears using a machine learning approach applied to mobile phone images. *PeerJ, 10*, e13470.

Müller, K. E., Zampieri, R. A., Aoki, J. I., Muxel, S. M., Nerland, A. H., & Floeter-Winter, L. M. (2018). Amino acid permease 3 (aap3) coding sequence as a target for Leishmania identification and diagnosis of leishmaniases using high resolution melting analysis. *Parasit Vectors, 11*(1), 421. doi: 10.1186/s13071-018-2989-z

Murray, H. W., Berman, J. D., Davies, C. R., & Saravia, N. G. (2005). Advances in leishmaniasis. *The Lancet, 366*(9496), 1561-1577.

Nguyen, L. D., Lin, D., Lin, Z., & Cao, J. (2018). *Deep CNNs for microscopic image classification by exploiting transfer learning*

and feature concatenation. Paper presented at the 2018 IEEE international symposium on circuits and systems (ISCAS).

Nirupama, & Virupakshappa. (2024). Mobilenet-v2: An enhanced skin disease classification by attention and multi-scale features. *Journal of Imaging Informatics in Medicine*, 1-21.

Niu, Y., Gu, L., Zhao, Y., & Lu, F. (2021). Explainable diabetic retinopathy detection and retinal image generation. *IEEE journal of biomedical and health informatics, 26*(1), 44-55.

Ong, W., Zhu, L., Tan, Y. L., Teo, E. C., Tan, J. H., Kumar, N., . . . Makmur, A. (2023). Application of machine learning for differentiating bone Malignancy on imaging: A systematic review. *Cancers, 15*(6), 1837.

Oryan, A., & Akbari, M. (2016). Worldwide risk factors in leishmaniasis. *Asian Pac J Trop Med, 9*(10), 925-932. doi: 10.1016/j.apjtm.2016.06.021

Öztürk, Ş. (2022). *Convolutional neural networks for medical image processing applications*: CRC Press Boca Raton, FL, USA:.

Pan American Health Organization. (2019). Manual of procedures for leishmaniases surveillance and control in the Americas. from file:///C:/Users/SC/Desktop/AI,%20ML%20AND%20DL/leishmania/book%20119789275120637_eng.pdf

Pattanaik, P. A., Mittal, M., Khan, M. Z., & Panda, S. N. (2022). Malaria detection using deep residual networks with mobile microscopy. *Journal of King Saud University-Computer and Information Sciences, 34*(5), 1700-1705.

Pedras, M. J., de Gouvêa Viana, L., de Oliveira, E. J., & Rabello, A. (2008). Comparative evaluation of direct agglutination test, rK39 and soluble antigen ELISA and IFAT for the diagnosis of visceral

leishmaniasis. *Trans R Soc Trop Med Hyg, 102*(2), 172-178. doi: 10.1016/j.trstmh.2007.11.004

Peixoto, H. M., de Oliveira, M. R., & Romero, G. A. (2015). Serological diagnosis of canine visceral leishmaniasis in Brazil: systematic review and meta-analysis. *Trop Med Int Health, 20*(3), 334-352. doi: 10.1111/tmi.12429

Pereira, A. S., Mazza, L. O., Pinto, P. C., Gomes, J. G. R., Nedjah, N., Vanzan, D. F., . . . Soares, J. G. (2022). Deep convolutional neural network applied to Trypanosoma cruzi detection in blood samples. *International Journal of Bio-Inspired Computation, 19*(1), 1-17.

Pigott, D. M., Bhatt, S., Golding, N., Duda, K. A., Battle, K. E., Brady, O. J., . . . Pratlong, F. (2014). Global distribution maps of the leishmaniases. *Elife, 3*, e02851.

Pulvertaft, R., & Hoyle, G. (1960). Stages in the life-cycle of Leishmania donovani. *Transactions of the Royal Society of Tropical Medicine and Hygiene, 54*(2), 191-196.

Qayyum, W., Ehtisham, R., Bahrami, A., Camp, C., Mir, J., & Ahmad, A. (2023). Assessment of convolutional neural network pre-trained models for detection and orientation of cracks. *Materials, 16*(2), 826.

Qiao, S., Wang, H., Liu, C., Shen, W., & Yuille, A. (2019). Micro-batch training with batch-channel normalization and weight standardization. *arXiv preprint arXiv:1903.10520*.

Quinnell, R. J., & Courtenay, O. (2009). Transmission, reservoir hosts and control of zoonotic visceral leishmaniasis. *Parasitology, 136*(14), 1915-1934.

Rajkomar, A., Dean, J., & Kohane, I. (2019). Machine learning in medicine. *New England Journal of Medicine, 380*(14), 1347-1358.

Rakha, E. A., Toss, M., Shiino, S., Gamble, P., Jaroensri, R., Mermel, C. H., & Chen, P.-H. C. (2021). Current and future applications of artificial intelligence in pathology: a clinical perspective. *Journal of clinical pathology, 74*(7), 409-414.

Ramos-Sanchez, E. M., Reis, L. C., Souza, M. d. A., Muxel, S. M., Santos, K. R., Lagos, D., . . . Goto, H. (2022). miR-548d-3p Is Up-Regulated in Human Visceral Leishmaniasis and Suppresses Parasite Growth in Macrophages. *Frontiers in Cellular and Infection Microbiology, 12*. doi: 10.3389/fcimb.2022.826039

Ready, P. (2010). Leishmaniasis emergence in Europe. *Eurosurveillance, 15*(10), 19505.

Reimão, J. Q., & Coser, E. M. (2020). Laboratory Diagnosis of Cutaneous and Visceral Leishmaniasis: Current and Future Methods. *8*(11). doi: 10.3390/microorganisms8111632

Reimão, J. Q., Coser, E. M., Lee, M. R., & Coelho, A. C. (2020). Laboratory diagnosis of cutaneous and visceral leishmaniasis: current and future methods. *Microorganisms, 8*(11), 1632.

Rogers, M. E., Chance, M., & Bates, P. (2002). The role of promastigote secretory gel in the origin and transmission of the infective stage of Leishmania mexicana by the sandfly Lutzomyia longipalpis. *Parasitology, 124*(5), 495-507.

Romero, G. A., & Boelaert, M. (2010). Control of visceral leishmaniasis in Latin America—a systematic review. *PLoS neglected tropical diseases, 4*(1), e584.

Romero, G. A., de Farias Guerra, M. V., Paes, M. G., & Macêdo, V. d. O. (2001). Comparison of cutaneous leishmaniasis due to

Leishmania (Viannia) braziliensis and L.(V.) guyanensis in Brazil: clinical findings and diagnostic approach. *Clinical Infectious Diseases, 32*(9), 1304-1312.

Roque, A. L. R., & Jansen, A. M. (2014). Wild and synanthropic reservoirs of Leishmania species in the Americas. *International Journal for Parasitology: Parasites and Wildlife, 3*(3), 251-262.

Rostami, M. N., Saghafipour, A., & Vesali, E. (2013). A newly emerged cutaneous leishmaniasis focus in central Iran. *International Journal of Infectious Diseases, 17*(12), e1198-e1206.

Saha, S., Goswami, R., Pramanik, N., Guha, S. K., Saha, B., Rahman, M., . . . Ali, N. (2011). Easy test for visceral Leishmaniasis and post-Kala-azar Dermal Leishmaniasis. *Emerg Infect Dis, 17*(7), 1304-1306. doi: 10.3201/eid1707.100801

Salam, M. A., Khan, M. G., & Mondal, D. (2011). Urine antigen detection by latex agglutination test for diagnosis and assessment of initial cure of visceral leishmaniasis. *Trans R Soc Trop Med Hyg, 105*(5), 269-272. doi: 10.1016/j.trstmh.2010.12.007

Salehi, A. W., Khan, S., Gupta, G., Alabduallah, B. I., Almjally, A., Alsolai, H., . . . Mellit, A. (2023). A study of CNN and transfer learning in medical imaging: Advantages, challenges, future scope. *Sustainability, 15*(7), 5930.

Salim, F., Saeed, F., Basurra, S., Qasem, S. N., & Al-Hadhrami, T. (2023). DenseNet-201 and Xception pre-trained deep learning models for fruit recognition. *Electronics, 12*(14), 3132.

Salimans, T., & Kingma, D. P. (2016). Weight normalization: A simple reparameterization to accelerate training of deep neural networks. *Advances in neural information processing systems, 29*.

Sandoval Pacheco, C. M., Araujo Flores, G. V., Favero Ferreira, A., Sosa Ochoa, W., Ribeiro da Matta, V. L., Zúniga Valeriano, C., . . .

Dalastra Laurenti, M. (2018). Histopathological features of skin lesions in patients affected by non-ulcerated or atypical cutaneous leishmaniasis in Honduras, Central America. *Int J Exp Pathol, 99*(5), 249-257. doi: 10.1111/iep.12295

Sandoval Pacheco, C. M., Araujo Flores, G. V., Favero Ferreira, A., Sosa Ochoa, W., Ribeiro da Matta, V. L., Zúniga Valeriano, C., . . . Dalastra Laurenti, M. (2018). Histopathological features of skin lesions in patients affected by non-ulcerated or atypical cutaneous leishmaniasis in Honduras, Central America. *International journal of experimental pathology, 99*(5), 249-257.

Sanghvi, H. A., Patel, R. H., Agarwal, A., Gupta, S., Sawhney, V., & Pandya, A. S. (2023). A deep learning approach for classification of COVID and pneumonia using DenseNet-201. *International Journal of Imaging Systems and Technology, 33*(1), 18-38.

Santos-Gomes, G., Gomes-Pereira, S., Campino, L., Araújo, M. D., & Abranches, P. (2000). Performance of immunoblotting in diagnosis of visceral Leishmaniasis in human immunodeficiency virus-Leishmania sp.-coinfected patients. *J Clin Microbiol, 38*(1), 175-178. doi: 10.1128/jcm.38.1.175-178.2000

Schuster, F. L., & Sullivan, J. J. (2002). Cultivation of clinically significant hemoflagellates. *Clin Microbiol Rev, 15*(3), 374-389. doi: 10.1128/cmr.15.3.374-389.2002

Seifert, K. (2011). Structures, targets and recent approaches in anti-leishmanial drug discovery and development. *Open Med Chem J, 5*, 31-39. doi: 10.2174/1874104501105010031

Seng, P., Rolain, J.-M., Fournier, P. E., La Scola, B., Drancourt, M., & Raoult, D. (2010). MALDI-TOF-mass spectrometry applications in clinical microbiology. *Future microbiology, 5*(11), 1733-1754.

Seyer Cagatan, A., Taiwo Mustapha, M., Bagkur, C., Sanlidag, T., & Ozsahin, D. U. (2022). An alternative diagnostic method for C. Neoformans: Preliminary results of deep-learning based detection model. *Diagnostics, 13*(1), 81.

Shaw, J. J., Marinho-Júnior, J. F., Courtenay, O., & Brandão-Filho, S. P. (2023). Assessing reservoir host status in leishmaniasis with special reference to the infectiousness of Leishmania (Viannia) braziliensis infections in wild rodents. *Revista da Sociedade Brasileira de Medicina Tropical, 56*, e0503-2023.

Silva, H., Liyanage, A., Deerasinghe, T., Chandrasekara, V., Chellappan, K., & Karunaweera, N. D. (2021). Treatment failure to sodium stibogluconate in cutaneous leishmaniasis: A challenge to infection control and disease elimination. *PloS one, 16*(10), e0259009.

Silveira, M. B., Gomes, R. S., Shio, M. T., Rugani, J. N., Paranaiba, L. F., Soares, R. P., & Ribeiro-Dias, F. (2022). Lipophosphoglycan From Dermotropic New World Leishmania Upregulates Interleukin-32 and Proinflammatory Cytokines Through TLR4 and NOD2 Receptors. *Frontiers in Cellular and Infection Microbiology, 12*. doi: 10.3389/fcimb.2022.805720

Singh, D. P., Goyal, R. K., Singh, R. K., Sundar, S., & Mohapatra, T. M. (2010). In search of an ideal test for diagnosis and prognosis of kala-azar. *J Health Popul Nutr, 28*(3), 281-285. doi: 10.3329/jhpn.v28i3.5557

Singh, O. P., Hasker, E., Boelaert, M., Sacks, D., & Sundar, S. (2020). Xenodiagnosis to address key questions in visceral leishmaniasis control and elimination. *14*(8), e0008363. doi: 10.1371/journal.pntd.0008363

Singh, O. P., Hasker, E., Sacks, D., Boelaert, M., & Sundar, S. (2014). Asymptomatic Leishmania infection: a new challenge for Leishmania control. *Clinical Infectious Diseases, 58*(10), 1424-1429.

Singh, R., Wu, W., Wang, G., & Kalra, M. K. (2020). Artificial intelligence in image reconstruction: the change is here. *Physica Medica, 79*, 113-125.

Siriwardana, Y., Deepachandi, B., Gunasekara, C., Warnasooriya, W., & Karunaweera, N. D. (2019). Leishmania donovani induced cutaneous leishmaniasis: an insight into atypical clinical variants in Sri Lanka. *Journal of tropical medicine, 2019*(1), 4538597.

Smith, P. (2007). *Smith P 2007. FAUNA Paraguay Handbook of the Mammals of Paraguay Number 1 Didelphis albiventris. p1-21*.

Soto, J., Gutiérrez, P., Soto, P., Paz, D., Cayhuara, E., Molina, C., . . . Berman, J. (2022). Treatment of Bolivian Leishmania braziliensis cutaneous and mucosal leishmaniasis. *The American Journal of Tropical Medicine and Hygiene, 106*(4), 1182.

Soto, J., & Toledo, J. T. (2007). Oral miltefosine to treat new world cutaneous leishmaniasis. *Lancet Infect Dis, 7*(1), 7. doi: 10.1016/s1473-3099(06)70665-x

Souza, M. A., Ramos-Sanchez, E. M., Muxel, S. M., Lagos, D., Reis, L. C., Pereira, V. R. A., . . . Goto, H. (2021). miR-548d-3p Alters Parasite Growth and Inflammation in Leishmania (Viannia) braziliensis Infection. *Front Cell Infect Microbiol, 11*, 687647. doi: 10.3389/fcimb.2021.687647

Srivastava, P., Dayama, A., Mehrotra, S., & Sundar, S. (2011). Diagnosis of visceral leishmaniasis. *Transactions of the Royal Society of Tropical Medicine and Hygiene, 105*(1), 1-6.

Suárez, M., Valencia, B. M., Jara, M., Alba, M., Boggild, A. K., Dujardin, J. C., . . . Adaui, V. (2015). Quantification of Leishmania (Viannia) Kinetoplast DNA in Ulcers of Cutaneous Leishmaniasis Reveals Inter-site and Inter-sampling Variability in Parasite Load. *PLoS Negl Trop Dis, 9*(7), e0003936. doi: 10.1371/journal.pntd.0003936

Sun, M., Song, Z., Jiang, X., Pan, J., & Pang, Y. (2017). Learning pooling for convolutional neural network. *Neurocomputing, 224*, 96-104.

Sundar, S., Chakravarty, J., Agarwal, D., Rai, M., & Murray, H. W. (2010). Single-dose liposomal amphotericin B for visceral leishmaniasis in India. *N Engl J Med, 362*(6), 504-512. doi: 10.1056/NEJMoa0903627

Sutherst, R. W. (2004). Global change and human vulnerability to vector-borne diseases. *Clinical microbiology reviews, 17*(1), 136-173.

Talo, M. (2019). Automated classification of histopathology images using transfer learning. *Artificial intelligence in medicine, 101*, 101743.

Tan, M., & Le, Q. (2019). *Efficientnet: Rethinking model scaling for convolutional neural networks.* Paper presented at the International conference on machine learning.

Thakur, S., Joshi, J., & Kaur, S. (2020). Leishmaniasis diagnosis: an update on the use of parasitological, immunological and molecular methods. *Journal of Parasitic Diseases, 44*, 253-272.

Thomaz-Soccol, V., Gonçalves, A. L., Piechnik, C. A., Baggio, R. A., Boeger, W. A., Buchman, T. L., . . . Salomon, O. D. (2018). Hidden danger: Unexpected scenario in the vector-parasite dynamics of leishmaniases in the Brazil side of triple border

(Argentina, Brazil and Paraguay). *PLoS Negl Trop Dis, 12*(4), e0006336. doi: 10.1371/journal.pntd.0006336

Tomiotto-Pellissier, F., Bortoleti, B., Assolini, J. P., Gonçalves, M. D., Carloto, A. C. M., Miranda-Sapla, M. M., . . . Pavanelli, W. R. (2018). Macrophage Polarization in Leishmaniasis: Broadening Horizons. *Front Immunol, 9*, 2529. doi: 10.3389/fimmu.2018.02529

Torres-Guerrero, E., Quintanilla-Cedillo, M. R., Ruiz-Esmenjaud, J., & Arenas, R. (2017). Leishmaniasis: a review. *F1000Research, 6*.

Tripathi, B. M. M., Kumar, N. H. N., Sharif, S. K., Chand, K. S., & Santosh, R. (2024). *Enhancing Microbes Prediction Accuracy Through Advanced Deep Learning Models.* Paper presented at the 2024 2nd World Conference on Communication & Computing (WCONF).

Tsukayama, P., Lucas, C., & Bacon, D. J. (2009). Typing of four genetic loci discriminates among closely related species of New World Leishmania. *Int J Parasitol, 39*(3), 355-362. doi: 10.1016/j.ijpara.2008.08.004

Uppamma, P., & Bhattacharya, S. (2023). Deep learning and medical image processing techniques for diabetic retinopathy: a survey of applications, challenges, and future trends. *Journal of Healthcare Engineering, 2023*(1), 2728719.

Valero, N. N. H., Prist, P., & Uriarte, M. (2021). Environmental and socioeconomic risk factors for visceral and cutaneous leishmaniasis in São Paulo, Brazil. *Science of The Total Environment, 797*, 148960. doi: https://doi.org/10.1016/j.scitotenv.2021.148960

Van der Auwera, G., & Dujardin, J. C. (2015). Species typing in dermal leishmaniasis. *Clin Microbiol Rev, 28*(2), 265-294. doi: 10.1128/cmr.00104-14

Van Griensven, J., Carrillo, E., López-Vélez, R., Lynen, L., & Moreno, J. (2014). Leishmaniasis in immunosuppressed individuals. *Clinical Microbiology and Infection, 20*(4), 286-299.

Van Veen, S., Claas, E., & Kuijper, E. J. (2010). High-throughput identification of bacteria and yeast by matrix-assisted laser desorption ionization-time of flight mass spectrometry in conventional medical microbiology laboratories. *Journal of clinical microbiology, 48*(3), 900-907.

Vaz, J. M., & Balaji, S. (2021). Convolutional neural networks (CNNs): Concepts and applications in pharmacogenomics. *Molecular diversity, 25*(3), 1569-1584.

Verma, S., Singh, R., Sharma, V., Bumb, R. A., Negi, N. S., Ramesh, V., & Salotra, P. (2017). Development of a rapid loop-mediated isothermal amplification assay for diagnosis and assessment of cure of Leishmania infection. *BMC Infect Dis, 17*(1), 223. doi: 10.1186/s12879-017-2318-8

Vink, M. M., Nahzat, S. M., Rahimi, H., Buhler, C., Ahmadi, B. A., Nader, M., . . . Schallig, H. D. (2018). Evaluation of point-of-care tests for cutaneous leishmaniasis diagnosis in Kabul, Afghanistan. *EBioMedicine, 37*, 453-460.

Volpedo, G., Huston, R. H., Holcomb, E. A., Pacheco-Fernandez, T., Gannavaram, S., Bhattacharya, P., . . . Satoskar, A. R. (2021). From infection to vaccination: reviewing the global burden, history of vaccine development, and recurring challenges in global leishmaniasis protection. *Expert review of vaccines, 20*(11), 1431-1446.

Vuola, A. O., Akram, S. U., & Kannala, J. (2019). *Mask-RCNN and U-net ensembled for nuclei segmentation.* Paper presented at the 2019 IEEE 16th international symposium on biomedical imaging (ISBI 2019).

Wang, C., Zhu, X., Hong, J. C., & Zheng, D. (2019). Artificial intelligence in radiotherapy treatment planning: present and future. *Technology in cancer research & treatment, 18*, 1533033819873922.

Wang, N., Liang, H., & Zen, K. (2014). Molecular mechanisms that influence the macrophage M1–M2 polarization balance. *Frontiers in immunology, 5*, 614.

Wang, T., Lei, Y., Fu, Y., Wynne, J. F., Curran, W. J., Liu, T., & Yang, X. (2021). A review on medical imaging synthesis using deep learning and its clinical applications. *J Appl Clin Med Phys, 22*(1), 11-36. doi: 10.1002/acm2.13121

Weirather, J. L., Jeronimo, S. M., Gautam, S., Sundar, S., Kang, M., Kurtz, M. A., . . . Wilson, M. E. (2011). Serial quantitative PCR assay for detection, species discrimination, and quantification of Leishmania spp. in human samples. *J Clin Microbiol, 49*(11), 3892-3904. doi: 10.1128/JCM.r00764-11

Wijerathna, T., & Gunathilaka, N. (2020). Morphological identification keys for adults of sand flies (Diptera: Psychodidae) in Sri Lanka. *Parasites & Vectors, 13*, 1-13.

Xu, F., Qin, Y., He, W., Huang, G., Lv, J., Xie, X., . . . Lan, R. (2021). A deep transfer learning framework for the automated assessment of corneal inflammation on in vivo confocal microscopy images. *PloS one, 16*(6), e0252653.

Yadav, A. C., Kolekar, M. H., & Zope, M. K. (2024). *ResNet-101 Empowered Deep Learning for Breast Cancer Ultrasound Image Classification.* Paper presented at the BIOSTEC (1).

Yu, D., Wang, H., Chen, P., & Wei, Z. (2014). *Mixed Pooling for Convolutional Neural Networks*.

Zampieri, R. A., Laranjeira-Silva, M. F., Muxel, S. M., Stocco de Lima, A. C., Shaw, J. J., & Floeter-Winter, L. M. (2016). High Resolution Melting Analysis Targeting hsp70 as a Fast and Efficient Method for the Discrimination of Leishmania Species. *PLoS Negl Trop Dis, 10*(2), e0004485. doi: 10.1371/journal.pntd.0004485

Zare, M., Akbarialiabad, H., Parsaei, H., Asgari, Q., Alinejad, A., Bahreini, M. S., . . . Amirmoezzi, Y. (2022). A machine learning-based system for detecting leishmaniasis in microscopic images. *BMC Infect Dis, 22*(1), 48.

Zerpa, O., & Convit, J. (2009). Leishmaniasis cutánea difusa en Venezuela. *Gazeta Médica da Bahia*(79).

Zhao, C., Shuai, R., Ma, L., Liu, W., & Wu, M. (2022). Improving cervical cancer classification with imbalanced datasets combining taming transformers with T2T-ViT. *Multimedia Tools and Applications, 81*(17), 24265-24300. doi: 10.1007/s11042-022-12670-0

Zink, A. R., Spigelman, M., Schraut, B., Greenblatt, C. L., Nerlich, A. G., & Donoghue, H. D. (2006). Leishmaniasis in ancient Egypt and Upper nubia. *Emerg Infect Dis, 12*(10), 1616.

Thesis

ORIGINALITY REPORT

18%	13%	15%	6%
SIMILARITY INDEX	INTERNET SOURCES	PUBLICATIONS	STUDENT PAPERS

PRIMARY SOURCES

1	img.medscape.com Internet Source	1%
2	wwwnc.cdc.gov Internet Source	1%
3	iris.paho.org Internet Source	1%
4	Abdullahi Umar Ibrahim, Fikret Dirilenoğlu, Uğuray Payam Hacisalihoğlu, Ahmet Ilhan, Omid Mirzaei. "Classification of H. pylori Infection from Histopathological Images Using Deep Learning", Journal of Imaging Informatics in Medicine, 2024 Publication	1%
5	www.dodl.klyuniv.ac.in Internet Source	1%
6	Juliana Quero Reimão, Elizabeth Magiolo Coser, Monica Ran Lee, Adriano Cappellazzo Coelho. "Laboratory Diagnosis of Cutaneous and Visceral Leishmaniasis: Current and Future Methods", Microorganisms, 2020 Publication	1%
7	Juliana P. B. de Menezes, Cláudia Brodskyn, Ricardo Gonçalves, Olivia Bacellar. "Editorial: Immunology and immunopathogenesis of human leishmaniasis", Frontiers in Cellular and Infection Microbiology, 2022 Publication	1%

9 Curriculum Vitae

Dr. Ali Mansour Abdelmula
Phone: +218 91 337 0979
Email: Ali.Hafeed85@gmail.com
Nationality: Libyan
Country of Residence: Libya
Date of Birth: 24 December 1985

Professional Summary

Dedicated medical microbiologist and clinical instructor with over a decade of experience in clinical laboratory diagnostics and higher education. Holder of a PhD in Medical and Clinical Microbiology with a strong academic foundation in biological sciences and bioengineering. Experienced in teaching, laboratory management, and scientific research in both academic and medical settings.

Education

PhD in Medical Microbiology and Clinical Microbiology
Near East University - [2025]

Master's Degree in Bioengineering
Cyprus International University - [2020]

Bachelor's Degree in Biological Sciences
High Institute of Biological Research Center, Massallate, Libya - [2010]

Professional Experience

Instructor
High Institute of Biological Research Center, Massallate, Libya
[2011] - Present

- Teaching core courses in biological and clinical microbiology.
- Supervising student research and lab projects.

- Contributing to curriculum development and academic planning.

Clinical Laboratory Specialist
Private Clinical Laboratory, Libya
2010 – 2016

- Performed diagnostic testing and clinical analysis in microbiology and hematology.
- Maintained quality control procedures in accordance with laboratory standards.
- Assisted in training junior staff and interns in laboratory techniques.

Skills

- Medical and Clinical Microbiology
- Laboratory Diagnostics and Analysis
- Teaching and Academic Supervision
- Bioengineering Applications in Medicine
- Research Design and Scientific Writing
- Laboratory Quality Control and Safety

Languages

- Arabic: Native
- English: Proficient